1-1-1990

The phase separation behavior of poly(vinyl methyl ether)/polystyrene semi-IPN/

Osamu, Aoki

University of Massachusetts Amherst

Recommended Citation

Aoki, Osamu,, "The phase separation behavior of poly(vinyl methyl ether)/polystyrene semi-IPN/" (1990). *Doctoral Dissertations 1896 - February 2014.* 761.

https://scholarworks.umass.edu/dissertations_1/761

THE PHASE SEPARATION BEHAVIOR OF
POLY(VINYL METHYL ETHER) / POLYSTYRENE SEMI-IPN

A Dissertation Presented

by

OSAMU AOKI

Submitted to the Graduate School of the

University of Massachusetts in partial fulfillment

of the requirements for the degree of

DOCTOR OF PHILOSOPHY

February 1990

Department of Polymer Science and Engineering

THE PHASE SEPARATION BEHAVIOR OF

POLY(VINYL METHYL ETHER) / POLYSTYRENE SEMI-IPN
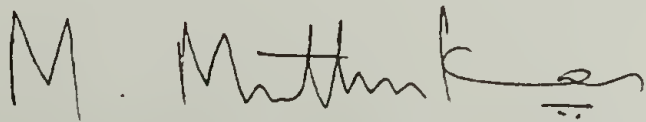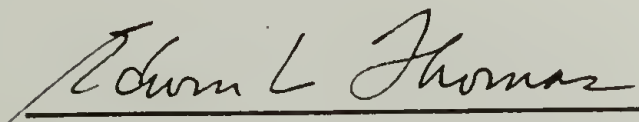

A Dissertation Presented

by

OSAMU AOKI

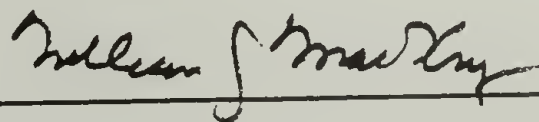Approved as to the style and content by:

Richard S. Stein, Chairperson of Committee

Murugappan Muthukumar, Member

Edwin L. Thomas, Member

William J. MacKnight, Department Head

Polymer Science and Engineering

Dedicated

to my Parents

ACKNOWLEDGEMENTS

ABSTRACT

THE PHASE SEPARATION BEHAVIOR OF
POLY(VINYL METHYL ETHER) / POLYSTYRENE SEMI-IPN

FEBRUARY 1990

OSAMU AOKI, B. S., KYOTO UNIVERSITY, JAPAN

M. S., KYOTO UNIVERSITY, JAPAN

Ph. D., UNIVERSITY OF MASSACHUSETTS

Directed by: Professor Richard S. Stein

The effect of crosslinking on the phase stability and phase separation behavior of poly(vinyl methyl ether) / polystyrene semi-IPN was studied by light scattering.

The cloud point temperature was measured as a function of degree of crosslinking and found to be constant within experimental precision. The result of this experiment was combined with a theoretical prediction of the phase diagram to determine conditions for the following experiment.

Wide angle light scattering was used to quantitatively analyze the mechanism and dynamics of the thermally induced phase separation with respect to the crosslinking density and the thermal condition. An apparatus with a one dimensional diode array was used to simultaneously monitor a wide range of scattering angles.

Analysis of the early stages of phase separation indicates that the spinodal temperature remained virtually constant whether or not crosslinks were present in the system. This was demonstrated to be consistent with theoretical prediction. However, the apparent diffusion coefficient decreased dramatically with the introduction of crosslinks thus the initial phase separation was slowed down significantly.

The final scattering intensity was shown to decrease with increasing crosslinking density. The scattering vector dependence of the scattering intensity was negligible compared with its overall time dependence. A plateau region was observed for some of the scattering intensity data of the semi-IPN systems with respect to time. This indicates that the crosslinks restrict terminal phase contrast and not the size of phase.

TABLE OF CONTENTS

LIST OF TABLES

LIST OF FIGURES

CHAPTER 1

INTRODUCTION

The objective of this dissertation is to determine the effect of crosslinking on the phase stability and phase separation behavior of a semi-interpenetrating network (semi-IPN) system. In recent years, the phase behavior of polymeric mixtures has been of considerable interest to industrial and academic research [1-7]. The phase behavior of polymer blends, especially polystyrene / poly(vinyl methyl ether) blends, has been investigated and modeled using statistical thermodynamics and measurable molecular parameters of their components [8-28]. Recently, the effect of crosslinks on this polymer blend system has been investigated in the one phase region using small angle neutron scattering [29-31].

1.1 Background

Many commercial polymer systems, such as acrylonitrile-butadiene-styrene copolymer (ABS)[32], and high impact polystyrene (HIPS)[33], involve not only the mixing of components but also their crosslinking. These systems are classified as interpenetrating polymer networks (IPN's)[5,7] in the broader sense. However, they are not true IPN's since they are phase separated on a microscopic

1

scale and do not form an interpenetrating network at the molecular level [29].

1.2 Semi-IPN's

A semi-IPN is a polymeric mixture of two homopolymers in which one of the components is crosslinked to form a network and the other is linear [5]. Usually, the linear polymer is added to the monomer mixture which is then crosslink-polymerized in its presence. This study will address the effect of a small amount of crosslinking on the phase behavior of a semi-IPN system.

Semi-IPN's have some similarities to homopolymer blends and polymer gels. Both semi-IPN's and homopolymer blends are mixtures of two homopolymers which have no covalent bonds between each another. A semi-IPN may be considered as a special case of a polymer gel where the solvent molecule is polymeric. The similarity of semi-IPN's to other systems enables us to describe their phase behavior using the theory of homopolymer blends, taking into account the perturbations caused by small amounts of crosslinks. These systems may also be described by the theory for swollen polymer networks with perturbations caused by the polymeric nature of the solvent. The unification of these theories to describe the semi-IPN system has been proposed for an undeformed system [34].

2

The primary goal of this thesis is to observe phase separation in the semi-IPN system and compare results with the theory using available molecular parameters. The expansion of the theory to describe the deformed semi-IPN system was considered using the theory for the deformed swollen polymer network [35,36].

1.3   Description of System

The system under consideration consists of linear poly(vinyl methyl ether) (PVME) and crosslinked polystyrene (PS) with varying crosslink densities. The linear blend of this polymer pair shows a rare case of lower critical solution temperature(LCST) behavior [8-28]. At ambient temperatures these two polymers have a negative χ-parameter and are miscible. They become immiscible at higher temperatures as the value of the χ-parameter increases to a point where it reaches a cirtain positive value determined by the molecular weights of polymers.

These characteristics of the PVME/PS system allow us to make a homogeneous semi-IPN system by preparing the sample at ambient temperature [29,31]. The homogeneous system offers an excellent reference state on which to base experiments. This system also offers control over the crosslink density. By varying the amount of crosslinking agent a series of samples can be made which vary only in

the degree of crosslink density since the crosslinking density is small enough not to affect any other physical properties.

This system was studied in the single phase regime by small angle neutron scattering [29,31]. In that study, the linear blend and the lowest crosslink density sample (N_{cPSD} = 2040) exhibited linear behavior for plots of inverse zero angle scattering, $S(0)^{-1}$, and inverse correlation length squared, ξ^{-2}, versus T^{-1}. The sample with higher crosslink density sample (N_{cPSD} = 380) showed pronounced curvature in the same plots, eventually crossing over the other samples. The highest crosslinking density sample (N_{cPSD} = 100) was phase separated at the temperature of polymerization (70 °C). Deformation studies were also done on these samples. The scattering intensities of deformed samples in the homogeneous state near the spinodal temperature depends not only on the magnitude of the scattering vector but also on its direction with respect to the deformation. This means that the static structure factor, which reflects mainly the thermal concentration fluctuation of components at this temperature, is anisotropic.

Conventional IPN's are in general somewhat phase separated on a microscopic scale [31]. The phase separation and network formation reaction occur simultaneously in the preparation of the system. The final state of the system is decided not by thermodynamic equilibrium but by the kinetic competition between rate of phase separation and rate of the crosslinking reaction. The size of the inhomogeneity depends on the outcome of this competition. If the chemical reaction is extremely fast, the system can be prepared "homogeneously" with

no large regions of phase separation [31]. Since most of the semi-IPN's reported as "homogeneous" are translucent [31], one may suspect that there still exist some phase separated regions which are on the order of the wavelength of light in size. Therefore such system is not truly homogeneous.

The concentration fluctuation caused by the phase separation is easily observed by light scattering since PS and PVME have significantly different refractive indices and since the size of fluctuation is on the order of the wavelength of light [8-28].

1.4   Experimental Methods

The cloud point temperature measurements were done to show that the homogeneously prepared semi-IPN system undergoes phase separation in a manner analogous to that of the corresponding linear polymer blends and to determine the cloud point temperature at which it happens. The results of these experiments were combined with the theoretical prediction of the phase diagram of this system with respect to temperature and composition to establish conditions for the following experiments.

Wide angle light scattering (WALS) experiments were used to observe the time dependent structural development of the system during phase separation. In these experiments, the system was driven

from the homogeneous state to the inhomogeneous state by instantaneously raising the temperature of the system (T-jump). The conditions for the T-jump were chosen using the results of the cloud point temperature measurements and the theoretical prediction of the phase diagram of this semi-IPN system. The various T-jump conditions were used for each sample to determine the spinodal temperature of the phase separating system.

CHAPTER 2

THEORY

A phenomenological theory was formulated for the semi-IPN system to interpret and predict the phase diagram and the phase separation kinetics. The free energy of the system, ΔF, was constructed by combining the free energy of mixing of the linear polymer blend and the free energy of the elastically deformed network following Binder's theory for the isotropic semi-IPN system [34]. This theory was extended to account for anisotropic deformation of the network following Onuki's theory for the swollen gel under anisotropic deformation [35]. The properties of this free energy were studied as a function of the volume fraction, ϕ, of one component and of temperature through the Flory-Huggins interaction parameter, $\chi(\phi, T)$ [37-40]. The effect of deformation on the free energy of semi-IPN system was also studied.

2.1 Description of System

The system under consideration is a semi-interpenetrating network (semi-IPN) in which component A is a network polymer and component B is a linear polymer. This description refers to a system in which a network polymer A is crosslinked in the presence of

7

polymer B. The notation convention for the parameters of interest in the following discussion is defined in Table 2.1.

2.2 Phase Diagram of a Semi-IPN

The phase diagram of a semi-IPN can be calculated from the free energy of the system, ΔF [34,35]. This total free energy is approximated by adding the free energy of mixing of the linear and the network polymer, ΔF_{mix}, and the free energy of elastic deformation of the network, $\Delta F_{network}$,

$$\Delta F = \Delta F_{mix} + \Delta F_{network} . \tag{2.1}$$

Each component of the free energy will be discussed in the following sections. The same approach is used in the Flory-Rehner theory which describes the swelling of a polymer network by a small molecule solvent [36,37-42] and has been moderately successful in describing this phenomena [43]. The semi-IPN system can be thought of as a special case of the Flory-Rehner theory where the solvent is a linear polymer molecule.

2.2.1 The Free Energy of Mixing

The free energy of mixing is approximated by the free energy of mixing for a linear polymer blend in which polymer A has a degree of polymerization νN_A [34,35].

$$\frac{\Delta F_{mix}}{k_B T} = \int_V dr^3 \left[\frac{\phi \ln\phi}{v_A \nu N_A} + \frac{(1-\phi) \ln(1-\phi)}{v_B N_B} + \frac{\chi \phi (1-\phi)}{v_0} \right], \quad (2.2)$$

As νN_A approaches infinity,

$$\frac{\Delta F_{mix}}{k_B T} = \int_V dr^3 \left[\frac{(1-\phi) \ln(1-\phi)}{v_B N_B} + \frac{\chi \phi (1-\phi)}{v_0} \right], \quad (2.3)$$

where v_0, the average lattice volume is given by

$$v_0 = \sqrt{v_A v_B} , \quad (2.4)$$

and χ is the Flory-Huggins interaction per segment (χ–parameter).

The χ–parameter for a semi-IPN is approximated well by that of a linear polymer blend of A and B. This has been shown to be true for the swelling of a network by a small molecule solvent (as described by the Flory-Rehner theory). In this case, the swelling is estimated using

the χ-parameter value for the solvent and the linear polymer. This estimate gives good agreement between experimental and calculated values of swelling.

2.2.2 The Free Energy of Elastically Deformed Network

The free energy of an elastically deformed network which consists of ν chains is approximated by ideal rubber elasticity theory for any small deformations,

$$\frac{\Delta F_{network}}{k_B T} = \nu \left[\frac{A}{2} (I_2 - 3) - B \ln(I_3) \right] ,$$ (2.5)

where A and B are constants that depend on the model of the network used to derive the ideal rubber elasticity theory [31,34,40-51]. I_2 and I_3 are the invariants of deformation defined by the elongation ratio along the principal axes, α_i, as,

$$I_2 = \alpha_x^2 + \alpha_y^2 + \alpha_z^2 ,$$ (2.6a)

$$I_3 = \alpha_x \alpha_y \alpha_z .$$ (2.6b)

10

The constant A depends on the fraction of elastically effective chains in the network. The constant B depends on the model of the network used to derive the ideal rubber elasticity theory as shown in Table 2.2.

In the case of no anisotropic external stress, the elongation ratios are identical due to symmetry and depend only on the local concentration,

$$\alpha_x = \alpha_y = \alpha_z = \left(\frac{\phi_0}{\phi}\right)^{1/3},$$ (2.7)

where, ϕ_0 and ϕ are volume fractions of the relaxed network and the deformed network respectively. The free energy of the elastically deformed network, $\Delta F_{network}$, is written under these isotropic constraints using the integral form as,

$$\frac{\Delta F_{network}}{k_B T} = \frac{v}{V_0} \int_{V_0} dr_0^3 \left\{ \frac{3A}{2} \left[\left(\frac{\phi_0}{\phi}\right)^{2/3} - 1 \right] + B \ln\left(\frac{\phi}{\phi_0}\right) \right\},$$ (2.8)

where V_0 is the volume of the relaxed network and r_0 is a fixed coordinate in the relaxed system. In the deformed system, the position vector, r, is defined and related to r_0 by

$$r = \left(\frac{\phi_0}{\phi}\right)^{1/3} r_0 .$$ (2.9)

11

Thus, using the relationship,

$$v_A \, N_A \, v = \phi_0 \, V_0 \, , \tag{2.10}$$

and converting the coordinate of the integral as,

$$\frac{v}{V_0} \int_{V_0} dr_0^3 = \frac{\phi_0}{v_A \, N_A} \int_V \left(\frac{\phi}{\phi_0} \right) dr^3 \, , \tag{2.11a}$$

$$= \frac{1}{v_A \, N_A} \int_V dr^3 \, \phi \, , \tag{2.11b}$$

we obtain an expression for $\Delta F_{network}$,

$$\frac{\Delta F_{network}}{k_B \, T} = \int_V dr^3 \left[\frac{B \, \phi \, \ln\left(\frac{\phi}{\phi_0} \right)}{v_A \, N_A} + \frac{3 \, A}{2 \, v_A \, N_A} \left(\phi^{1/3} \, \phi_0^{1/3} - \phi \right) \right].$$

$$\tag{2.12}$$

2.2.3 The Total Free Energy of Semi-IPN system

The total free energy of a semi-IPN system (equation 2.1) is explicitly written by combining the free energy of mixing (equation 2.3) with the free energy of the network (equation 2.12),

$$\frac{\Delta F}{k_B T} = \int_V dr^3 \left[\frac{B \, \phi \ln\phi}{v_A \, N_A} + \frac{(1-\phi) \ln(1-\phi)}{v_B \, N_B} + \frac{\chi \, \phi \, (1-\phi)}{v_0} \right.$$

$$\left. + \frac{3 \, A}{2 \, v_A \, N_A} \phi^{1/3} \, \phi_0^{2/3} \right]. \quad (2.13)$$

This equation bears a strong resemblance to the free energy of a linear polymer blend[12],

$$\frac{\Delta F}{k_B T} = \int_V dr^3 \left[\frac{\phi \ln\phi}{v_A \, N_A} + \frac{(1-\phi) \ln(1-\phi)}{v_B \, N_B} + \frac{\chi \, \phi \, (1-\phi)}{v_0} \right], \quad (2.14)$$

where N_A in this equation is the degree of polymerization of the A, linear chain component. The only significant difference in these two equations 2.12 and 2.13 is the last term in equation 2.12 for the free energy of the semi-IPN system which accounts for the elastic energy contribution from the network deformation due to the local swelling.

2.2.4 Binodal Temperature

The binodal temperature for a semi-IPN network is implicitly defined as the temperature and the composition where the linear polymer within the network and that outside of the network are in equilibrium. The schematic diagram is shown in Figure 2.1. In other words, the chemical potentials of each phase must be equal,

$$\mu_B(\phi, T) = \mu_B(\phi = 0, T) .$$ (2.15)

This definition of the binodal temperature is the same as that of a small molecule solvent in swelling equilibrium with a network polymer[32]. The chemical potential of polymer B is defined in general as,

$$\mu_B(\phi, T) = \left(\frac{\partial \Delta F}{\partial n_B} \right),$$ (2.16)

where n_B is the number of monomer units of polymer B in the system.

The condition for the binodal temperature in the semi-IPN system is obtained by inserting the chemical potential given by equations 2.13 and 2.16 into equation 2.15 [31].

$$0 = \frac{A\,\phi^{1/3}\,\phi_0^{2/3}}{v_A\,N_A} - \frac{B\,\phi}{v_A\,N_A} + \frac{\phi}{v_B\,N_B} + \frac{\ln(1-\phi)}{v_B\,N_B} + \frac{\chi\,\phi^2}{v_0}. \qquad (2.17)$$

From this equation, the χ-parameter at the binodal temperature, χ_b, is given explicitly as,

$$\frac{\chi_b}{v_0} = \left(\frac{1}{\phi^2}\right)\left[\frac{B\,\phi - A\,\phi^{1/3}\,\phi_0^{2/3}}{v_A\,N_A} - \frac{\phi + \ln(1-\phi)}{v_B\,N_B}\right] \qquad (2.18)$$

In the case of linear polymer blends with polymer A having an infinite degree of polymerization, $N_A \rightarrow \infty$, the condition for the binodal temperature is approximated by equation 2.15. The formula is obtained by inserting the chemical potential given by the equations 2.14 and 2.16 into the equation 2.15 and and taking N_A to the limit of infinity as,

$$\frac{\chi_b}{v_0} = \left(\frac{1}{\phi^2}\right)\left[-\frac{\phi + \ln(1-\phi)}{v_B\,N_B}\right]. \qquad (2.19)$$

It should be noted that equation 2.18 becomes identical to equation 2.19 in the limit of $N_A \rightarrow \infty$ and that the difference between these equations is only a term involving N_A in equation 2.18 accounting for the contribution from elastic deformation of network.

2.2.5 Spinodal Temperature

The spinodal temperature of a semi-IPN system is implicitly defined by the equation,

$$\left(\frac{\partial^2 \Delta F}{\partial \phi^2} \right) = 0 .$$

(2.20)

Beyond this condition, spontaneous nucleation and phase separation occur everywhere in the system. This is called spinodal decomposition and the schematic diagram is given in Figure 2.1. The explicit formula for the spinodal temperature in the semi-IPN system is [31],

$$\chi_s - \chi(\phi,T) = 0 ,$$

(2.21)

where χ_s is defined as,

$$\frac{\chi_s}{v_0} = \frac{1}{2} \left\{ \frac{1}{v_A N_A \phi} \left[B - \frac{A}{3} \left(\frac{\phi_0}{\phi} \right)^{2/3} \right] + \frac{1}{v_B N_B (1-\phi)} \right\} .$$

(2.22)

The explicit formula for the spinodal temperature in the linear polymer blend is the same as equation 2.21 except that the definition of χ_s in equation 2.22 is replaced by [12],

16

$$\frac{\chi_s}{v_0} = \frac{1}{2}\left[\frac{1}{v_A \, N_A \, \phi} + \frac{1}{v_B \, N_B \, (1-\phi)}\right]. \tag{2.23}$$

It should be noted that equations 2.22 and 2.23 become identical in the limit of $N_A \rightarrow \infty$.

2.2.6 Examination of Phase Diagram

The phase diagram of the semi-IPN system is defined by equations 2.18 and 2.22. It is informative to examine the effect of parameters to these equations. For simplicity, we assume $v_0 = v_B = v_A$, $\phi = \phi_0$, and $A = 1$. The constant B is expected to be between 0.5 and 1 for the network having a functionality of four as described in section 2.2.2. We assumed $B = 0.5$ in following calculation. Equation 2.18 was simplified as,

$$N_B \, \chi_b = \left(\frac{1}{\phi^2}\right)\left\{\left[-0.5 \, \phi\left(\frac{N_B}{N_A}\right)\right] - \left[\phi + \ln(1-\phi)\right]\right\}. \tag{2.24}$$

Equation 2.22 was simplified as,

$$N_B \, \chi_s = \frac{1}{2}\left[\frac{1}{6\,\phi}\left(\frac{N_B}{N_A}\right) + \frac{1}{(1-\phi)}\right]. \tag{2.25}$$

17

It should be remembered that the elastic contributions are the terms involving (N_A/N_B) for both equations 2.24 and 2.25. It is apparent that the important parameters in the system are $N_B \chi_b$, $N_B \chi_s$, (N_B/N_A) and ϕ.

The spinodal and binodal conditions are plotted against $N_B \chi$ versus ϕ for special cases $N_A = N_B$ and $N_A = \infty$ in Figure 2.2. The dotted curves indicate the spinodal conditions and the solid lines indicate the binodal conditions. The intermediate set of curves are for the case $N_A = \infty$, and the others are for the case $N_A = N_B$. The case $N_A = \infty$ is equivalent to the case of a linear blend with one component having infinite molecular weight but having no crosslinks. It is clear that the presence of the elastic terms in free energy causes the downward curve for binodal at dilute network concentrations, ϕ, indicating that even for a large negative χ-parameter the semi-IPN system will be inherently unstable and tend to phase separate if the concentration of network component is small.

Figure 2.3 is a plot of $N_B \chi$ versus N_B/N_A for $\phi = 0.5$ to indicate the effect of the crosslink density and the molecular weight of the linear component. The elastic terms in the free energy decrease the one phase region as defined by the binodal condition, $N_B \chi_b$, with respect to the ratio N_B/N_A while the unstable region as defined by the spinodal condition, $N_B \chi_s$, is actually decreased. It should also be noted that the binodal condition is six times more sensitive to the ratio N_B/N_A than the spinodal condition.

Numerical evaluation is necessary in order to further evaluate the phase diagram of a semi-IPN system with respect to temperature and composition. This analysis is discussed in chapter 5 describing the theoretical prediction of the phase diagram for the PVME/PS semi-IPN.

2.3 Dynamics of a Semi-IPN

In order to study the dynamics of the system, one must also take into account the contribution of the concentration fluctuation to the free energy [34,35,52-58]. This allows us to evaluate the static structure factor and the spinodal decomposition.

The free energy of concentration fluctuation, $\Delta F_{fluct.}$, can be estimated by the Ginzburg-Landau approximation,

$$\frac{\Delta F_{fluct.}}{k_B T} = \int_V dr^3 \left[\kappa_A \ |\nabla\phi|^2 + \kappa_B \ |\nabla(1 - \phi)|^2 \right], \qquad (2.26)$$

where κ_A and κ_B are constants related to the dispersion of acoustic waves [34]. The values of κ_A and κ_B were estimated by random phase approximation for the polymer system [59-61]. The total free energy of a semi-IPN system, ΔF, which accounts for the fluctuation term is given by,

$$\Delta F = \Delta F_{mix} + \Delta F_{network} + \Delta F_{fluct.} \ .$$ (2.27)

The functions $f(\phi)$ and κ are defined in the following equation:

$$\frac{\Delta F}{k_B T} = \int_V dr^3 \left[f(\phi) + \kappa \ | \nabla \phi |^2 \right].$$ (2.28)

In order to determine an expression for the static structure factor we first obtain the local chemical potential difference $\mu(r)$ which is normalized so that it is a thermodynamic variable conjugate to the volume fraction using a functional derivative [35],

$$\mu(r) = \frac{\delta\left(\dfrac{\Delta F}{k_B T} \right)}{\delta\phi} = \left(\frac{\partial f(\phi)}{\partial\phi} \right) - \kappa \nabla^2 \phi \ .$$ (2.29)

Expanding $\mu(r)$ by putting $\phi(r) = \phi_0 + \delta\phi(r)$ where ϕ_0 is an average concentration and keeping only the terms linear in $\delta\phi(r)$, we obtain,

$$\delta\mu(r) = \mu(r) - \mu(r)_{\delta\phi = 0}$$

$$= \left\{ \left[\frac{\partial^2 f(\phi)}{\partial\phi^2} \right]_{\phi = \phi_0} - \kappa \nabla^2 \right\} \delta\phi(r) \ .$$ (2.30)

Defining the Fourier transforms,

$$\mu_{\mathbf{q}} = \frac{(2\pi)^3}{V} \int_V d\mathbf{r}^3 \exp(\, i\,\mathbf{q}\,\mathbf{r}\,)\, \delta\mu \, , \qquad (2.31)$$

$$\phi_{\mathbf{q}} = \frac{(2\pi)^3}{V} \int_V d\mathbf{r}^3 \exp(\, i\,\mathbf{q}\,\mathbf{r}\,)\, \delta\phi \, . \qquad (2.32)$$

we obtain the relationship,

$$\mu_{\mathbf{q}} = \left[\left(\frac{\partial^2 f(\phi)}{\partial\phi^2} \right)_{\phi = \phi_0} + \kappa\, q^2 \right] \phi_{\mathbf{q}} \, , \qquad (2.33)$$

where V is the total volume of the system. The wave dependent, collective static structure factor, S(q), is defined as,

$$S^{-1}(\mathbf{q}) = \left(\frac{\mu_{\mathbf{q}}}{\phi_{\mathbf{q}}} \right). \qquad (2.34)$$

Thus, we have derived the static structure factor for semi-IPN's [31],

$$S^{-1}(q) = 2\, (\chi_s - \chi(\phi,T)\,) + \kappa q^2 \, , \qquad (2.35)$$

where χ_s is the χ-parameter at the spinodal temperature defined in equation 2.20. This formula shows that the static structure factor of both semi-IPN and polymer blend systems can be written as the same Lorentzian function except that the definition of χ_s differs slightly for

each system in equations 2.22 and 2.23. The difference between the two systems relies only upon the definition of χ_s.

It is also known that the scattering intensity is proportional to the structure factor,

$$I(q) \propto S(q) , \tag{2.36}$$

and that the scattering intensity at zero angle is proportional to S(0), as follows:

$$I(0) \propto S(0) = \frac{1}{2(\chi_s - \chi(\phi,T))} . \tag{2.37}$$

Furthermore, the correlation length, ξ, is defined by the slope of $I(q)^{-2}$ vs. q^2 divided by $I(0)^{-2}$,

$$\xi^2 = I(0)^2 \left(\frac{d(I(q)^{-2})}{d(q^2)} \right)$$

$$= \left(\frac{\kappa}{2(\chi_s - \chi(T))} \right) . \tag{2.38}$$

If the system is miscible, where χ is definitely smaller than χ_s, both the zero angle scattering intensity and the correlation length have finite positive values. As the χ-parameter approaches χ_s (i.e. the system approaches its spinodal temperature), both the zero angle

scattering intensity and the correlation length diverge toward infinity. This result is used in small angle neutron scattering (SANS) to detect the spinodal temperature [31].

As χ becomes larger than χ_s (i.e the system is brought into the two phase region), the static structure factor becomes negative. This $S(q)$ is called a virtual scattering factor to indicate that it has no direct relationship to the scattering intensity. In this region, a large concentration fluctuation is created by the spontaneous phase separation of the system. This makes it possible to observe scattering by light.

The early stages of this kind of phase separation can be described by the Cahn-Hilliard spinodal decomposition theory [52-58]. In this regime, the scattering intensity grows exponentially as follows:

$$I(q,t) = I(q,0) \exp(2 R(q) t) , \qquad (2.39)$$

where $R(q)$ is the growth rate which is related to the virtual static scattering factor and the Onsager coefficient, $\Lambda(q)$,

$$R(q) = - q^2 \Lambda(q) S^{-1}(q) . \qquad (2.40)$$

The Onsager coefficient is a measure of the entropic contribution to the driving force of demixing, and the virtual static structure factor is a measure of the excess free energy contribution to demixing.

The apparent diffusion coefficient is given by,

$$D_{app} = \lim_{q \to 0} \Lambda(q) \, S(q)^{-1} \, .$$ (2.41)

The equations 2.35 and 2.40 indicate that the apparent diffusion coefficient is zero at the spinodal temperature, T_s:

$$\lim_{T \to T_s} D_{app} = 2 \, \Lambda(0) \, (\, \chi_s - \chi(T_s) \,) = 0 \, .$$ (2.42)

The apparent diffusion coefficient is measured experimentally using equations 2.39 and 2.41,

$$D_{app} = \lim_{q \to 0} (\, q^{-2} \, R(q) \,) \, .$$ (2.43)

We can therefore experimentally determine the spinodal temperature by extrapolating temperature to where the apparent diffusion coefficient is zero from light scattering data of the phase separating system.

2.4   The Effect of Anistropic Deformation

The assumption of isotropic deformation in equation 2.8 is no longer true for the system under anisotropic deformation. Onuki considered the effect of anisotropic deformations on the free energy of the swollen gel [35]. This theory can be adopted to the semi-IPN system since the semi-IPN system is a special case of the swollen gel in which solvent is polymeric. This results in a static structure factor of the deformed semi-IPN system given by,

$$S(\mathbf{q})^{-1} = 2(\chi_s - \chi) + \kappa\, q^2 + \frac{1}{N_A}\left(\sum_i \frac{\alpha_i^2\, q_i^2}{|\mathbf{q}|^2}\right).$$

$$\hspace{10cm} (2.44)$$

where α_i and q_i are the elongation ratio and the scattering vector along the i-th direction, respectively. The constant χ_s is defined as equation 2.22 for the semi-IPN system in order to account for the polymeric nature of solvent in semi-IPN system. It is very important to note that $S(\mathbf{q})$ of the deformed semi-IPN system has a third term which depends only on the direction of scattering vector, $\mathbf{q}/|\mathbf{q}|^2$, even in the limit of $|\mathbf{q}| \to 0$.

This formula does not account for the fact that the deformation of the polymer network may cause a large change in the single chain structure factor of the polymer chains constituting the network. The corresponding prefactor, κ, of the q^2-term in equation 2.44 for the

undeformed network appears in equation 2.35 and was determined by the argument of the random phase approximation [59-61] using the single chain structure factor. Thus, the prefactor κ in equation 2.44 should actually be considered as a tensor and depends on the direction of the scattering vector with respect to the deformation of the network and on the extent of the deformation.

CHAPTER 3

SAMPLE DESCRIPTION

3.1   Sample Preparation

PVME/PS semi-IPN samples are prepared by polymerizing styrene monomer in the presence of PVME and a crosslinking agent in the sample cell. An ultraviolet sensitive initiator, benzoin, was used to initiate radical polymerization at ambient temperature by ultraviolet light irradiation. A bifunctional monomer, divinylbenzene(DVB), was used as the crosslinking agent. This preparation procedure ensured that the sample was homogeneously mixed and that there were no covalent bonds formed between linear PVME and PS network.

3.1.1 Poly(vinyl methyl ether)

The phase diagram of the PVME/PS system can be strongly affected by a trace amount of water present in the system [24]. Extreme care was taken to keep water away from the sample throughout the sample preparation and experiments.

Poly(vinyl methyl ether) (PVME - Scientific Polymer Products, Mw = 99,000; Mn = 46,500; 50% water solution) was carefully dried

and purified using the following procedures. Toluene (3 parts) and as-received PVME solution(1 part) were combined in a large (1000 ml) beaker. They were vigorously mixed using a mechanical stirrer over a twelve hour period. After mixing the toluene became thick and the PVME solution became translucent and white in color. This beaker was left overnight to let the toluene and water separate. The clear, yellowish toluene/PVME solution was transferred to an Erlenmeyer flask (7 l). The PVME was then precipitated from the toluene solution using heptane. Approximately seven parts of heptane for one part of the toluene solution were required to precipitate the polymer. The Erlenmeyer flask was heated to about 50° C for twenty minutes to redissolve the PVME. This resulted in a clear one phase solution. The Erlenmeyer flask was set aside overnight so that the PVME would precipitate to the bottom of the flask. The top layer was removed and a small quantity of toluene was added to dissolve the remaining precipitated PVME. This solution was poured into an evaporation dish which was kept in a vacuum oven for three days to remove any residual solvent. The PVME was then transferred to a vacuum desiccator for storage.

3.1.2 Monomer Mixture

Styrene monomer and DVB were vacuum distilled over CaH_2 for purification and drying. They were then mixed in various proportions to achieve a range of crosslinking densities for the semi-IPN's. The

composition of PVME and PS was 50/50 weight ratio for all the samples prepared. The composition of crosslinking agent, DVB, is listed in Table 3.1 with its sample codes. The #0 sample was prepared as a reference sample and is not a semi-IPN system but a linear blend system since it used no crosslinking agent.

Benzoin, the ultraviolet light sensitive radical initiator was dissolved into the monomer mixture (0.1 wt %). Next, the PVME was dissolved into the monomer mixture and kept in a sealed test tube. After three days, homogeneous mixing of the monomers and the PVME were confirmed by observing the homogeneity of viscosity of the sample.

3.1.3 Sample Cell

The sample cell consists of two circular quartz plates separated by a thin Teflon washer as shown in Figure 3.1. The quartz plate is 1/16" thick with a diameter of 7/8". The thin Teflon washer is 5 mil (0.127 mm) thick, has an outer diameter of 7/8" and an inner diameter of 3/4". This sample cell was designed to fit into the sample holder on the WALS equipment. The viscous mixture of monomer and PVME was transferred into a quartz cell and kept sealed by clamping the quartz plates together on either side of the washer, during the polymerization procedure described below.

29

3.1.4 Polymerization

The monomers mixed with PVME were polymerized at ambient temperature using ultraviolet irradiation to form a homogeneously mixed semi-IPN system in which there are no covalent bonds formed between the linear PVME and the PS network. A long wavelength ultraviolet lamp (100 W, λ = 300nm) was kept 40 cm away from the sample cell. The cell was held fixed in the clamp with the quartz window facing the lamp for proper irradiation by the ultraviolet light. This wavelength was chosen to specifically initiate the benzoin but not the styrene monomer. Sample irradiation and thus polymerization was maintained for three days. This is twice as long as the time required for the bulk polymerization of styrene in a comparable environment. The sample was inspected for clarity to ensure that there was no phase separation during polymerization. The sample was then transferred to a vacuum oven at 80 °C for three days to remove any residual monomer. Before each experiment, all samples were held at 100 °C for 60 minutes in order to insure consistent initial condition.

3.2   Sample Characterization

The results of the characterization for all the samples are tabulated in Table 3.1 with sample codes. The stoichiometrically

estimated average molecular weight was calculated assuming the purity of divinylbenzene to be 55% and the remainder to be primarily 3- and 4 - ethylvinylbenzene as stated in the supplier's specifications (Aldrich Chemical). We also assumed that the copolymerization of styrene and DVB is completely random and consumes all of the monomer in the system.

The gel fraction and the average molecular weight between crosslinks were determined by solvent extraction and swelling experiments after all other experiments were complete since these are destructive tests. The quartz sample cell was broken, and the sample recovered. The sample(ca. 10 µg) was then weighed, W_0, and soaked in an excess of toluene(ca. 10 ml) for one month. At the end of one month, the sample had become a highly swollen gel. In order to ensure that all the linear polymer components had been extracted out of the semi-IPN system and that an equilibrium swelling state had been achieved, the toluene was replaced with fresh toluene and left for another two weeks. At the end of two weeks, no further change in the swelling of the sample was observed. We therefore concluded that the sample consisted only by the swollen polystyrene network which had reached its swelling equilibrium with pure toluene. The swollen gel was then taken out of the toluene and weighed immediately in its wet state, W_{wet}. The gel was then dried for one day in air followed by drying for one day in a vacuum oven at 50 °C to remove the toluene. The sample was weighed again in its dry state, W_{dry}.

The gel fraction is given by,

$$(\text{gel fraction}) = \frac{W_{dry}}{W_0} . \tag{3.1}$$

Since sample #0 is a linear blend, it dissolved into solvent and did not have any gel fraction. Samples #1 to #4 have gel fractions of 0.50 ±0.06 which means that the polymerization process to prepare the semi-IPN samples formed no covalent bonds between PS network and linear PVME, i.e., covulcanization between PS and PVME does not occur. All the semi-IPN samples should have gel fraction of 0.5 since PVME is not crosslinked and should be extracted as sol fraction. Large deviation from 0.50 for the gel fraction of sample #5 was observed. Higher crosslink density causes diffusion of linear PVME through the PS network to slow down. This results in incomplete solvent extraction of PVME from the semi-IPN system.

The average molecular weight between crosslinks, $M_{C(swell)}$ was obtained from the swelling of the PS network in toluene. The weight ratio W_{wet} / W_{dry} was converted to a swelling ratio, Q, using the density of toluene, ρ_{tol}, to be 0.867 and that of PS, ρ_{PS}, to be 1.04.

$$Q = \left(\frac{W_{wet}}{W_{dry}} - 1 \right) \left(\frac{\rho_{PS}}{\rho_{tol}} \right) + 1 . \tag{3.2}$$

The volume fraction of the PS network as it was prepared, ϕ_0, is 0.5. The volume fraction of the swollen PS network, ϕ, is given by Q^{-1}.

Flory-Rehner theory relates the swelling of the network to the average molecular weight between crosslinks, $M_{C(swell)}$ [40-42].

$$M_{C(swell)} = M_{w(toluene)} \left(\frac{\rho_{PS}}{\rho_{toluene}} \right) \left(\frac{\phi_0^{2/3} \phi^{1/3} - 0.5 \phi}{- \ln(1- \phi) - \phi - \chi \phi^2} \right). \quad (3.3)$$

where χ for PS and toluene at 25 °C is 0.44 [62].

The stoichiometrically estimated average molecular weight between crosslinks of PVME/PS semi-IPN system, $M_{c(st.)}$, and that experimentally determined from swelling of the network by toluene, $M_{c(swell)}$ are compared in Figure 3.2. They have a linear relationship with a factor of 3.09 except for sample #1. This discrepancy happens because the stoichiometrical calculations do not account for the fact that the polymerization is not ideal. The deviation from linearity for sample #1 is due to its low crosslink density. At such low crosslink densities there are many dangling chain ends which are elastically inactive.

CHAPTER 4

CLOUD POINT

The cloud point temperature measurement was used to study the onset of phase separation in the PVME/PS semi-IPN system. The cloud point temperature is determined by monitoring the onset of the light scattering intensity increase caused by concentration fluctuations induced by the phase separation. The result of this experiment was combined with the theoretical prediction of the phase diagram of this system to establish conditions for the following experiments.

4.1   Cloud Point Apparatus

The schematic of the cloud point apparatus at the University of Massachusetts is shown in Figure 4.1. The optical geometry of the system is shown in Figure 4.2. The intensity of scattered light at scattering angles between 42° and 138° are reflected at the glass-to-air surface by the total reflection, emitted from the edge of a microscope slide, and collected by a integrating sphere. This corresponds to scattering vectors, $q = 20 - 28\ \mu m^{-2}$. The scattering from small concentration fluctuations caused by phase separation can be detected in this scattering vector range [9,10,22,27].

34

The sample was subjected to temperatures from 80 to 150 °C with an increasing temperature rate of 2 °C per minute while the scattering intensity was monitored with the apparatus depicted in Figure 4.1.

4.2   Results

The phase separation of the corresponding linear polymer blend is known and has been detected by the cloud point experiment. The data for the control sample #0, which is not crosslinked and is a linear polymer blend, shows a typical upturn in the scattering intensity at the cloud point temperature upon heating as shown in Figure 4.3.

The homogeneously prepared semi-IPN samples, #1 - #5, which are crosslinked, undergo phase separation in a manner analogous to that of the corresponding linear polymer blend with the reduction in the scattering intensity with the increase in crosslinking density as shown in Figure 4.3.

In order to determine where the onset of the increase in the scattering intensity occurs, the light scattering data were normalized with respect to the scattering intensities at 100 °C and 150 °C in Figure 4.4. This figure indicates that the onset of an increase in the scattering intensity is constant within the precision of these experiments(116 °C ± 2 °C).

The reduction of the scattering intensity with increasing crosslink density was empirically analyzed by plotting the scattering intensity at 150 °C against the molecular weight between crosslinks of the polystyrene network in the semi-IPN system on a log-log scale as shown in Figure 4.5. This analysis shows that the scattering intensity from the phase separated system is proportional to the molecular weight between crosslinks. This may be due to the fact that the concentration fluctuation caused by the phase separation is limited by the elastic restoration force of the polymer network which increases with higher crosslink density or that the size of phase is limited by the existence of crosslinks. In order to further investigate the cause of this effect, the angular dependance of scattering intensity should be measured for the phase separated system as described in Chapter 6.

CHAPTER 5

THEORETICAL PREDICTION OF PHASE DIAGRAM

The effect of crosslinks on the phase diagram for the PVME/PS semi-IPN system is numerically evaluated using the theory in Chapter 2. The explicit formulae for both the binodal temperature and spinodal temperature require the knowledge of the composition and temperature dependent χ-parameter, $\chi(\phi,T)$, of the system.

5.1 The Molecular Parameters for the PVME/PS System

The molecular parameters needed for the evaluation of the phase diagram of the semi-IPN system are the degree of polymerization of each chain, N_A and N_B, the average lattice volume, v_0, and the χ-parameter, $\chi(\phi,T)$. The degree of polymerization was obtained by dividing the molecular weight by the monomer molecular weight. The volume of monomer unit was obtained by dividing the monomer molecular weight by the density. The density of PS and PVME are 1.044 and 1.047 respectively [26].

Unfortunately, there are no good experimentally obtained χ-parameter values available for the PS(hydrogenous)/PVME system. As a close approximation therefore, we used the χ-parameter value

between deuterated PS and PVME. A correction factor was used to account for the isotope effect [26] and the tacticity effect [29].

The χ-parameter between PS(deuterated) and PVME was experimentally determined using a small angle neutron scattering technique and is described by the following equation for a wide range of temperatures and compositions [28].

$$\frac{\chi}{v_0} = (A + B \phi) + \left(\frac{C + D \phi}{T} \right)$$

(5.1)

where T is the absolute temperature, and ϕ is the volume fraction of PS. Numerical values of A, B. C, and D are

A = $8.714*10^{-4}$,

B = $4.749*10^{-4}$,

C = $-3.543*10^{-1}$, and

D = $-2.461*10^{-1}$.

The phase diagram of the PVME/PS system is reported to shift to a higher temperature by more than 30°C if the hydrogen on the PS is substituted by deuterium [26]. This is explained in that the χ-parameter for this blend is not highly dependent on changes in temperature. However, the small changes in cohesive energy densities between the deuterated and hydrogenated PS do cause large shifts in the phase diagram. The spinodal temperature of the

38

PS(deuterated)/PVME system prepared by radical polymerization of PS is reported to shift to a lower temperature by 7° to 10°C compared to that of the anionically polymerized one [29]. This was attributed to the very slight difference in χ-parameter which comes from the difference in tacticity between the radically and anionically polymerized materials.

In our studies, the PS component in the PS(hydrogenous)/PVME system was prepared by radical polymerization. A parameter, E, was introduced into equation 5.1 to account for the very small difference in the χ-parameter due to isotope and tacticity effects.

$$\frac{\chi}{v_0} = (A + B\,\phi) + \left(\frac{C+D\,\phi}{T}\right)E \ , \tag{5.2}$$

where E is chosen to be 0.897 so that the theoretical prediction of the binodal temperature using equation 2.19 and this χ-parameter matches that of sample #0 which is simply the linear PVME/PS blend system.

5.2 The Phase Diagram of Linear Blend

The phase diagram of linear blend is plotted as a function of temperature and composition using equations 2.19, 2.23 and 5.2 in

figure 5.1 for sample #0. The critical composition of this system, ϕ_c, is nearly zero due to the fact that the molecular weight of the PS is much larger than that of the PVME. The entire phase diagram is shifted to the left until $\phi_c = 0$. The non-parabolic nature of this phase diagram comes from the fact that the χ-parameter is strongly composition dependent. From this theoretical phase diagram it is also observed that the difference between the binodal and the spinodal at $\phi = 0.5$ is less than 2°C.

5.3   The Effect of Crosslinks on Binodal Temperature

The binodal temperature for each sample is also plotted as a function of temperature and composition in Figure 5.2. using equations 2.24 and 5.2. The degrees of polymerization for each of the components,N_A and N_B, were chosen to correspond to the samples used in the experiments described in this dissertation described in Table 3.1.

Table 5.1 lists the theoretical prediction of binodal temperature for each sample prepared. This shows that the binodal temperature at $\phi = 0.5$ becomes significantly lower than that of the linear blend. Some initial attempts to make semi-IPN systems with $\phi = 0.2$ failed to achieve homogeneity during sample preparation. This is because at room temperature the system is above the binodal temperature and phase separates during polymerization.

5.4   Effect of Crosslinks on the Spinodal Temperature

The spinodal temperature for each sample is also plotted as a function of temperature and composition in Figure 5.3. using equations 2.25 and 5.2. The degrees of polymerization for each of the components, N_A and N_B, were chosen to correspond to the samples used in the experiments described in this dissertation which are described in Table 3.1.

Table 5.1 lists the theoretical prediction of spinodal temperature for each sample prepared. This shows that the difference in the spinodal temperature at $\phi = 0.5$ is smaller than 2°C even for the most extreme case.

CHAPTER 6

WIDE ANGLE LIGHT SCATTERING

Wide angle light scattering(WALS) was used to quantitatively analyze the mechanism and dynamics of the thermally induced phase separation. The corresponding linear polymer blend is known to scatter light in the 1 to 10 μm^{-1} range while undergoing phase separation [9,10,22,27]. A linear polymer blend control sample #0 and two semi-IPN samples #1, and #2 were used for this experiment. The other semi-IPN samples did not scatter enough light to be able to measure them with WALS apparatus.

6.1   Wide Angle Light Scattering Apparatus

In order to make rapid measurement of scattering intensity over a range of scattering angles, the WALS apparatus depicted in Figure 6.1 was used [27]. A vertically polarized helium-neon laser with wavelength λ = 632 nm was used as a light source to scatter light from the sample held in a hot stage. The scattered light was focused onto a one-dimensional photo diode array. The transmitted light was monitored using a photocell. These data were collected by the OMA-III system with a programmed timing sequence.

6.1.1 Detection of Scattered Light

The scattering image was projected onto a one dimensional photodiode array with 512 pixel elements (PAR model 1452) using two sets of four element lenses (ORIEL ASPHERAB MODEL 66063, f/0.7, 50 mm focal length). This combination of lenses gives an aperture angle of up to 70°. The two sets of lenses were collimated so that their optical axes coincided with each other, and were also in line with the center of the detector and the sample. The sample was located such that its center coincided with the center of the goniometer with a tilt angle. The entire assembly, consisting of the two lenses and the detector is attached to the arm fixed to the goniometer and can be rotated to the desired angle. The sample was tilted in order to have access to higher scattering angles.

The first set of lenses (L1) was located at a distance equal to its focal length away from the sample. This ensures that the Fourier image of the sample is focused at the focal length of the lens on the other side of the lens. The second set of lenses (L2) was located such that the inverted and reduced image of the Fourier image was focused onto the detector.

The relationship between the scattering angle and the detector channel position was calibrated using the main beam at reduced

intensity. The goniometer was rotated so that the main beam went through both lenses to the detector. The various goniometer angle readings and the corresponding peak channel positions were reduced to a best fit third order polynomial function which related the detector position and the offset angle from the center of the detector.

6.1.2 Detection of Transmitted Light

The transmitted light intensity was monitored by a photocell located at the beam stop in order to evaluate the absorption of light by the sample, and to compensate for absorption in the scattering intensity readings. A diffuser located before the photocell was used to suppress the position sensitivity of the photocell.

A preamplifier was built to interface the output of the photocell to the Source Comp. input of the OMA-III. This preamplifier consists of three operational amplifiers. It reverses the polarity of the signal, compensates the offset of the photocell, amplifies the output of the photocell with variable gain to the level suitable for the input of the OMA-III, and adjusts the time constant.

6.1.3 OMA-III

The OMA-III consists of a timing pulse generator, a 14 bit analog-to-digital converter and a programmable microcomputer. It was interfaced to both the one dimensional diode array and the preamplifier of the photocell. For each 150 msec exposure, it reads all channels on the one dimensional detector to detect the scattered light and the Source Comp. input to detect the transmitted light intensity. It stores the digitized values as an array in its memory. Throughout this experiment, the 32 bit numerical summation of 400 consecutive data points in the memory is used to achieve an equivalent of six seconds of exposure time to improve the precision of data.

A timed sequence of data was taken by programming the OMA-III with increasing intervals and is stored as a two dimensional array in its memory. This arrangement ensures the best efficiency of memory use without degrading the quality of the data or the precision of the time interval. After each experiment, the data in the memory is transferred to a diskette for further analysis.

6.1.4 T-jump Experiment

In order to have well defined conditions for the quantitative analysis of phase separation, the system was driven from a

homogeneous state to an inhomogeneous state by instantaneously increasing the temperature (T-jump). The conditions for the T-jump were chosen using the results of the cloud point temperature measurements and the theoretical prediction of the phase diagram for this semi-IPN system. The initial temperature of the T-jump experiments was chosen to be 100°C where samples #0, #1, and #2 are below the experimentally observed cloud point temperature and the theoretically calculated binodal temperature. The various final temperatures of the T-jump experiments were used for each sample to determine the spinodal temperature of the phase separating system.

The sample was kept for 60 minutes in an auxiliary heating block located right next to the main heating block and heated to 100°C. The main heating block on the WALS equipment was kept at the temperature to which the sample is subjected after the T-jump. The sample was quickly transfered from auxiliary heating block to the main heating block to change the sample temperature instantaneously. Monitoring of the scattered intensity and the transmitted intensity was begun immediately using a pre-programmed time sequence.

The temperature of these heating blocks was regulated by PID controllers with an accuracy of ±0.02°C. The speed of the T-jump was calibrated by using a platinum resistance thermometer located in the empty sample cell. The temperature reached within 10% of the terminal temperature in 15 seconds.

6.2   Data Correction and Conversion

47

The raw data was corrected for the absorption and the sensitivity of the detector, converted to the scattering intensity as a function of the scattering vector, and reduced the number of data points by averaging data over several channels [63-65]. A program, OMA-III.PAS, was written in Turbo Pascal to do all of this on a MS-DOS microcomputer and is attached as Appendix C.

6.2.1 The Scattering Vector

A schematic of the optical geometry around the sample is shown in Figure 6.2. The vertically polarized incident light arrives at the sample at the angle, θ_1. The scattered light leaves the sample with an angle, θ_4, to a detector channel. The angles θ_1 and θ_4 can be determined by reading the goniometer position and using the polynomial function which relates the detector channel and the offset angle from the center of the detector obtained in section 6.1.1.

Snell's law describes the refraction of light:

$$\frac{\sin \theta_1}{\sin \theta_2} = \frac{\sin \theta_4}{\sin \theta_3} = n \, , \tag{6.1}$$

where n is the refractive index of the sample and angles, θ_2 and θ_3, are defined in the Figure 6.2. Thus, θ_2 and θ_3 can be solved using known parameters:

$$\theta_2 = \sin^{-1}\left(\frac{\sin \theta_1}{n}\right), \tag{6.2a}$$

$$\theta_3 = \sin^{-1}\left(\frac{\sin \theta_4}{n}\right). \tag{6.2b}$$

The scattering vector is given by

$$q = \frac{2 \pi n}{\lambda} \sin\left(\frac{\theta_2 + \theta_3}{2}\right), \tag{6.3}$$

where λ is the wavelength of light in a vacuum, which is 632 nm for a helium-neon laser.

6.2.2 Absorption Correction

Lambert's equation describes the absorption of light as follows:

$$I_{trans.} = I_{in.} \exp\left(-\frac{\mu x_0}{\cos \theta_2}\right),\qquad\qquad (6.4)$$

where μ is the absorption coefficient, $I_{in.}$ is the incident light intensity, $I_{trans.}$ is the transmitted light intensity, and x_0 is the thickness of the sample. The absorption coefficient was obtained by monitoring the reduction of transmitted light using equation 6.4. The scattering intensity, $I_{scatt.}$, is reduced by the absorption of light in the same manner. The optical path length within the sample is given as

$$(\text{Optical path length}) = \frac{x_1}{\cos \theta_2} + \frac{x_0 - x_1}{\cos \theta_3},\qquad (6.5)$$

for the light path scattered at x_1. The average absorption by the sample for scattered light [63] is given as

$$(\text{Average absorption}) = \int_0^{x_0} dx_1 \left\{ \exp\left[-\mu \left(\frac{x_1}{\cos \theta_2} + \frac{x_0 - x_1}{\cos \theta_3} \right) \right] \right\}$$

$$= \exp\left(-\frac{\mu x_0}{\cos \theta} \right),$$

$$\text{for } \theta = \theta_2 = \theta_3 , \quad (6.6a)$$

or,

$$= \left(\frac{-1}{\mu\,x_0}\right)\left[\frac{\exp\left(\frac{-\mu\,x_0}{\cos\theta_2}\right) + \exp\left(\frac{-\mu\,x_0}{\cos\theta_3}\right)}{\left(\cos\theta_2\right)^{-1} - \left(\cos\theta_3\right)^{-1}}\right],$$

$$\text{for } \theta_2 \neq \theta_3 \, . \quad (6.6b)$$

The measured scattering intensity was multiplied by the inverse of equation 6.6 to cancel the absorption effect from the scattering intensity. The effect of multiple scattering was not corrected since the scattering intensity was not strongly dependent on the scattering vector [64,65].

6.2.3 Sensitivity Calibration

The correction factor for effects other than the absorption by the sample was obtained as an overall value using the non-directional nature of the fluorescent emission from the dye kept in the sample cell which was excited by the laser beam. Nile blue (Aldrich) was chosen as a dye. The stock solution of nile blue was prepared by dissolving 11.4 mg of nile blue into 4.00 ml of water. The 20 ml of water solution of gelatine (Kodak, class 88 type IV, deionized NVAB 400F, lot #RD-44) was prepared and kept heated to 60°C. The mixture of 1 ml of nile blue stock solution and 10 ml of water solution of gelatine was made and kept heated to 60°C. These pure and dyed

samples were cast into the same type of cell as the one containing the semi-IPN sample.

These calibration samples were placed into the sample cell and the equipment was aligned to the same experimental configuration as that for the next T-jump experiment. The results from the wide angle light scattering experiments were calibrated using these data.

The sharp cut filter (ORIEL 03FCG109) was used before the detector to eliminate the scattered light from the fluorescent light in this calibration measurement. The fluorescent light is measured as a difference between the measured intensities for dyed and pure gelatine solution.

6.3   Results

Figure 6.3 is a plot of the initial scattering intensity with respect to the scattering vector for the linear blend, sample #0, and the semi-IPN samples, #1 and #2. All the samples have the same thickness and were measured in an arbitrary unit. Since the linear blend sample #0 is annealed below cloud point temperature, sample #0 is surely homogeneous. The semi-IPN samples show similar scattering intensities indicating that they are also homogeneously prepared.

51

The scattering intensities through out these experiments are not smooth due to the effect of speckle pattern, even though the scattering intensities were averaged over 16 channels of detector pixels.

Though we chose T-jump conditions such that the system would undergo phase separation by spinodal decomposition, the system simultaneously undergoes phase separation by the nucleation and growth mechanism. The compositions of PVME/PS systems were 50/50 for our samples which is far from their critical compositions, 100/0. The contribution of the nucleation and growth mechanism to the scattering intensity is mainly in the low scattering vector regime [14,15].

Figures 6.4 and 6.5 are examples of the scattering intensities of the linear blend, sample #0, plotted against the scattering vectors for a series of times after the T-jump from 100°C to 120°C and to 150°C respectively. Large changes in scattering intensity with respect to time were observed and the scattering intensity dependence is weaker than that of the scattering vector.

Figures 6.6 to 6.9 are examples of the scattering intensity of semi-IPN samples #1 and #2 plotted against the scattering vector for a series of times after the T-jump from 100°C to 120°C and to 150°C. A smaller change in scattering intensity with respect to time was observed than in that of the linear blend. The scattering intensity dependence is weaker than that of the scattering vector.

The initial scattering intensities of the scattering vector larger than 6 μm^{-1} grow exponentially. This is behavior characteristic of spinodal decomposition. The growth of the scattering intensities in this range of the scattering vector is considered to be dominated by the spinodal decomposition mechanism. Thus initial scattering intensities in this range of scattering vector were analyzed using the theory for the dynamics of spinodal decomposition presented in chapter 2.

Figure 6.10 is a plot of the logarithm of scattering intensity against time for the initial 200 seconds for linear blends after a T-jump from 100°C to 150°C. Since the T-jump takes about 15 seconds, the initial 15 seconds of data were disregarded and the slope between 18 to 60 seconds was used as an initial slope. In this range the data was linear indicating exponential growth characteristic of spinodal decomposition. According to Cahn-Hilliard theory of spinodal decomposition, this initial slope gives the growth rate, R(q) in equation 2.39.

Figures 6.11 and 6.12 are plots of the logarithm of the scattering intensity against time for the initial 200 seconds for semi-IPN samples after a T-jump from 100°C to 150°C. The change is smaller than that of a linear blend, however, similar exponential growth was observed and the same analysis was done.

Figures 6.13 to 6.18 are plots of $R(q)/q^2$ against q^2 for samples #0, #1, and #2. Using the relationship described by equation 2.43, the apparent diffusion coefficient,$D_{app.}$, was extrapolated from these plots.

Figure 6.19 plots the apparent diffusion coefficient, $D_{app.}$ against temperature, T, for each sample. The intercept of the temperature axis gives the spinodal temperature, T_s, for each sample according to equation 2.42. The spinodal temperature is found to be virtually constant, 116°C±2°C, whether or not crosslinks are present in the system. The theoretical prediction of the spinodal temperature shown in Table 5.1 predicted less than a 0.5°C increase and is thus consistent with the experimental result. However, the apparent diffusion coefficient decreased dramatically with the introduction of crosslinks and with increase of crosslinking density. Thus, the initial phase separation was slowed down significantly. This is in agreement with the fact that the mobility of polymer chain is reduced in a network matrix and the reduction of the mobility increases with the crosslinking density.

The change of the scattering intensity at longer time periods is plotted for the scattering vector, $q=11.42 \ \mu m^{-1}$, and is shown in Figures 6.20 and 6.21 for each sample at 120°C and 150°C respectively. The scattering vector dependence of the scattering intensity was negligible compared with its overall time dependance. The final scattering intensity was shown to decrease with increasing crosslinking density. The plateau region was observed for some of the

54

scattering intensities of the semi-IPN system with respect to time indicating that the crosslinks restrict terminal phase contrast.

55

CHAPTER 7

DISCUSSION

7.1 Conclusion

The cloud point temperature, T_c, is constant for different crosslinking densities within the limits of our experimental precision. The phase stability does not depend on the degree of crosslinking for the low degrees of crosslinking used in these experiments.

The scattering intensity decreases with an increase in crosslink density. Both cloud point and WALS measurements strongly confirm this result. Empirical linear relationship between crosslinks and the scattered intensity from the phase separated system was observed in cloud point experiments. The elastic restraining force of the network is working against the phase separation in the semi-IPN system and limits the phase contrast resulting in the decrease of the scattered intensity from phase separated system.

The excess scattering intensity for semi-IPN samples does not exhibit a strong scattering vector(q) dependence. The excess scattering intensity, $I(q,t) - I(q,0)$, reflects the change in concentration fluctuation of wavelength $2\pi/q$. The lack of

dependence on the scattering vector indicates a broad distribution of phase separated domain size.

The analysis of light scattering data leads to the conclusion that we may be able to describe the early stages of phase separation using the spinodal decomposition theory since these data exhibit an initial exponential growth which is characteristic of spinodal decomposition. The spinodal temperatures deduced from this analysis using equation 2.39 are listed in Table 5.1 for each sample and fall within experimental precision of each other. This indicates that the spinodal temperature is not affected significantly by low degrees of crosslinking. These results coincide with the result of the theoretical prediction where the effect of crosslinking on the spinodal temperature for #1 or #2 samples was predicted to be less than 0.5°C in Table 5.1.

The change in scattering intensity for the semi-IPN samples does show a strong dependence on time. The phase separation behavior of the linear PVME/PS blend and the semi-IPN systems show similar power-law dependence in the early stages. However, at longer time scales, the crosslinked samples show a marked decrease in power law dependence of phase separation compared to the PVME/PS blend. At a given point the phase separation of the semi-IPN systems seems to reach a constant value. It is proposed that this is due to a balancing of the entropy of mixing and the elastic restoration energy of the crosslinked system. When these energies balance, further phase separation of the semi-IPN does not occur.

These results indicate that crosslinking limits the speed of the phase separation and the ultimate phase contrast in the phase separated system of the semi-IPN system. Crosslinking for the M_C studied does not affect the thermodynamic stability of the system since the spinodal temperature is virtually constant. The experimental stability of the system in terms of the cloud point temperature is not affected by crosslinking even though the binodal is expected to be affected. The phase separation of the semi-IPN system at its binodal requires deswelling of the network and synergistic movement of the homopolymer out of the network which will not happen within experimental time scale considered here. The polymeric nature of the solvent molecule makes diffusion through the network extremely slow. The actual cloud point temperature should occur near or at the spinodal temperature where the system is unstable enough to spontaneously phase separate. This explains the observation that the spinodal temperature and the cloud point temperature of this semi-IPN system are very close to each other.

7.2   Suggestions for Future Work

Future studies on the phase behavior of the semi-IPN system should consider the effect of an external force field on the phase behavior of the semi-IPN system. Since semi-IPN's are crosslinked, they can be exposed to static stress and reach equilibrium. I propose

the study of the phase behavior of the semi-IPN under uniaxial stress. The sample cam be made using a similar system of semi-IPN used in this study. The sample is first exposed to uniaxial deformation in its single phase regime. Then the sample is exposed to T-jump into two phase temperature. The wide angle light scattering from the sample is observed in a similar equipment with a two dimensional detector which enables us to monitor azimuthal dependence of the scattering intensities.

The result of these experiments should be analyzed by combination of the theories of Binder and Onuki described in chapter 2. This theoretical approach should predict that the concentration fluctuation of the homogeneous phase and the growth rate of the scattering intensity of the phase separating system should depend on the scattering vector anisotropically for the deformed semi-IPN system. The detail of the theories still need to be elaborated.

Some related topics should be referenced to understand the phase behavior of the semi-IPN under uniaxial stress. A related topic is the phase behavior of the linear polymer blend under the shear force field, i.e., the flow induced phase separation [66]. There have been proposed several theories [67,68,69]. Another related topic is the single chain static structure factor of network chain and has been studied by the small angle neutron scattering.[70-73]. This is important because the constant κ in Chapter 2 is obtained by the random phase approximation which uses the single chain static structure factor.

In order to proceed to the next experiments, the improvement of the experimental procedure is desirable. The precision of the experiment is an area which can be improved. Sources of error in the measured intensity can be attributed to a.) error in system calibration (scattering intensity jitter - 5%), b.) statistical error due to low count of intensity(< 1%), c.) instability of solid state over one dimensional optical detector unit(~ 1%) d.) modulation of the scattered intensity by speckle patterns (reduced by averaging 16 channels). In future experiments the possibility of shaking the sample should be considered as this would decrease speckle pattern effects which are a major source of data deterioration. The quality of the sample is another area which needs attention. Dust free environments such as semiconductor fabrication clean rooms and microfiltration of all the polymer components should be used for sample preparation. The photo crosslinking techniques used to immobilize transient structures in the phase separating system may be used to prepare the styrene network for the PVME/PS semi-IPN system [74]. The evolution of the microstructure can be visualized using transmission electron microscopy on the immobilized system.

APPENDIX A

TABLES

Table 2.1   The convention of notations for the parameters of interest in the following discussion.

Component	A	B
Volume fraction	ϕ	$1-\phi$
Average degree of polymerization	$N_A{}^*$	N_B
Volume of monomer unit	v_A	v_B .
Number of lattice sites	y_A	y_B
Average end-to-end distance	$R_A{}^*$	R_B
Segment length	σ_A	σ_B

    *   Indicates value for network chains between

crosslinks for the semi-IPN system.

Table 2.2   The comparison of front factors for various rubber
elasticity theories [51].

Theory	Value of B in equation 2.5
James and Guth	0
Kuhn(Affine deformation)	1
Flory(Phantom network)	$1 - \left(\dfrac{2}{f}\right)$
Flory-Erman	varies between $1 - \left(\dfrac{2}{f}\right)$ and 1 (with mobility of crosslink point)

In the above table, f is the functionality of crosslinks.

Table 3.1 Composition of divinyl benzene (DVB) in polystyrene (PS) network; stoichiometrically estimated average molecular weight between crosslinks of PVME/PS semi-IPN system, $M_{c(st.)}$; that experimentally determined from swelling of network by toluene, $M_{c(swell)}$; gel fraction of semi-IPN, and weight ratio of wet and dry gels.

| Sample	DVB/PS (weight %)	$M_{c(st.)}$	$M_{c(swell)}$*	Gel fraction	W_{wet}/W_{dry}
#0	0.0	(not crosslinked)		0.00	(dissolved)
#1	0.1	$1.04*10^5$	$4.58*10^5$	0.50	34.1
#2	0.2	$5.20*10^4$	$1.64*10^5$	0.45	19.8
#3	0.4	$2.60*10^4$	$7.42*10^4$	0.46	13.4
#4	0.6	$1.73*10^4$	$4.33*10^4$	0.56	10.4
#5	0.8	$1.30*10^4$	$4.16*10^4$	0.70	10.2

* $M_{c(swell)}$ involves 10 % error.

Table 5.1   The theoretical prediction of the binodal temperature and spinodal temperature for the samples prepared.
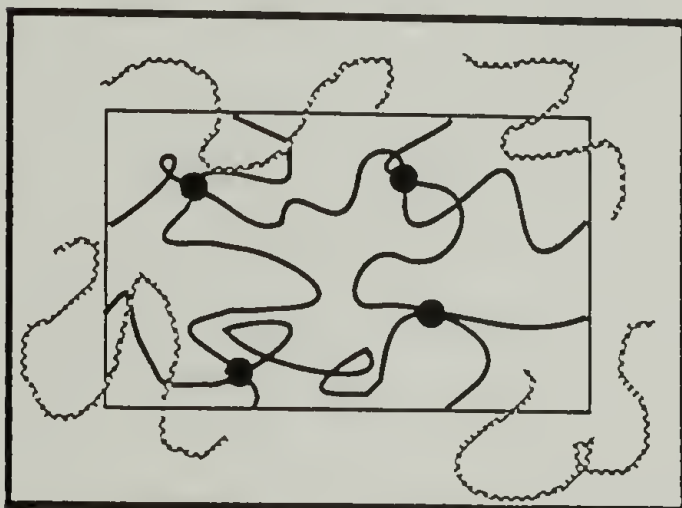
64

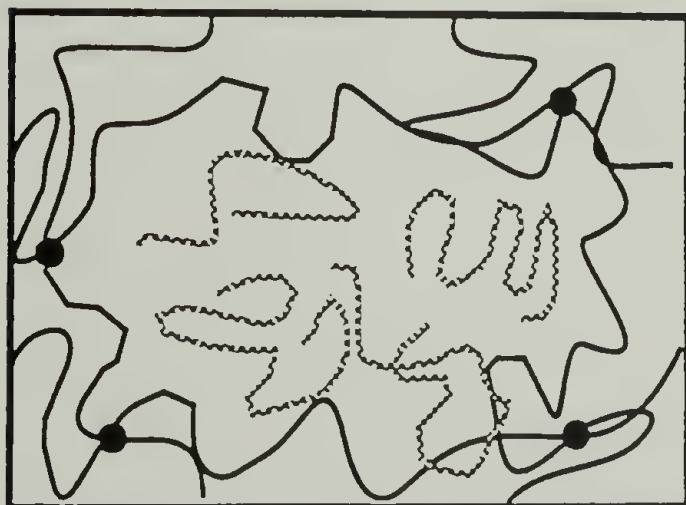| Sample code	Molecular Weight between crosslinks	Binodal Temperature (°C)	Spinodal Temperature (°C)
#0	(not crosslinked)	116.00	116.86
#1	458000	115.20	117.00
#2	164000	113.77	117.23
#3	74200	111.11	117.69
#4	43300	107.69	118.29
#5	41600	107.36	118.34
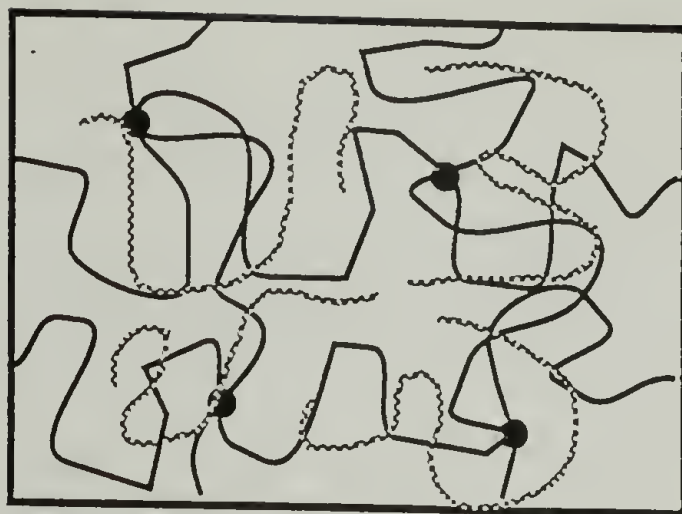
FIGURES

Homogeneous

Binodal

Spinodal

Figure 2.1 Schematics of phase behavior in the semi-IPN system under homogeneous state, binodal decomposition, and spinodal decomposition.
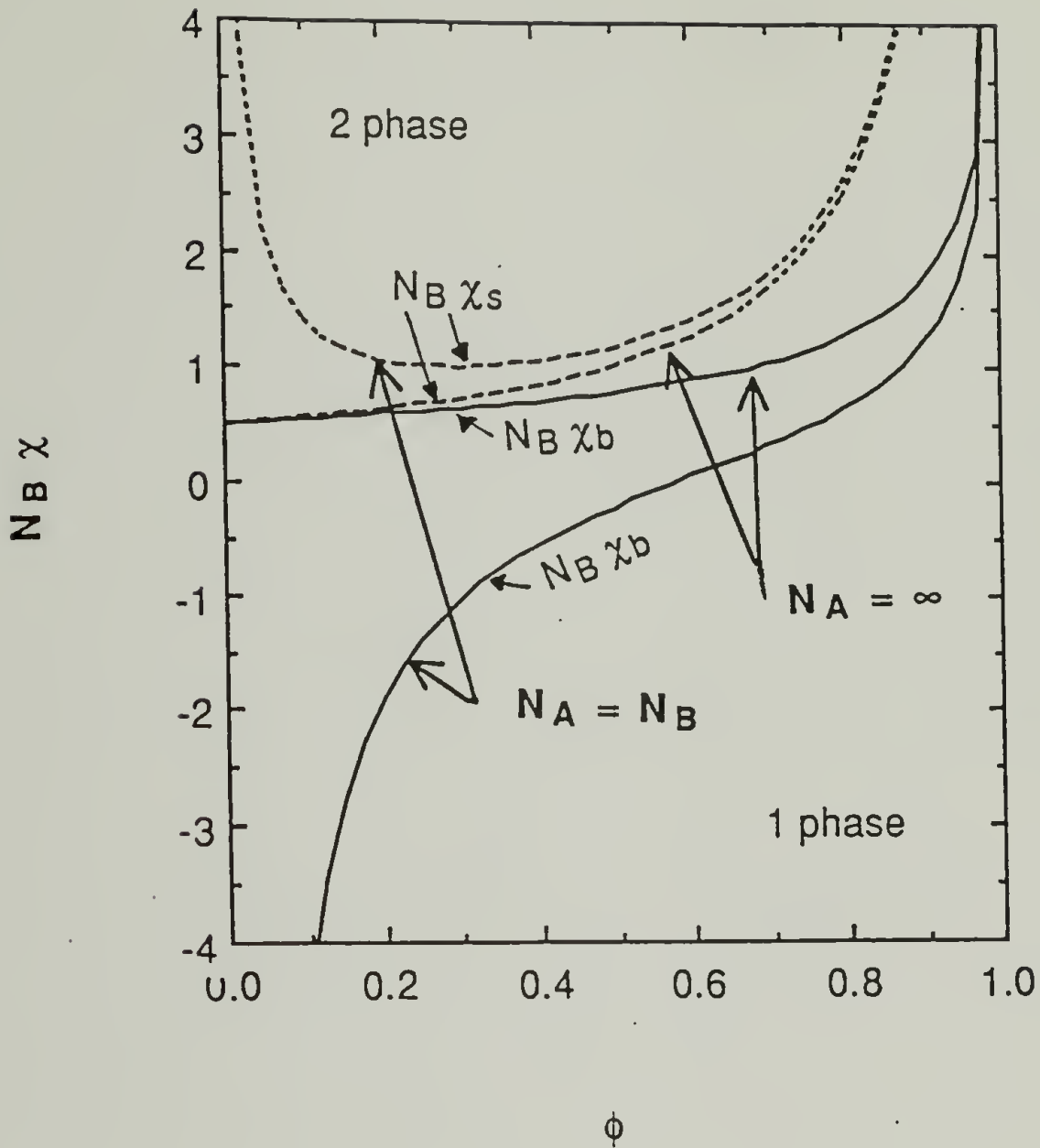
Figure 2.2 The spinodal and binodal conditions are plotted against $N_B \chi$ versus ϕ for special cases $N_A = N_B$ and $N_A = \infty$. The dotted curves indicate the spinodal conditions and the solid ones indicate the binodal ones. The intermediate set of curves are for the case $N_A = \infty$, and the others are for the case $N_A = N_B$.
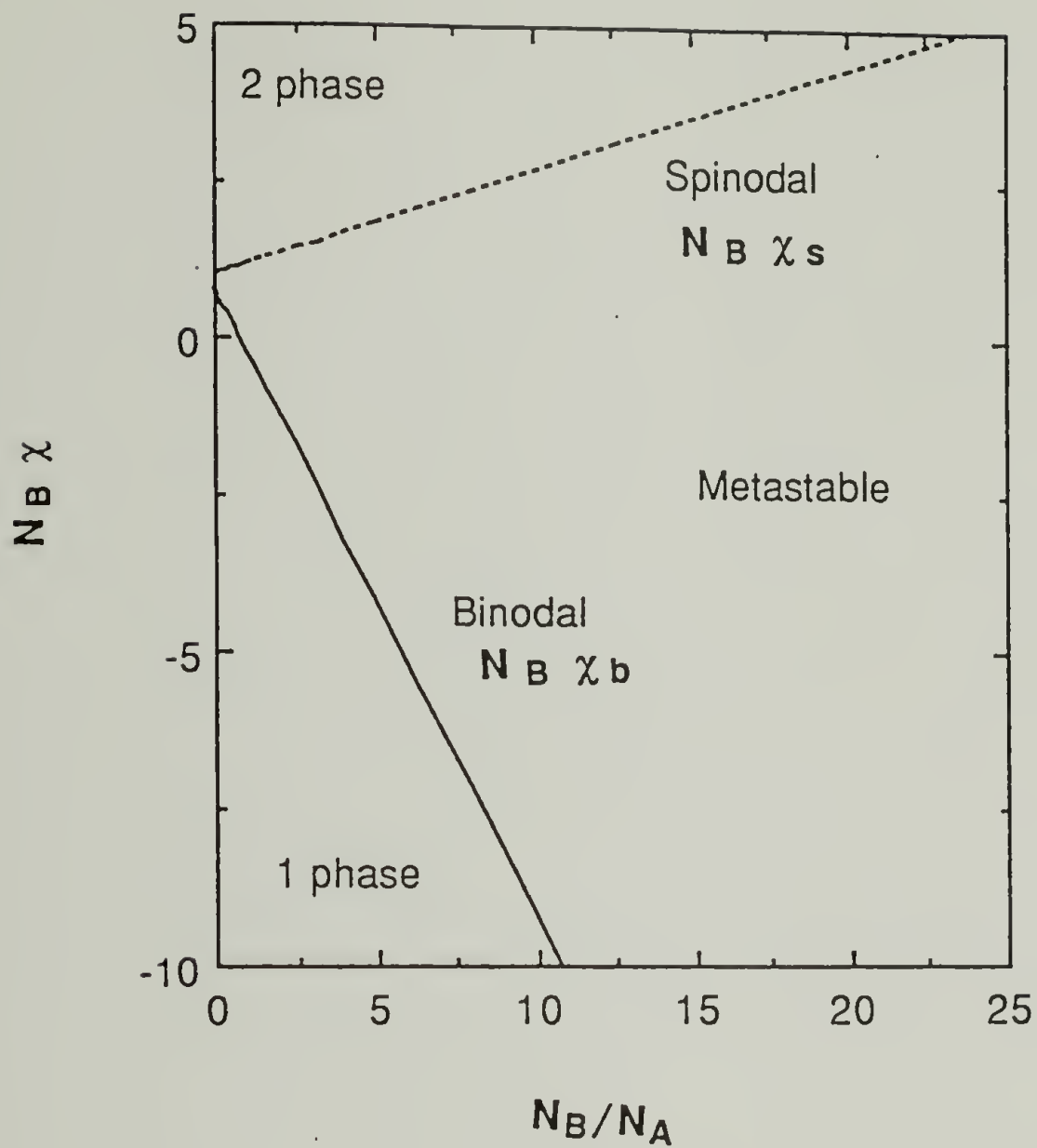
Figure 2.3 A plot of χ N_B versus N_B/N_A for $\phi = 0.5$ to indicate the effect of the crosslink density and the molecular weight of the linear component.
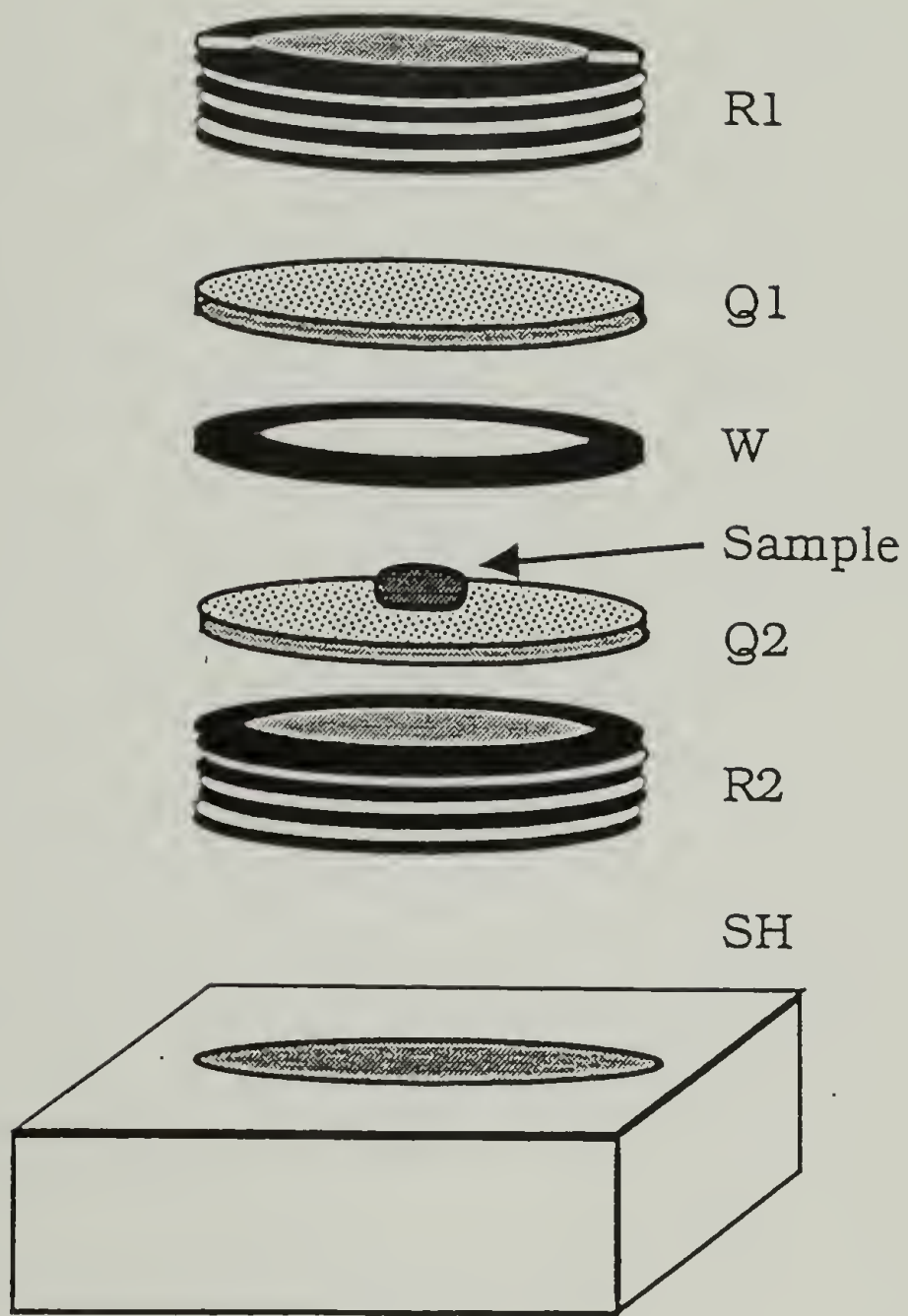
Figure 3.1   A schematic of the sample cell and its clamp used during polymerization.
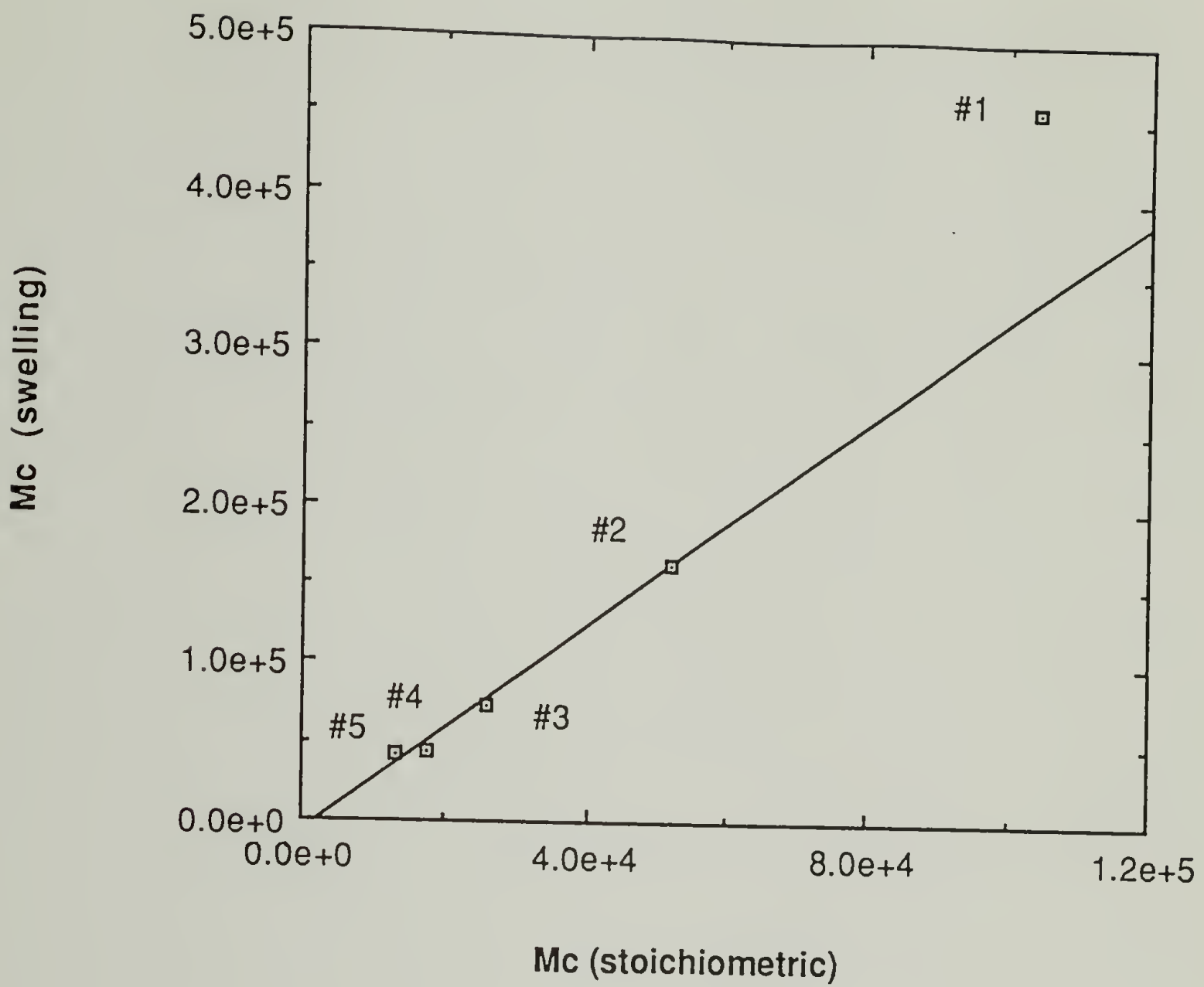
Figure 3.2   Relationship between stoichiometrically determined average molecular weight and experimentally determined molecular weight from swelling experiments.
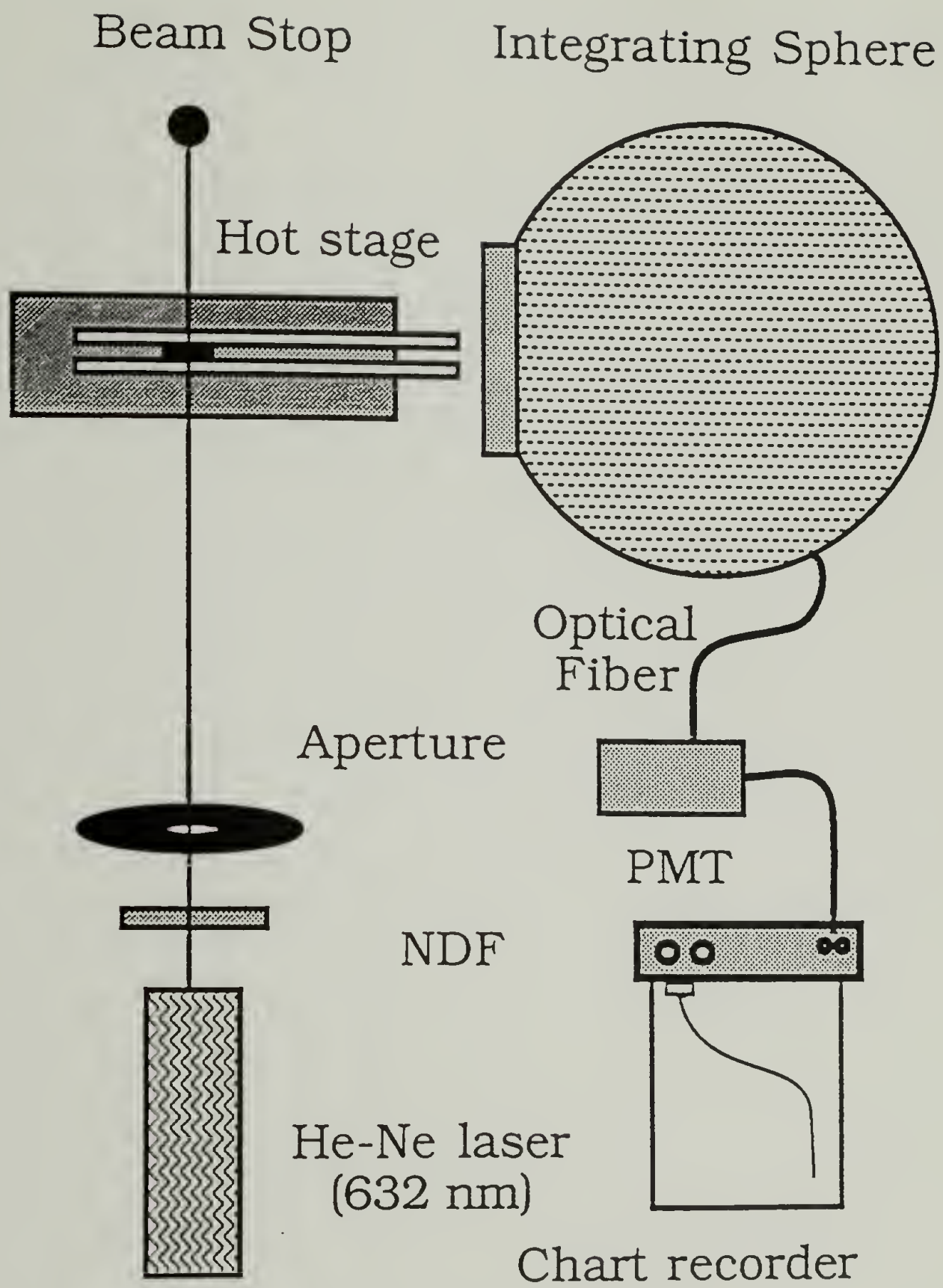
Figure 4.1 Schematic diagram of the cloud point apparatus.
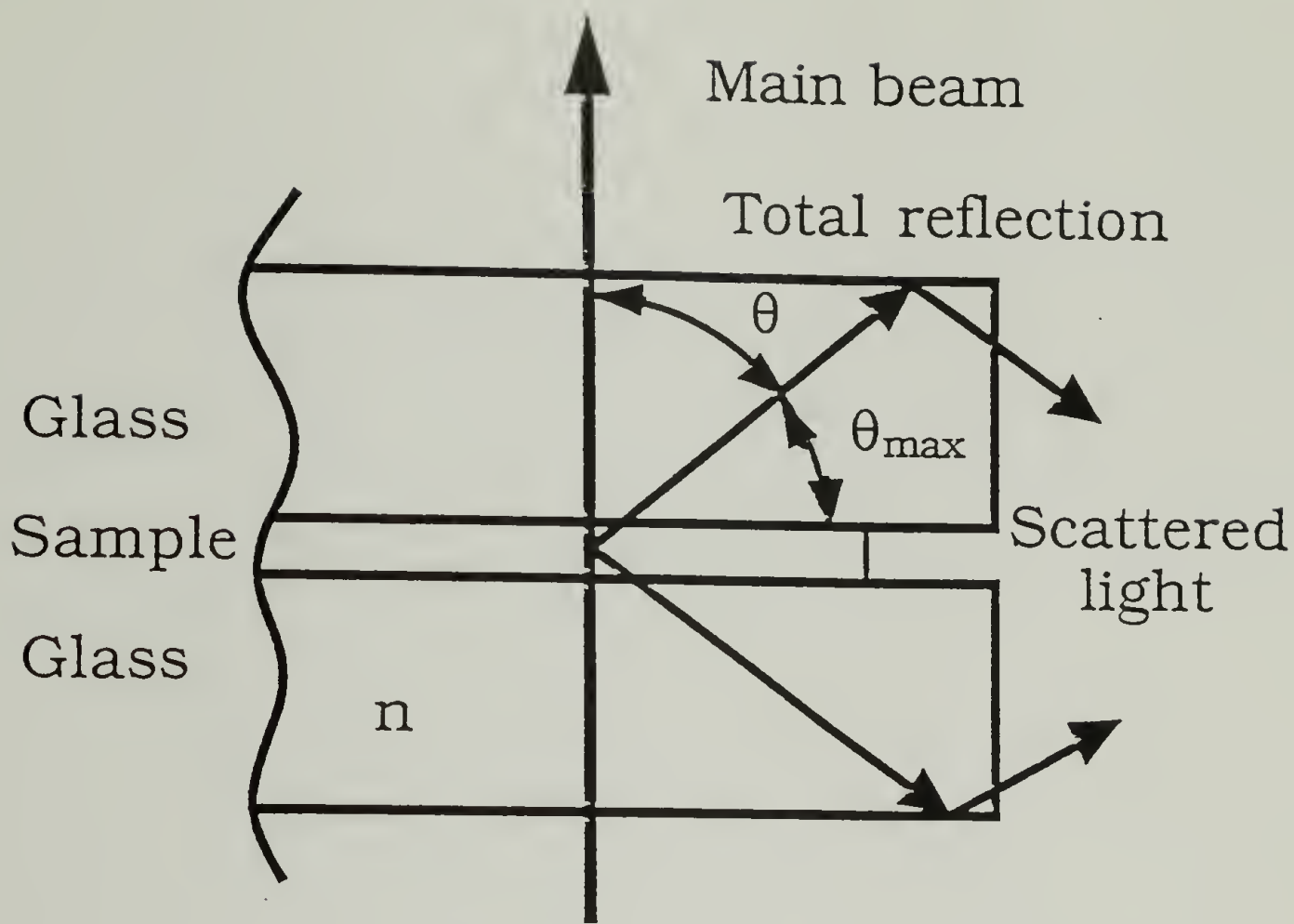
Figure 4.2 The optical geometry of the cloud point apparatus.
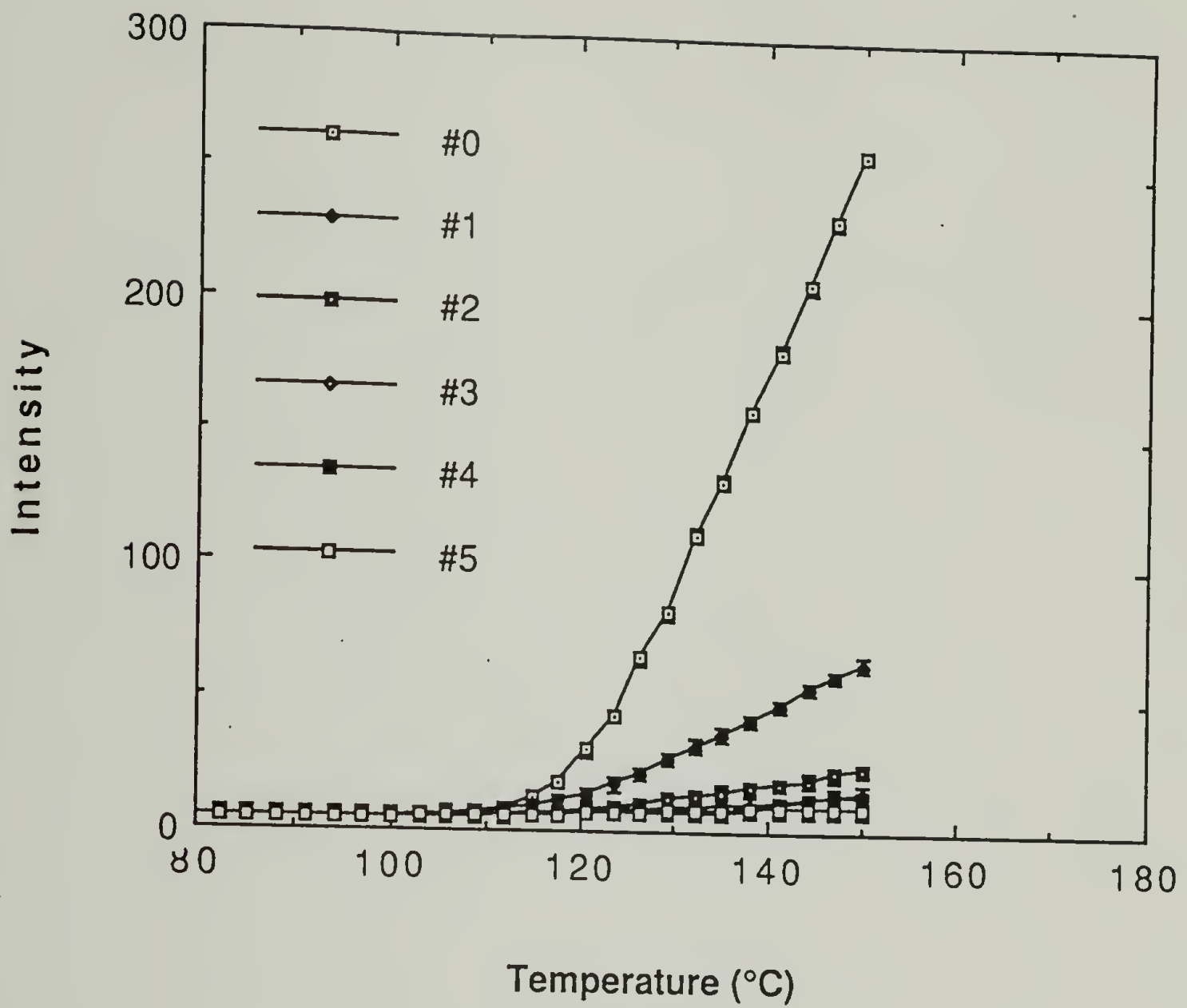
Figure 4.3 The scattering intensity measured by the cloud point apparatus for samples #0 to #5 with a temperature increase rate of 2°C/min. from 80°C to 150°C.
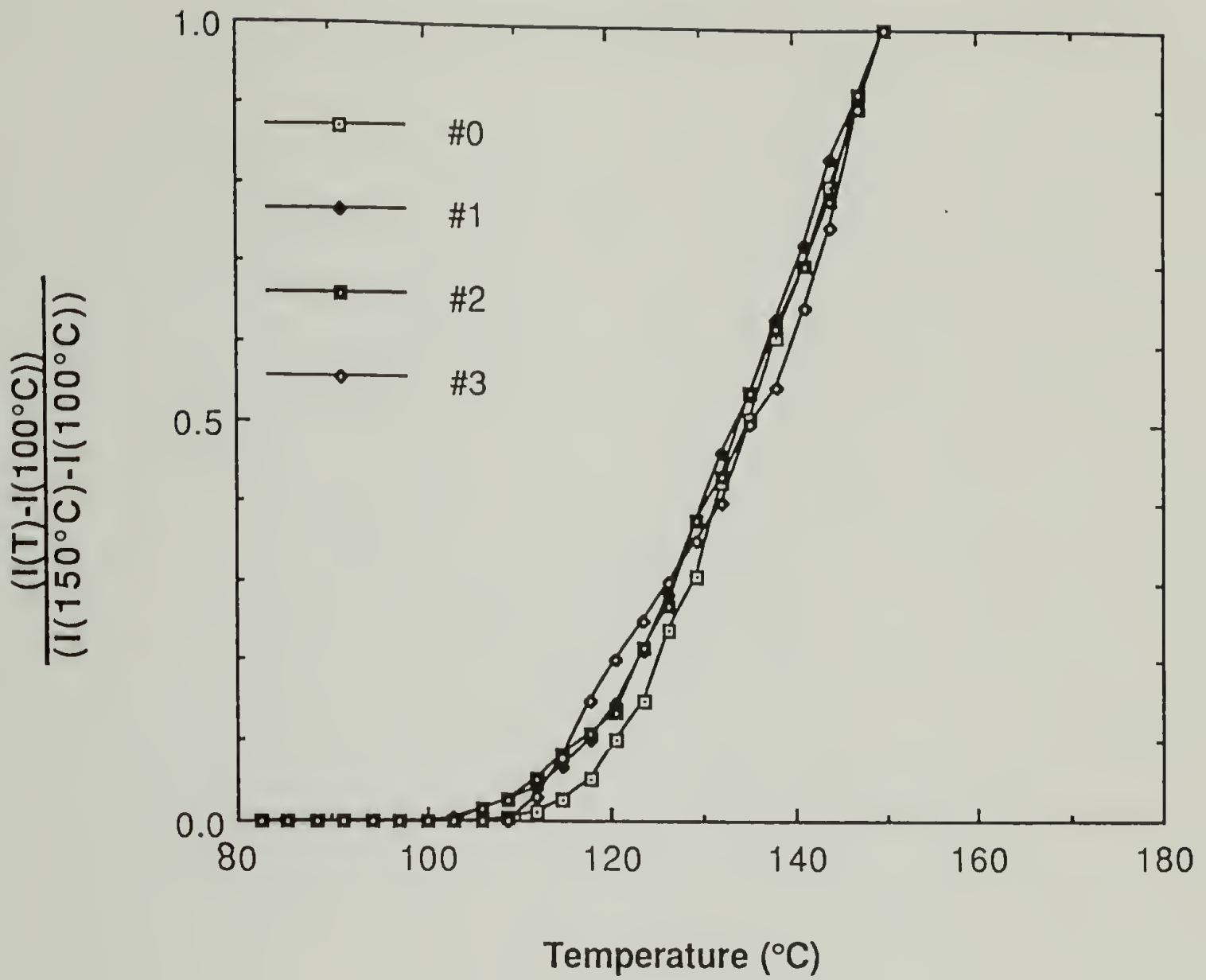
Figure 4.4 The normalized scattering intensity measured by the cloud point apparatus for samples #0 to #3 with the scattering intensity of 100°C and 150°C.
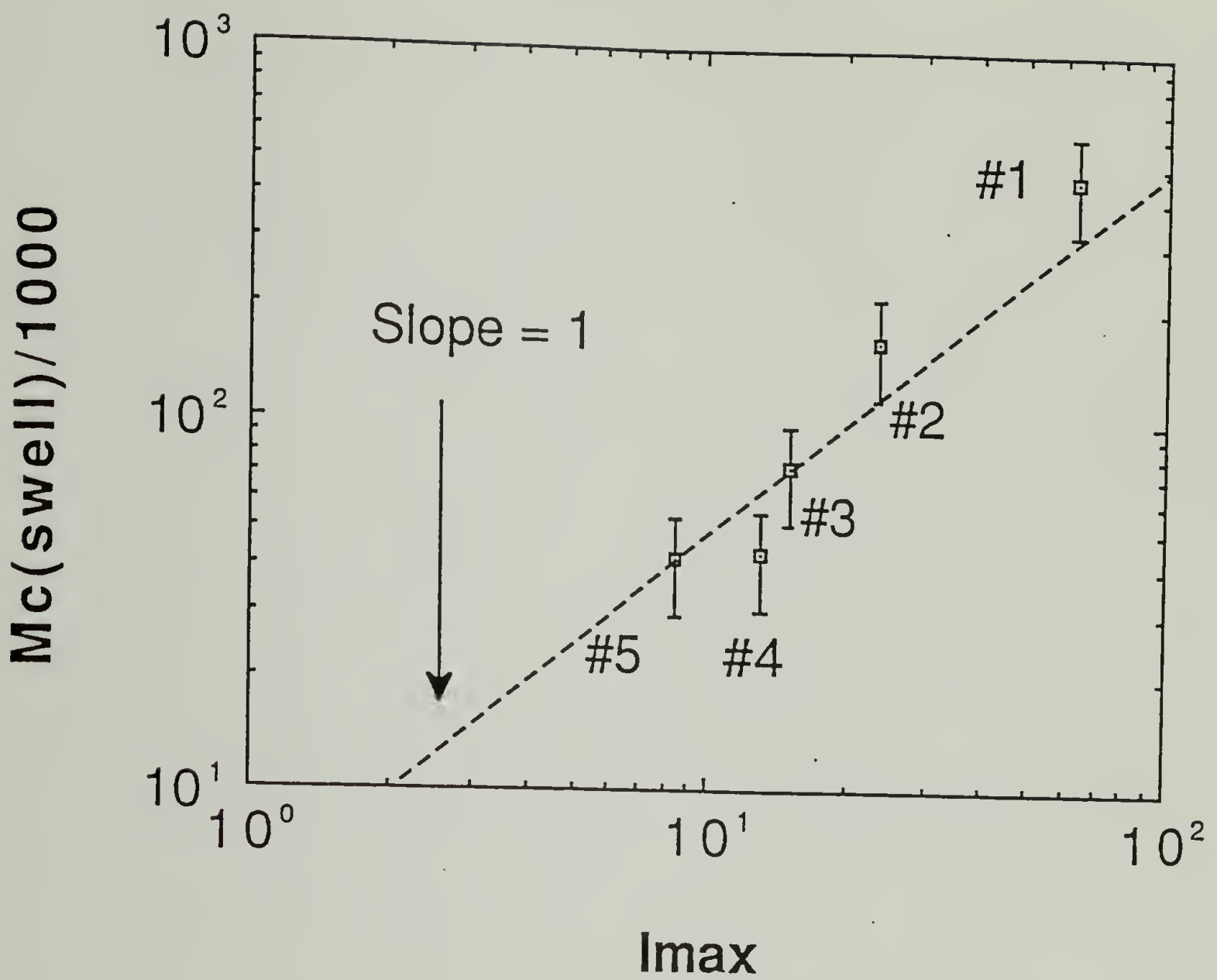
Figure 4.5 The relationship between scattering intensity measured by the cloud point apparatus at 150°C and the average molecular weight between crosslinks for samples #1 to #5 measured by the swelling experiments.

Phase Diagram for PVME/PS linear blend (NA=∞)
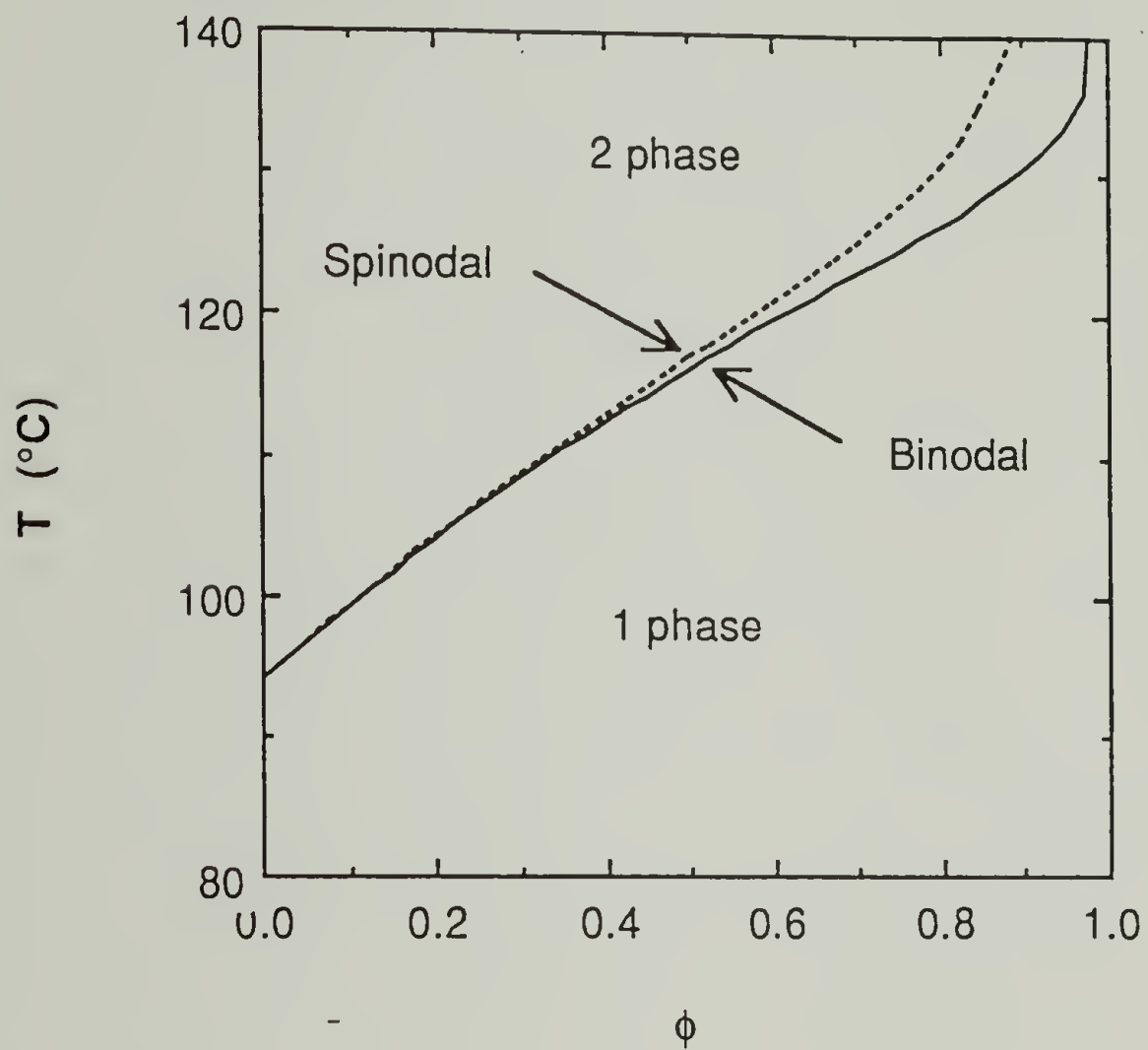
Figure 5.1   The phase diagram of sample #0 with the adjustable parameter, E=0.897, in equation 5.2 to match the temperature of cloud point of sample #0 to that of binodal for linear polymer blend.
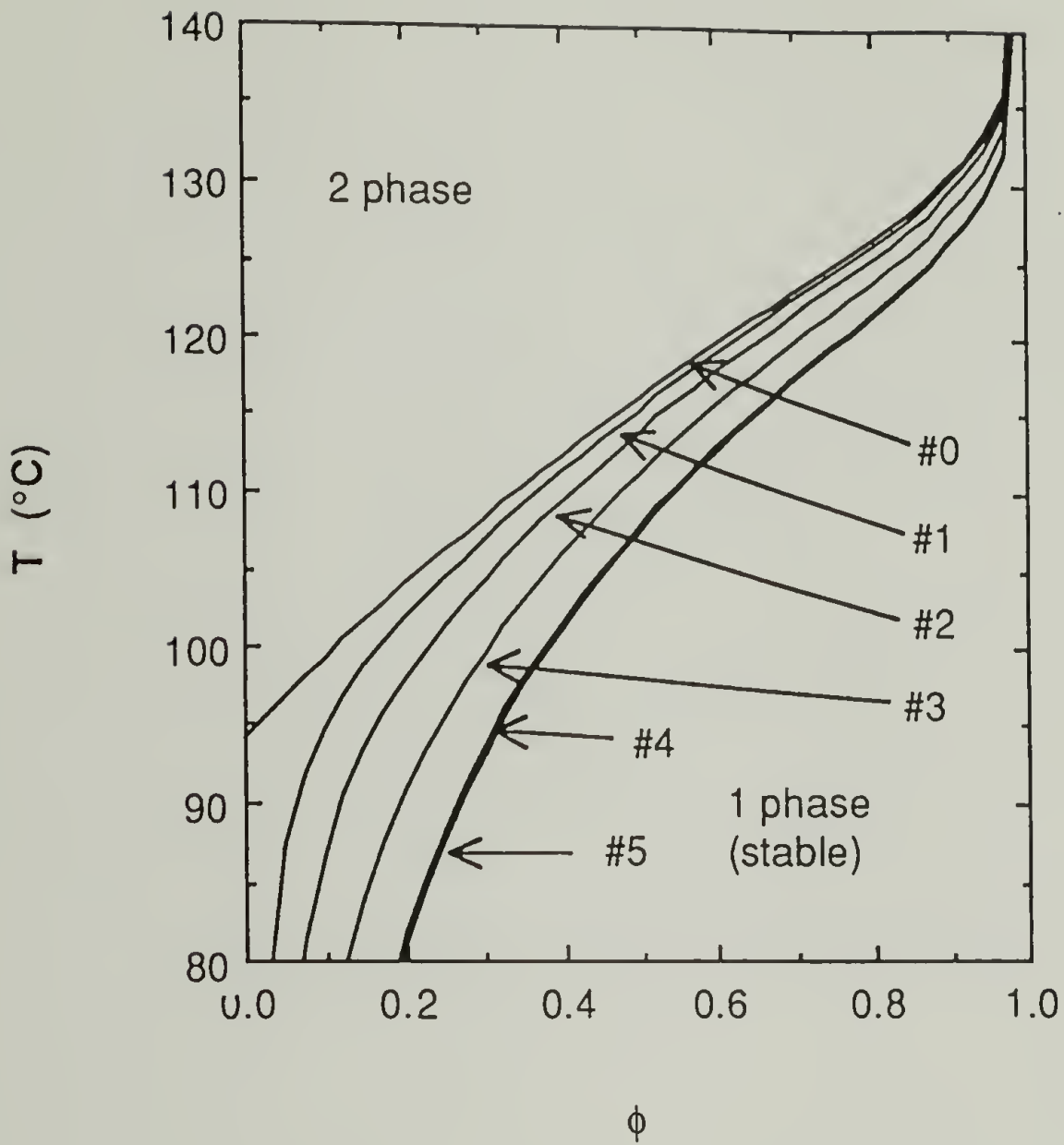
Figure 5.2 The effect of crosslinks on the binodal point of semi-IPN
systems. Sample #0 is the control sample which is a
linear polymer blend. The others are semi-IPN systems
with increasing crosslink densities with an increase in
the sample indices.
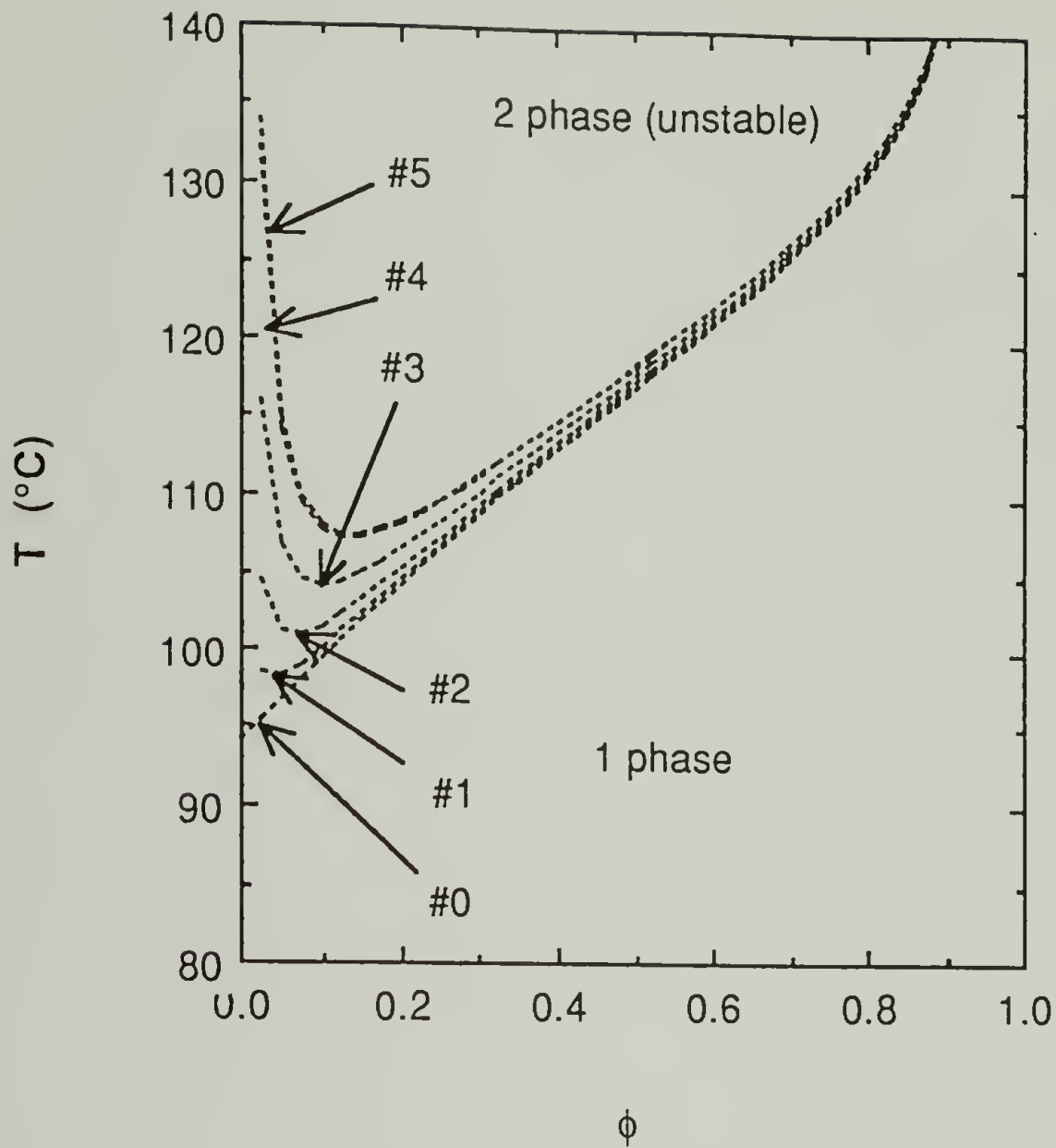
Figure 5.3 The effect of crosslinks on the spinodal point of semi-IPN systems. Sample #0 is the control sample which is a linear polymer blend. The others are of the semi-IPN system with increasing crosslink densities with an increase in the sample indices.
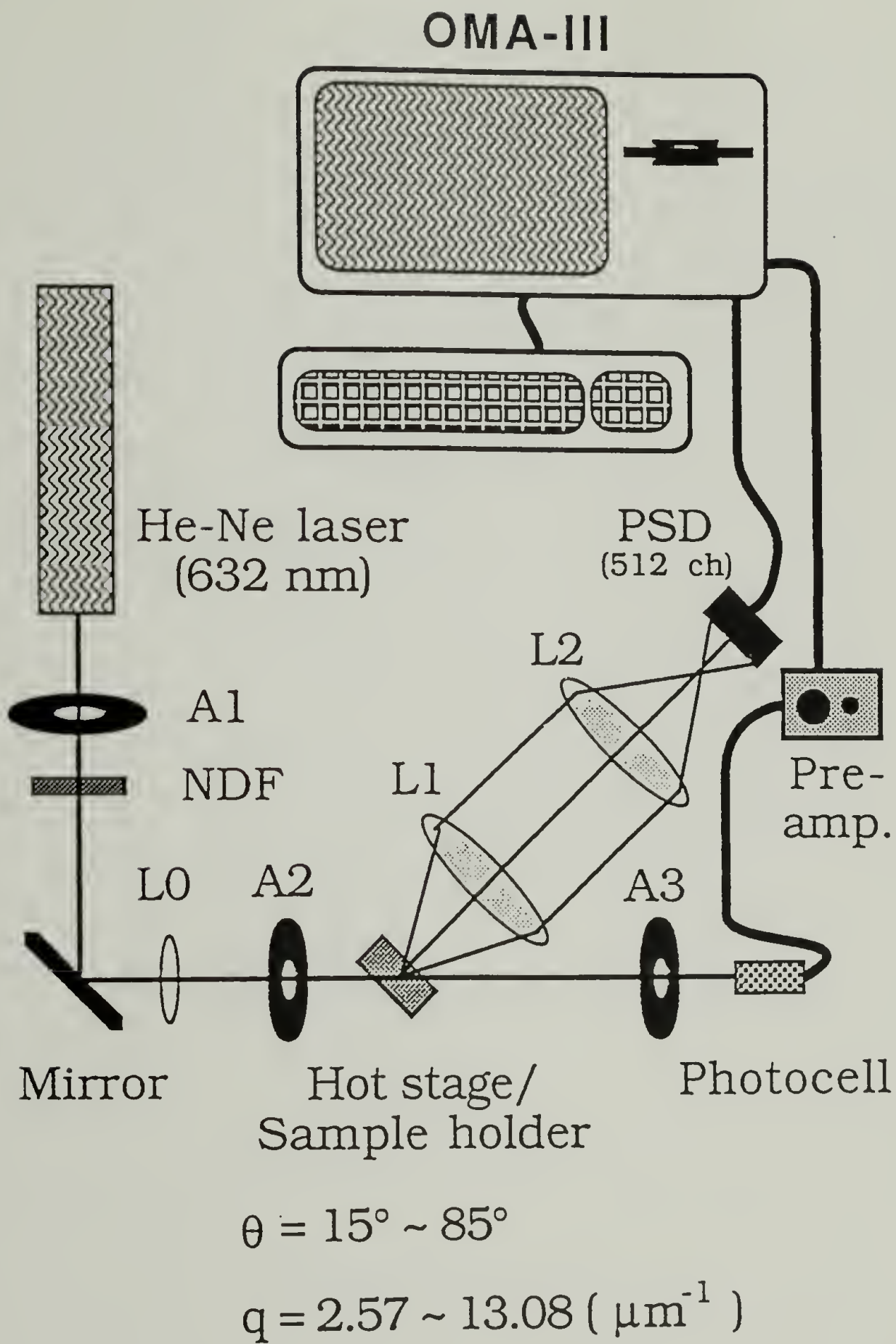
Figure 6.1 Schematic diagram of the wide angle light scattering apparatus.
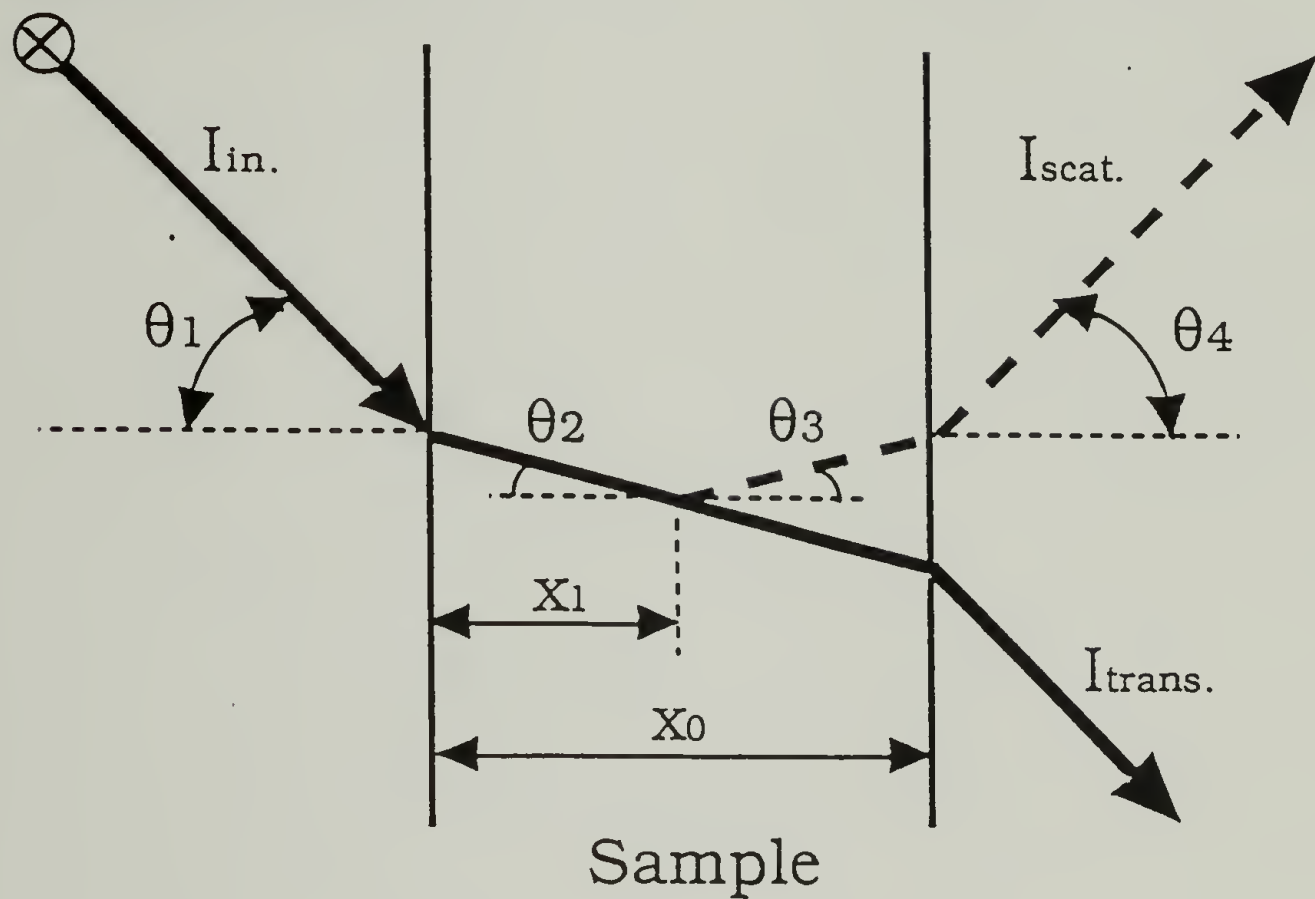
Figure 6.2   The optical geometry of the wide angle light scattering apparatus.
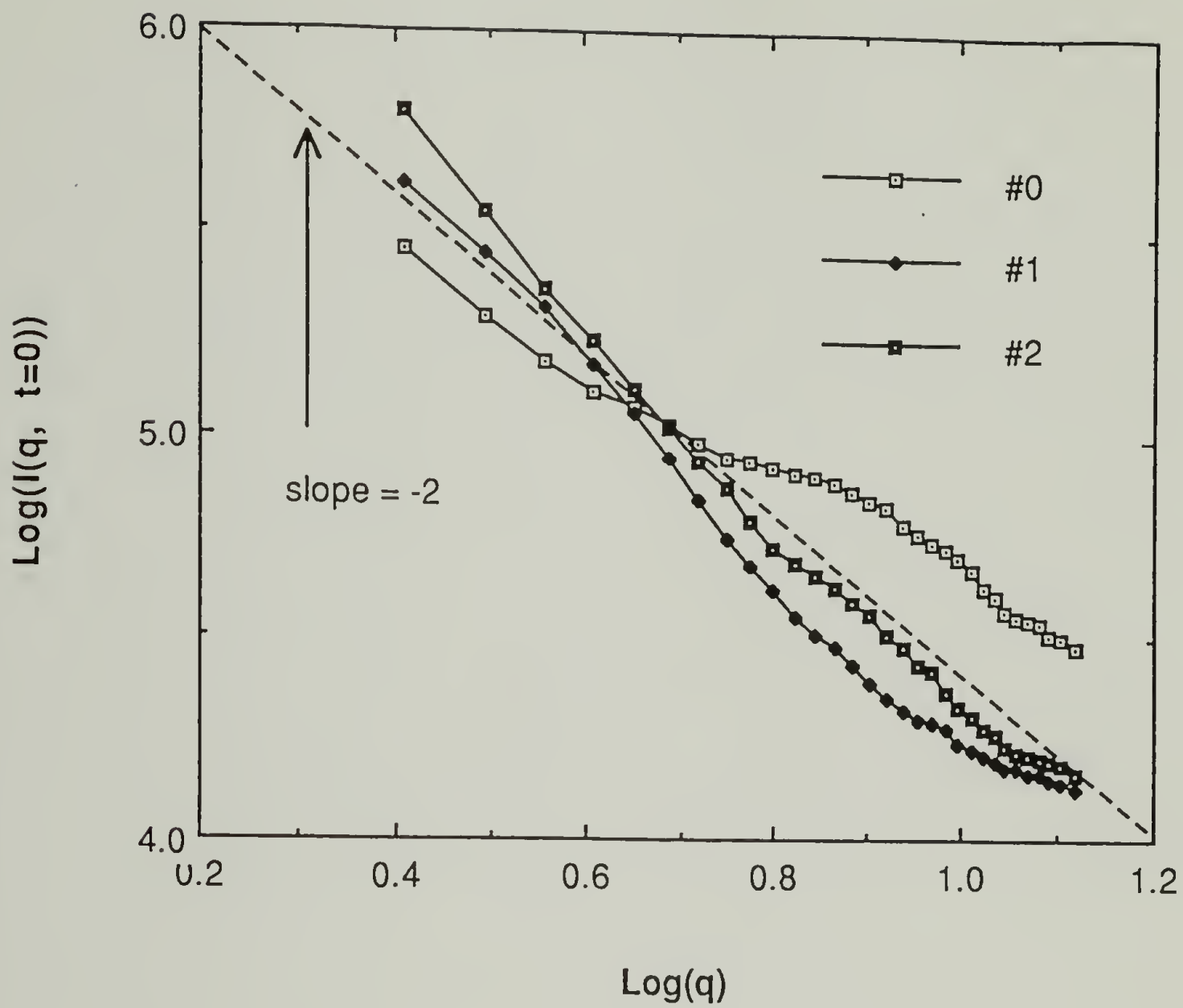
Figure 6.3 The initial scattering intensity of samples #0, #1, and #2.
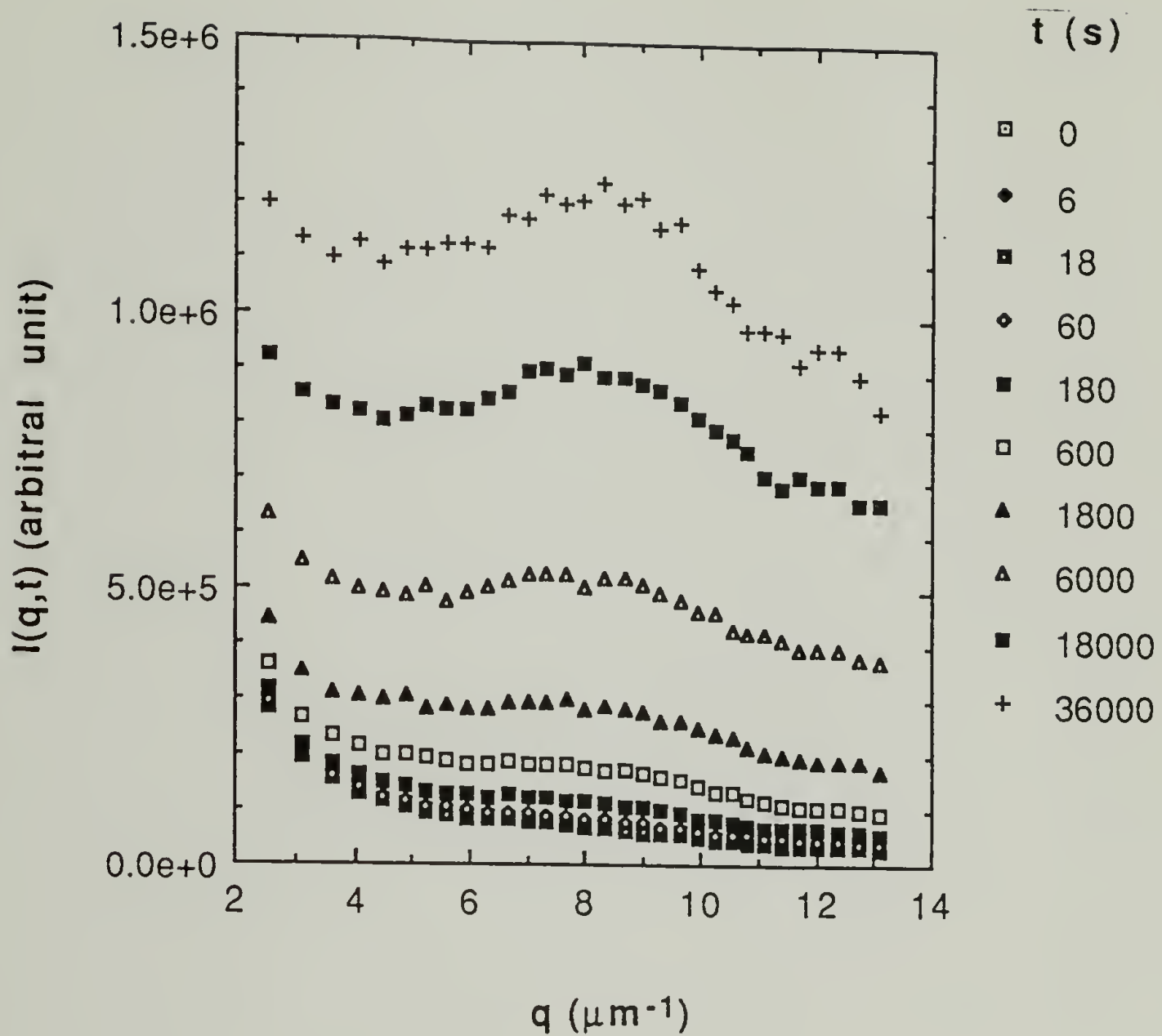
Figure 6.4 The time dependent wide angle light scattering intensity
measured as a function of the scattering vector for
sample #0 subjected to the T-jump from 100°C to 120°C.

Figure 6.5 The time dependent wide angle light scattering intensity measured as a function of the scattering vector for sample #0 subjected to the T-jump from 100°C to 150°C.

Figure 6.6 The time dependent wide angle light scattering intensity measured as a function of the scattering vector for sample #1 subjected to the T-jump from 100°C to 120°C.
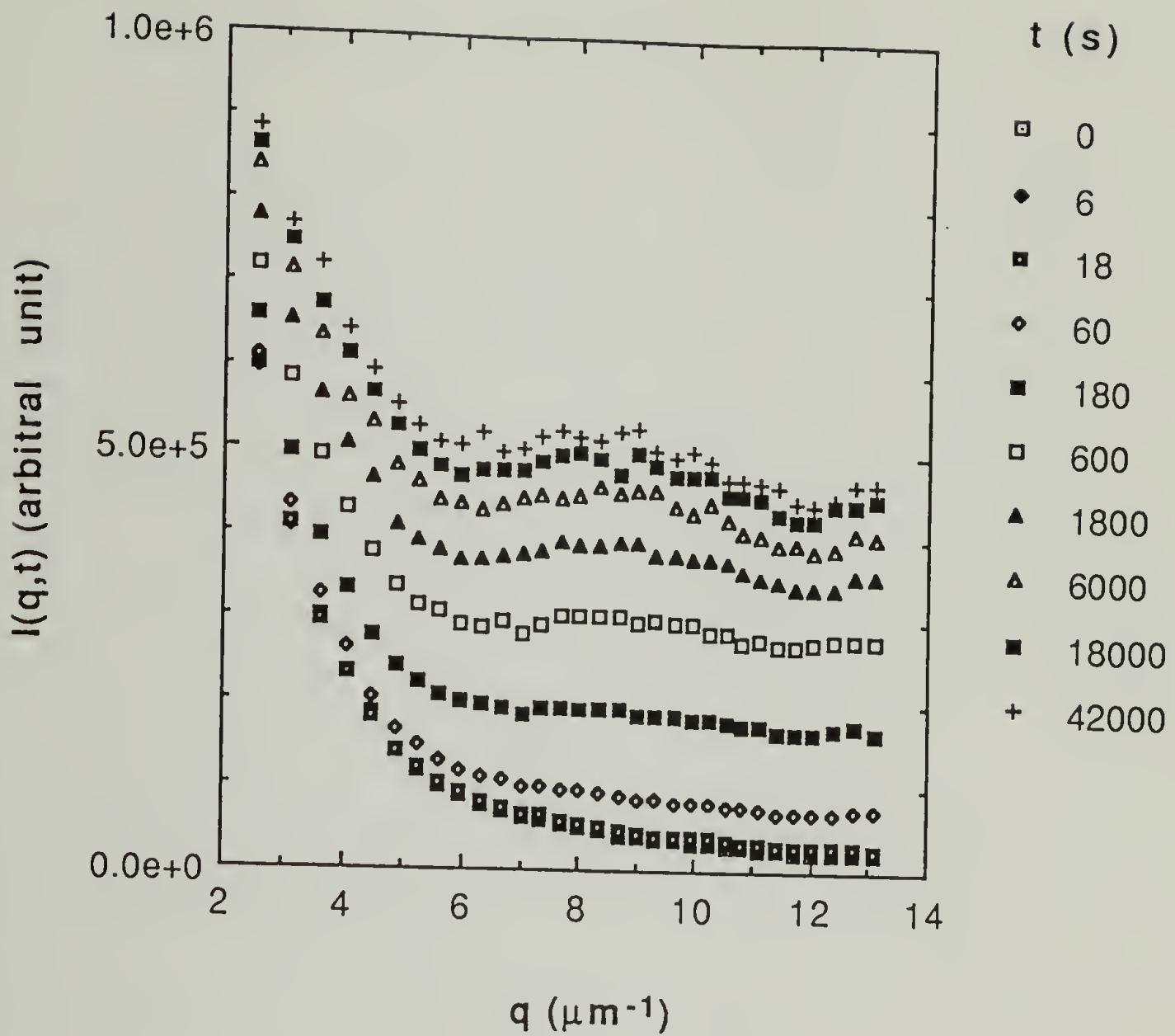
Figure 6.7 The time dependent wide angle light scattering intensity measured as a function of the scattering vector for sample #1 subjected to the T-jump from 100°C to 150°C.
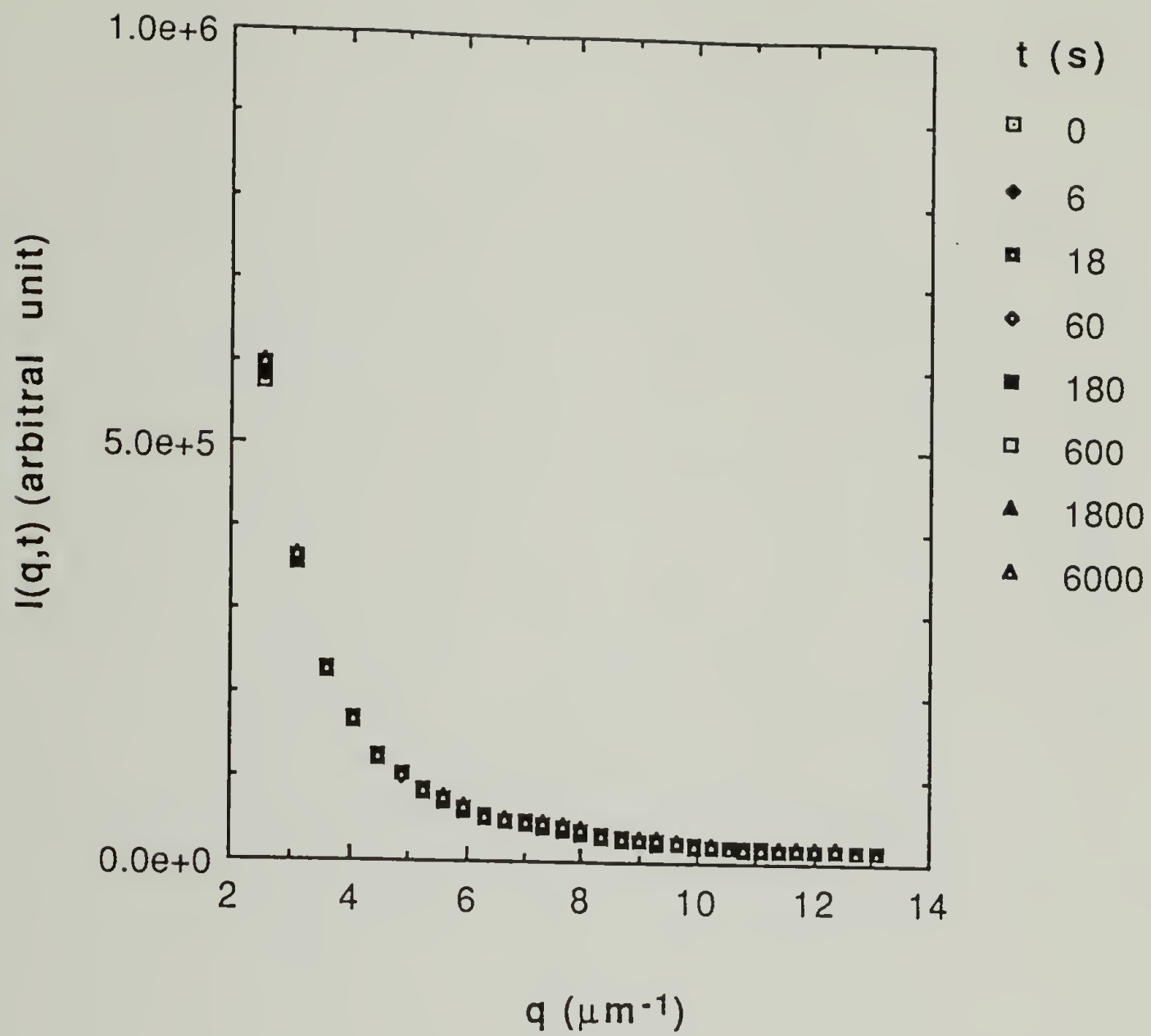
Figure 6.8 The time dependent wide angle light scattering intensity measured as a function of the scattering vector for sample #2 subjected to the T-jump from 100°C to 120°C.
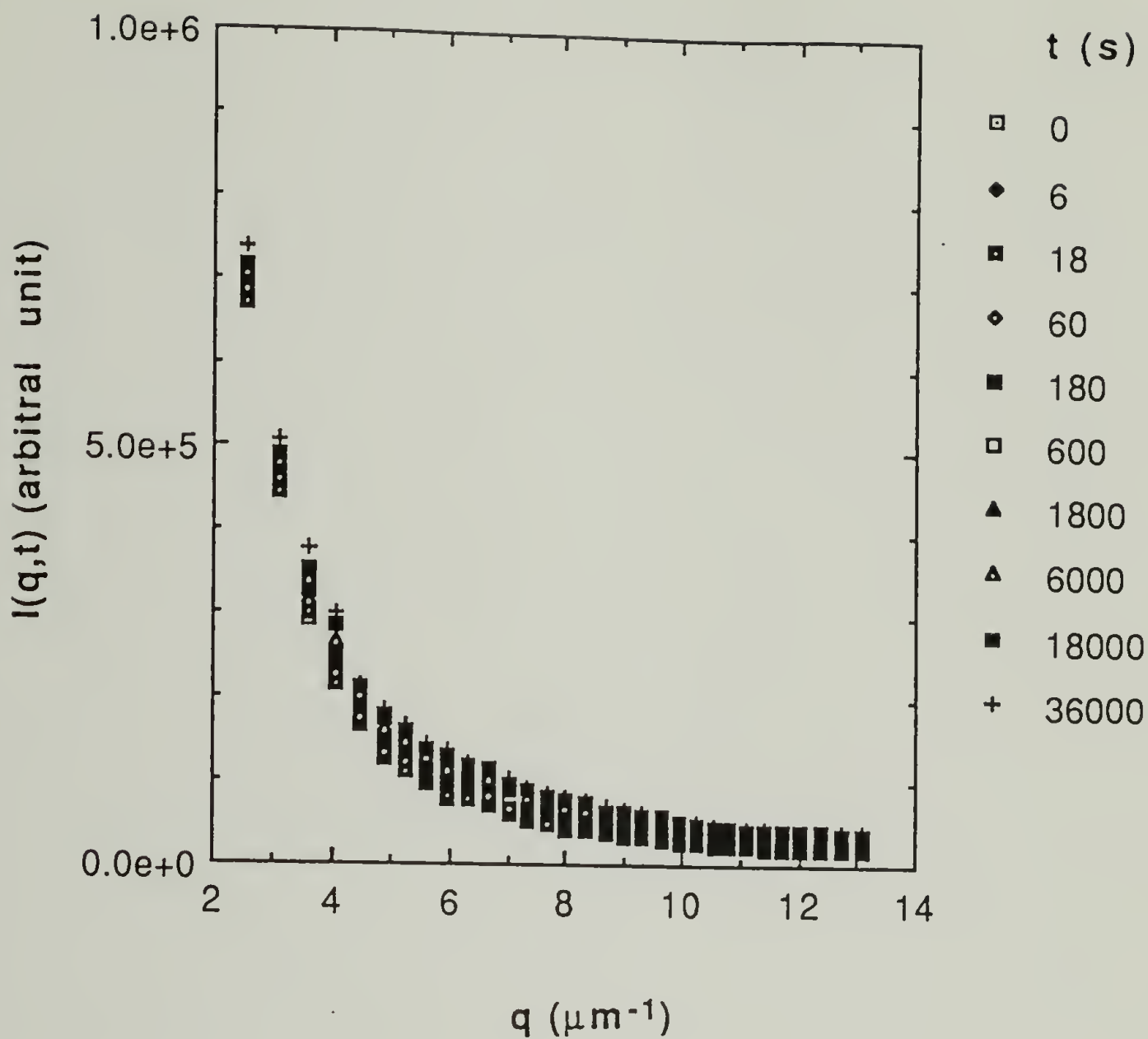
Figure 6.9 The time dependent wide angle light scattering intensity
measured as a function of the scattering vector for
sample #2 subjected to the T-jump from 100°C to 150°C.
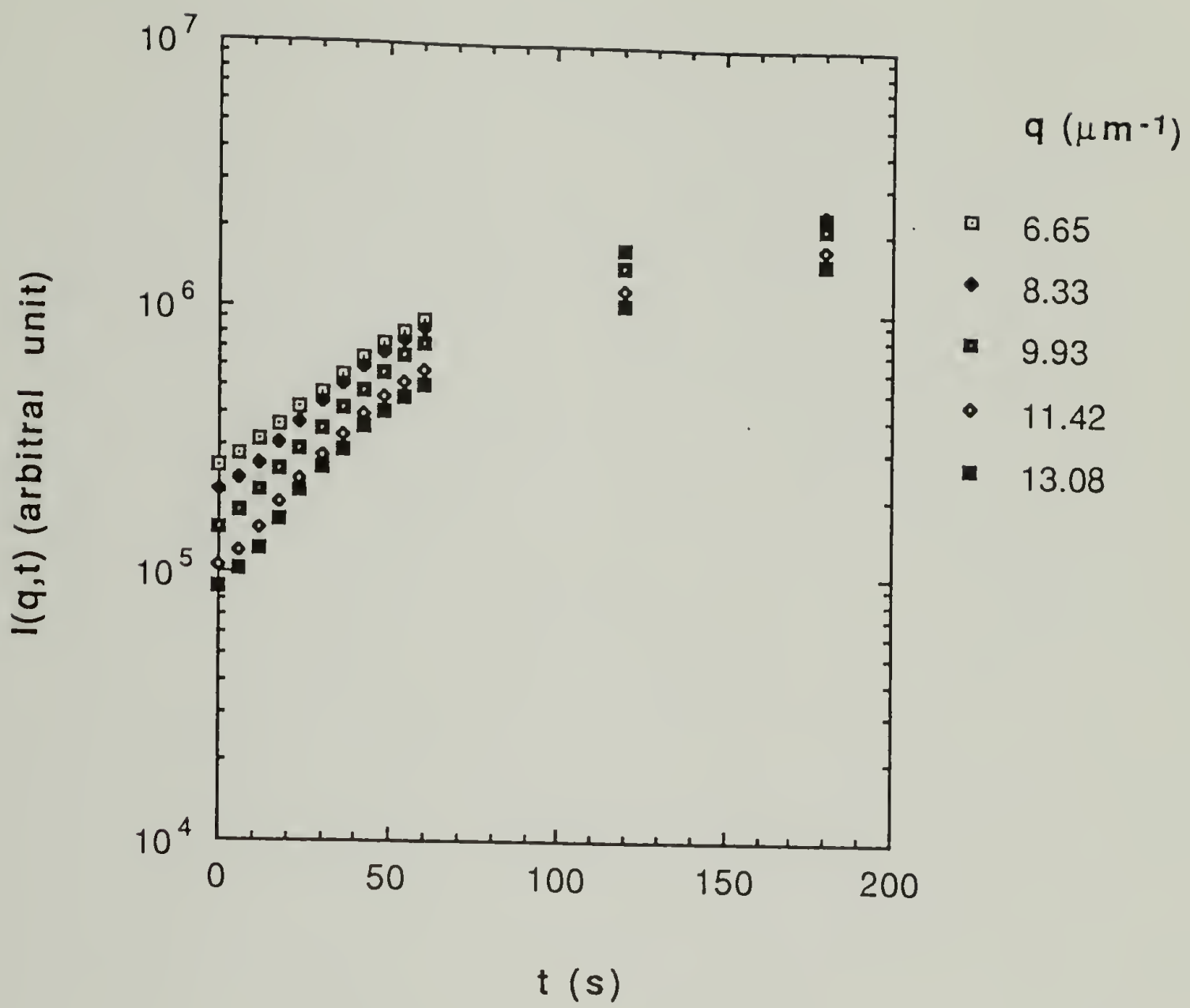
Figure 6.10 The initial time dependence of the wide angle light scattering intensity for the different scattering vectors for sample #0 subjected to the T-jump from 100°C to 150°C.
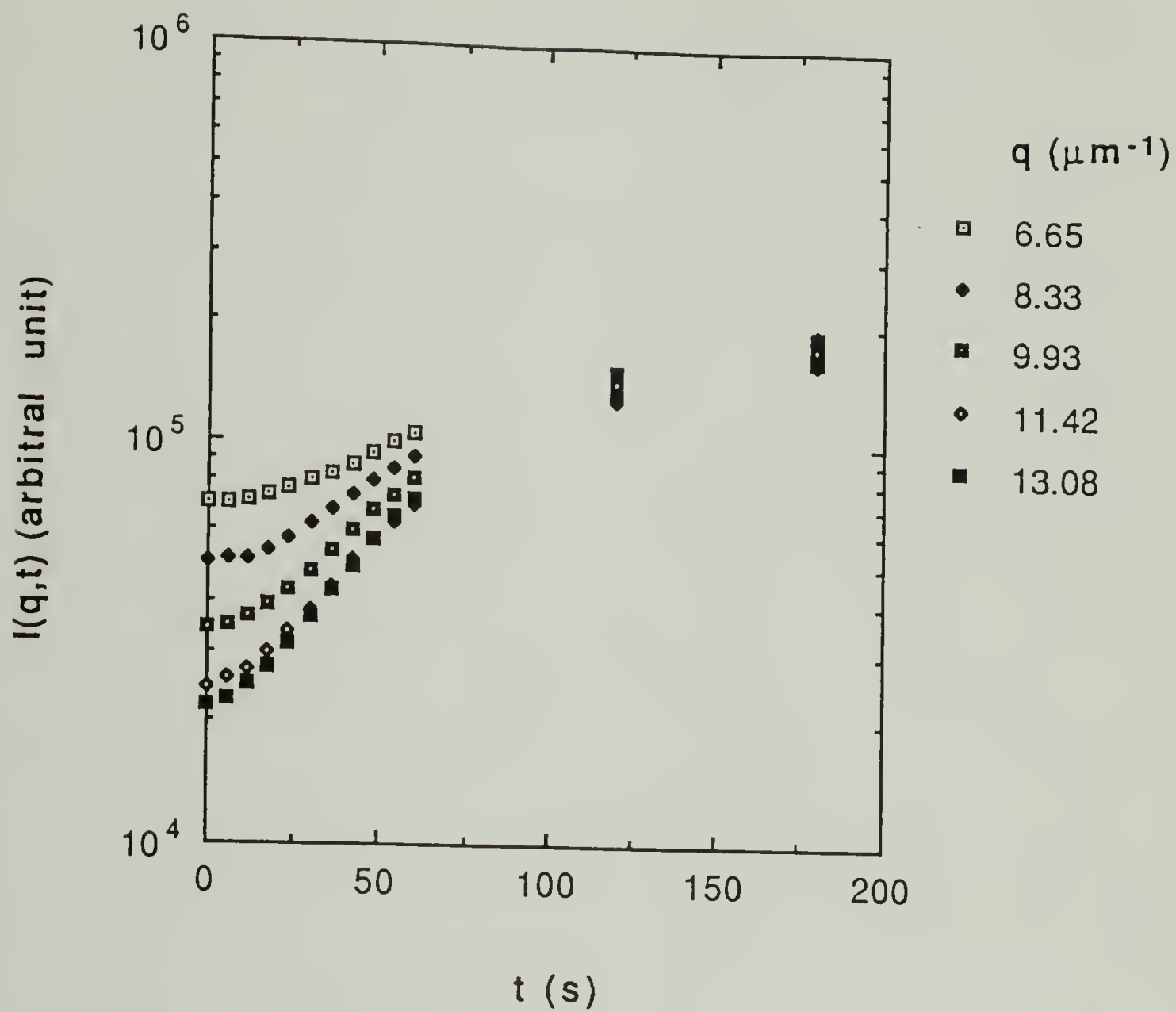
Figure 6.11 The initial time dependence of the wide angle light scattering intensity for the different scattering vectors for sample #1 subjected to the T-jump from 100°C to 150°C.
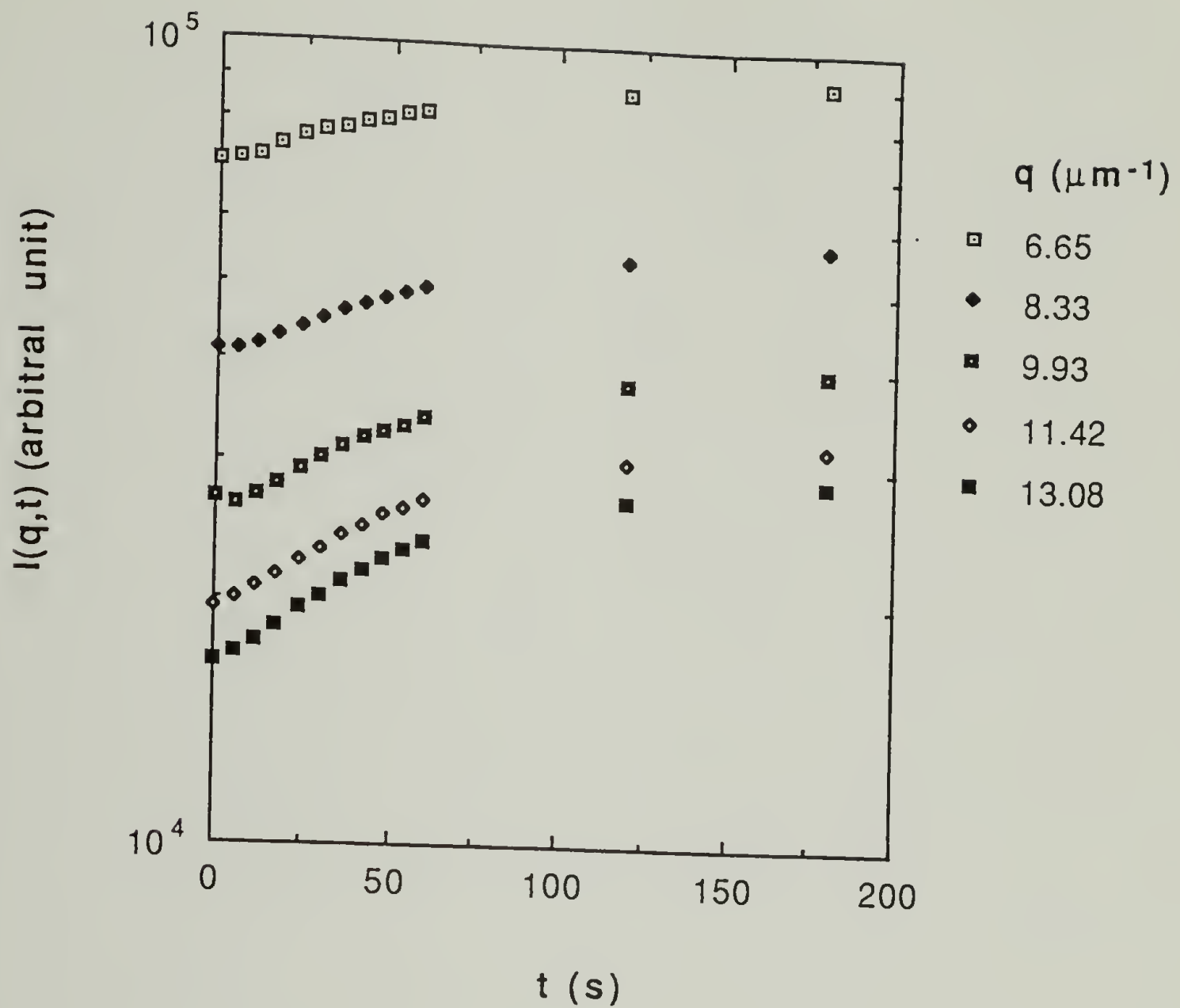
Figure 6.12 The initial time dependence of the wide angle light scattering intensity for the different scattering vectors for sample #2 subjected to the T-jump from 100°C to 150°C.
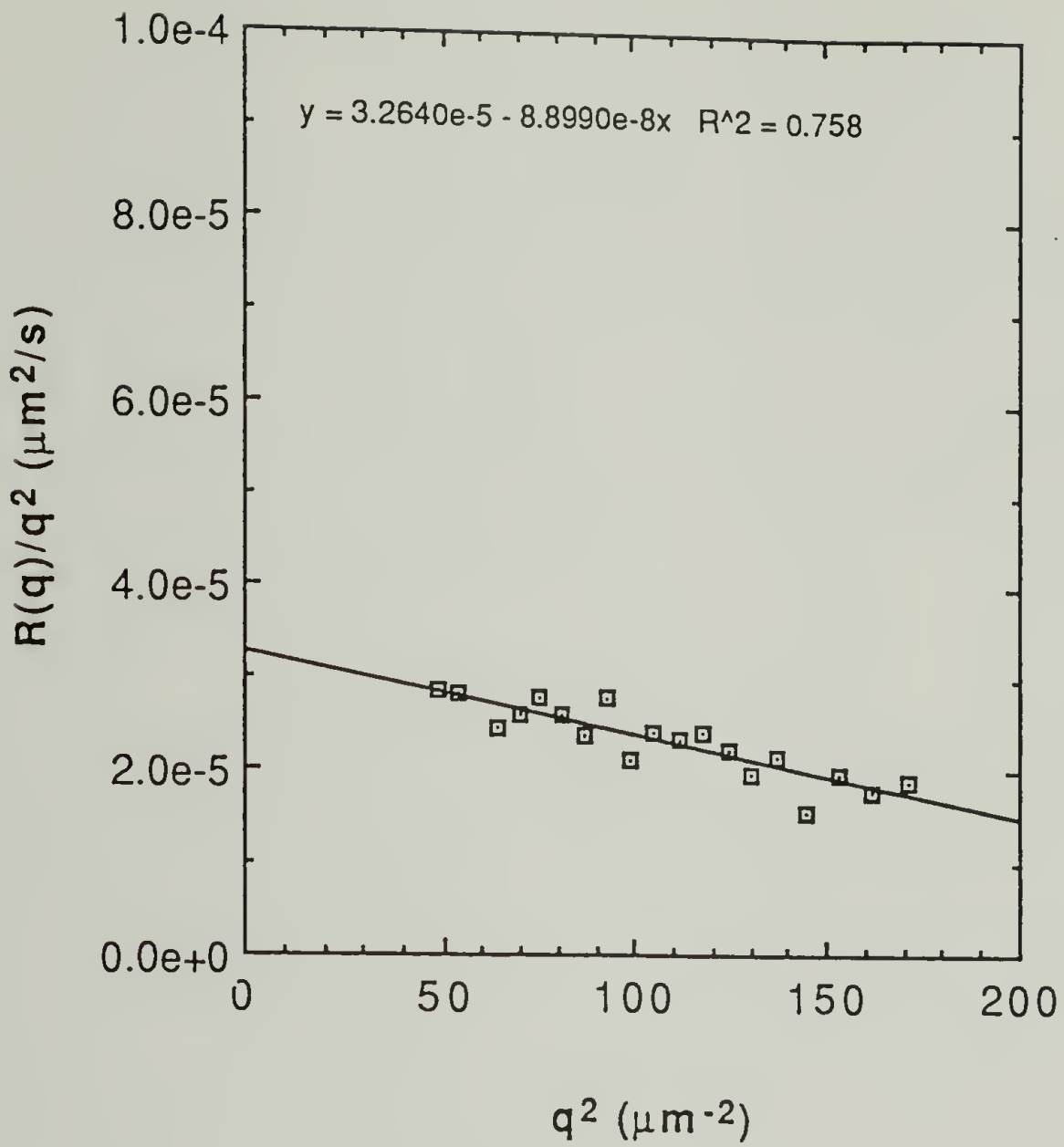
Figure 6.13 The relationship between the initial growth rate, R(q) of the wide angle light scattering intensity and the scattering vector for sample #0 subjected to the T-jump from 100°C to 120°C.
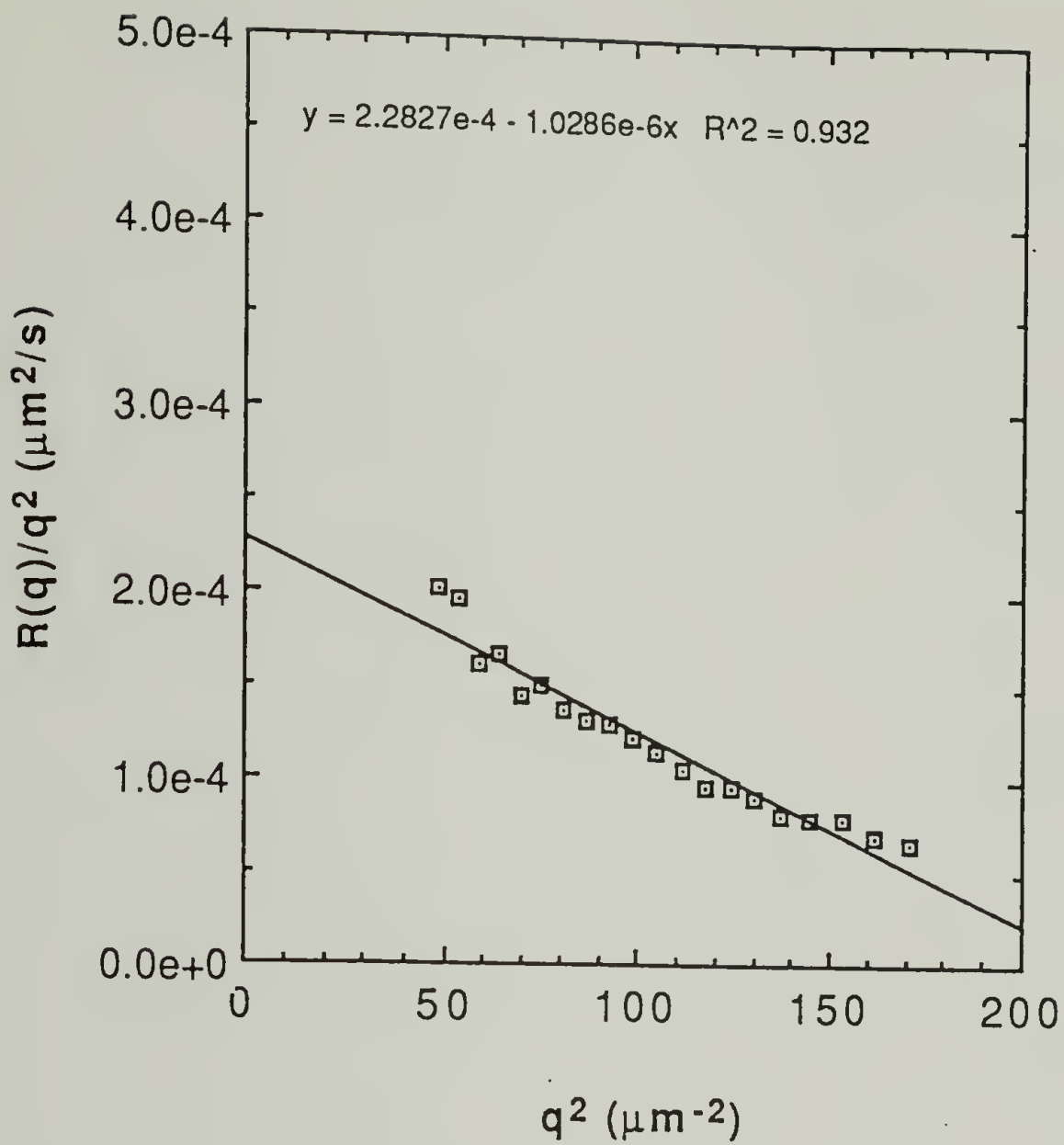
Figure 6.14 The relationship between the initial growth rate, R(q) of the wide angle light scattering intensity and the scattering vector for sample #0 subjected to the T-jump from 100°C to 150°C.
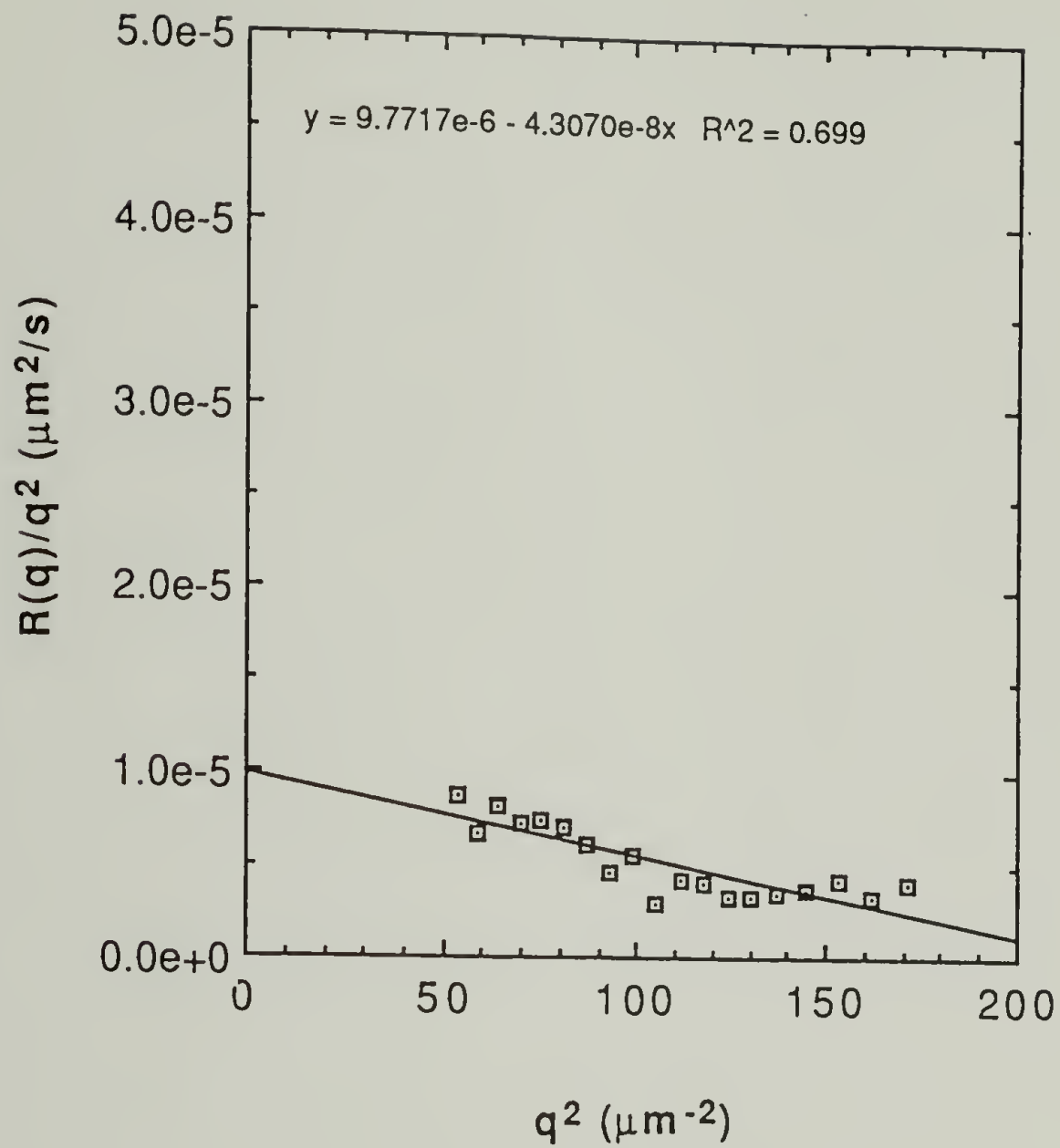
Figure 6.15 The relationship between the initial growth rate, R(q) of
the wide angle light scattering intensity and the
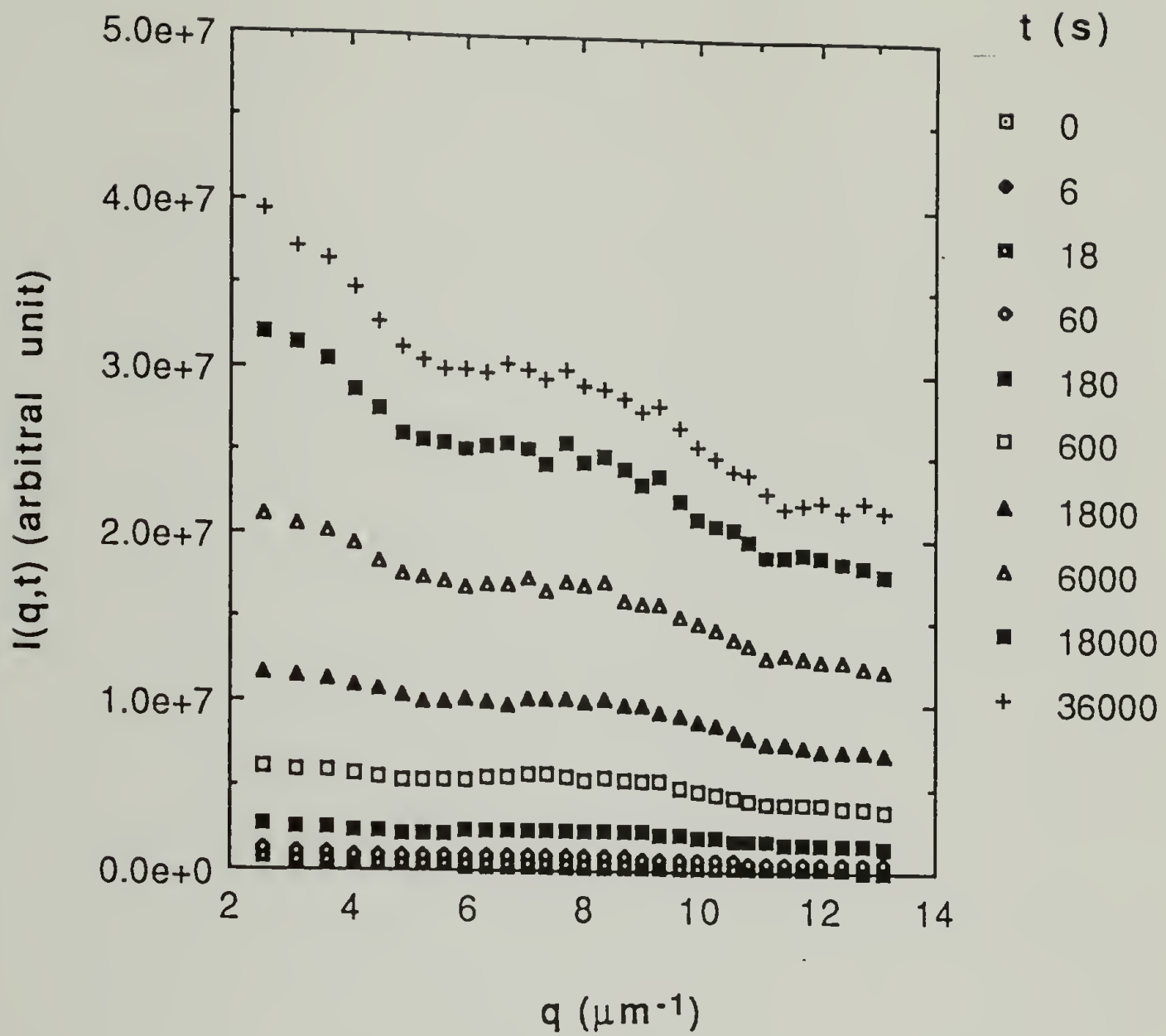scattering vector for sample #1 subjected to the T-jump
from 100°C to 120°C.
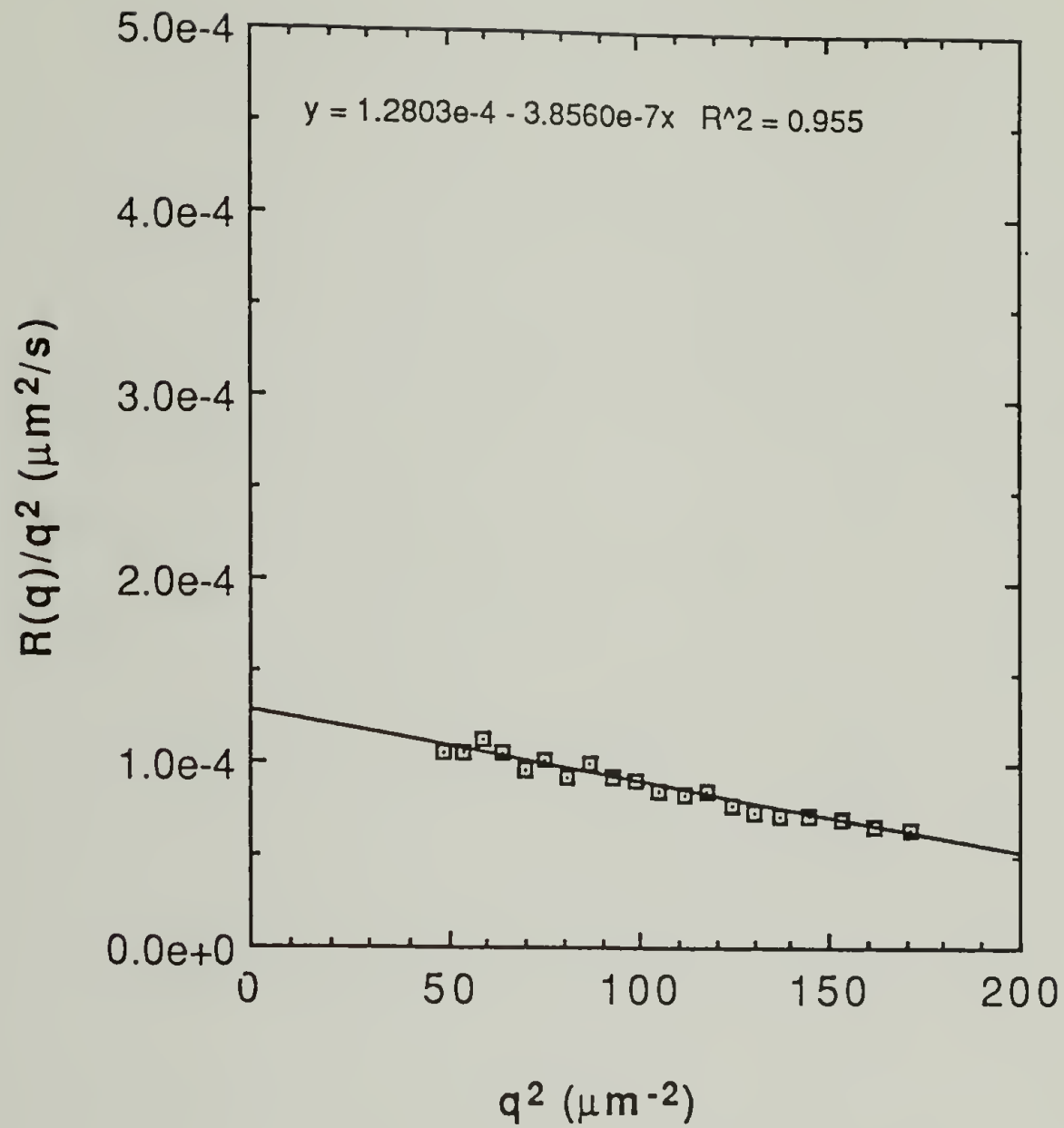
Figure 6.16 The relationship between the initial growth rate, R(q) of the wide angle light scattering intensity and the scattering vector for sample #1 subjected to the T-jump from 100°C to 150°C.
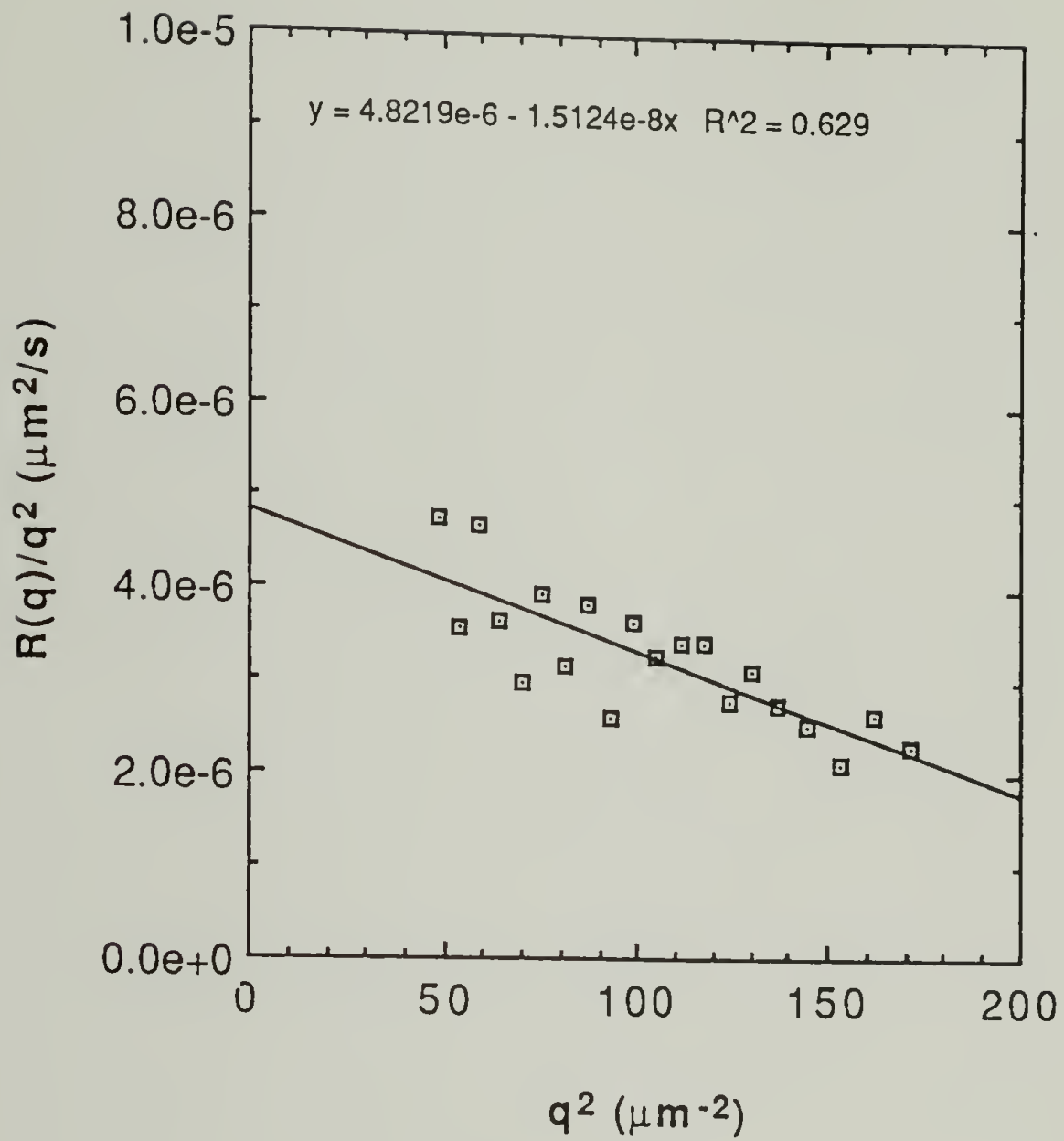
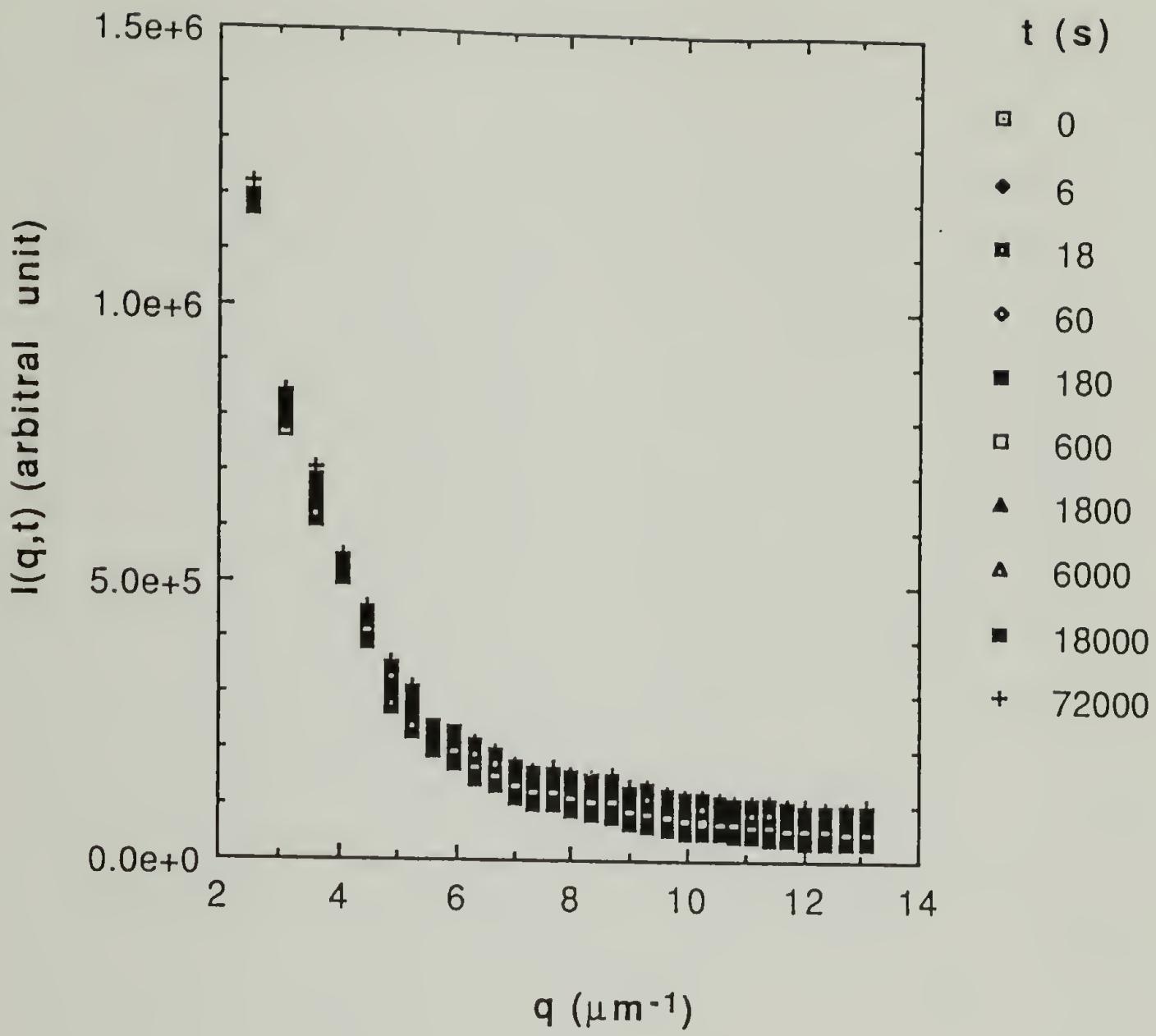Figure 6.17 The relationship between the initial growth rate, R(q) of the wide angle light scattering intensity and the scattering vector for sample #2 subjected to the T-jump from 100°C to 120°C.
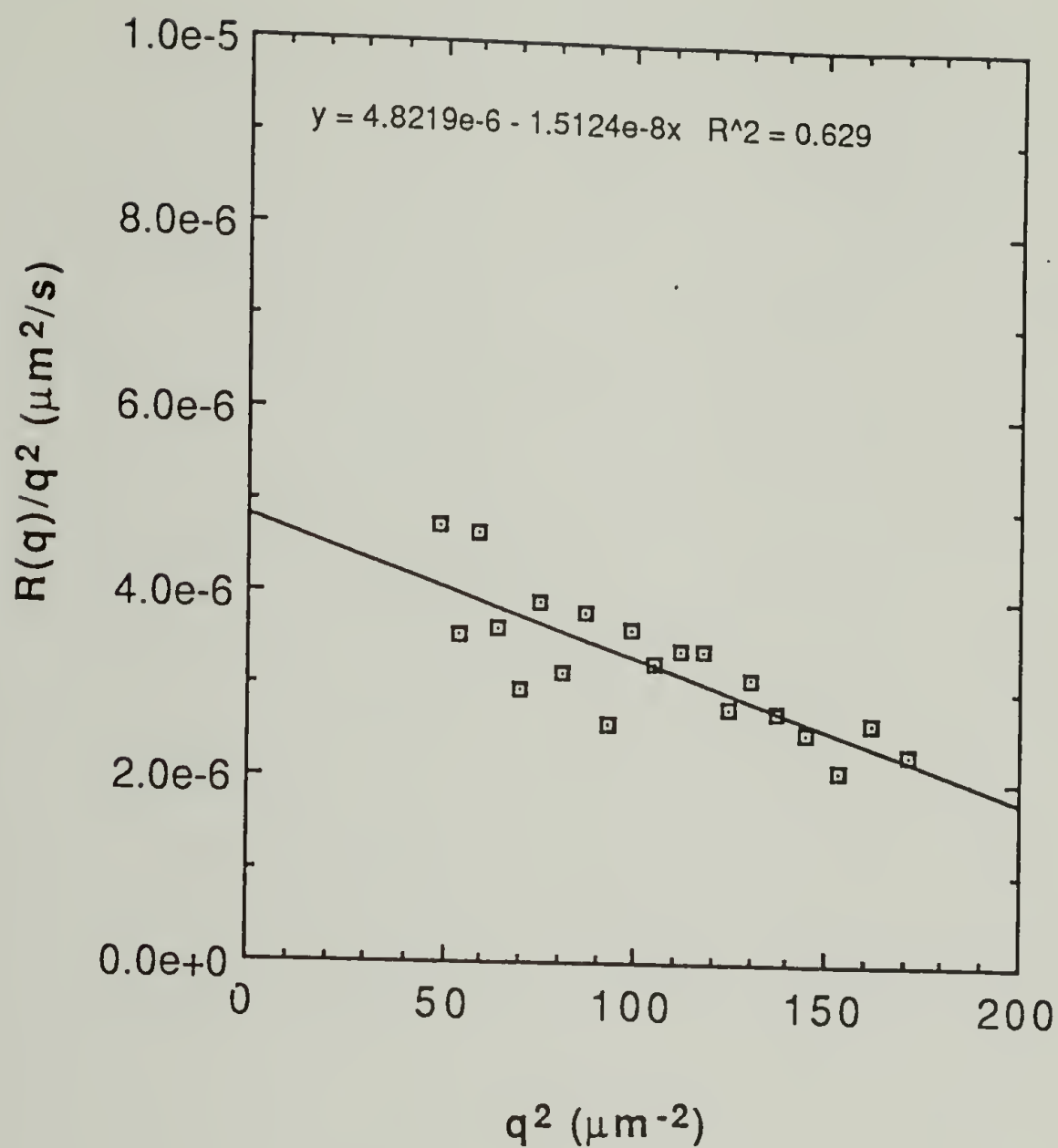
Figure 6.18 The relationship between the initial growth rate, R(q) of the wide angle light scattering intensity and the scattering vector for sample #2 subjected to the T-jump from 100°C to 150°C.
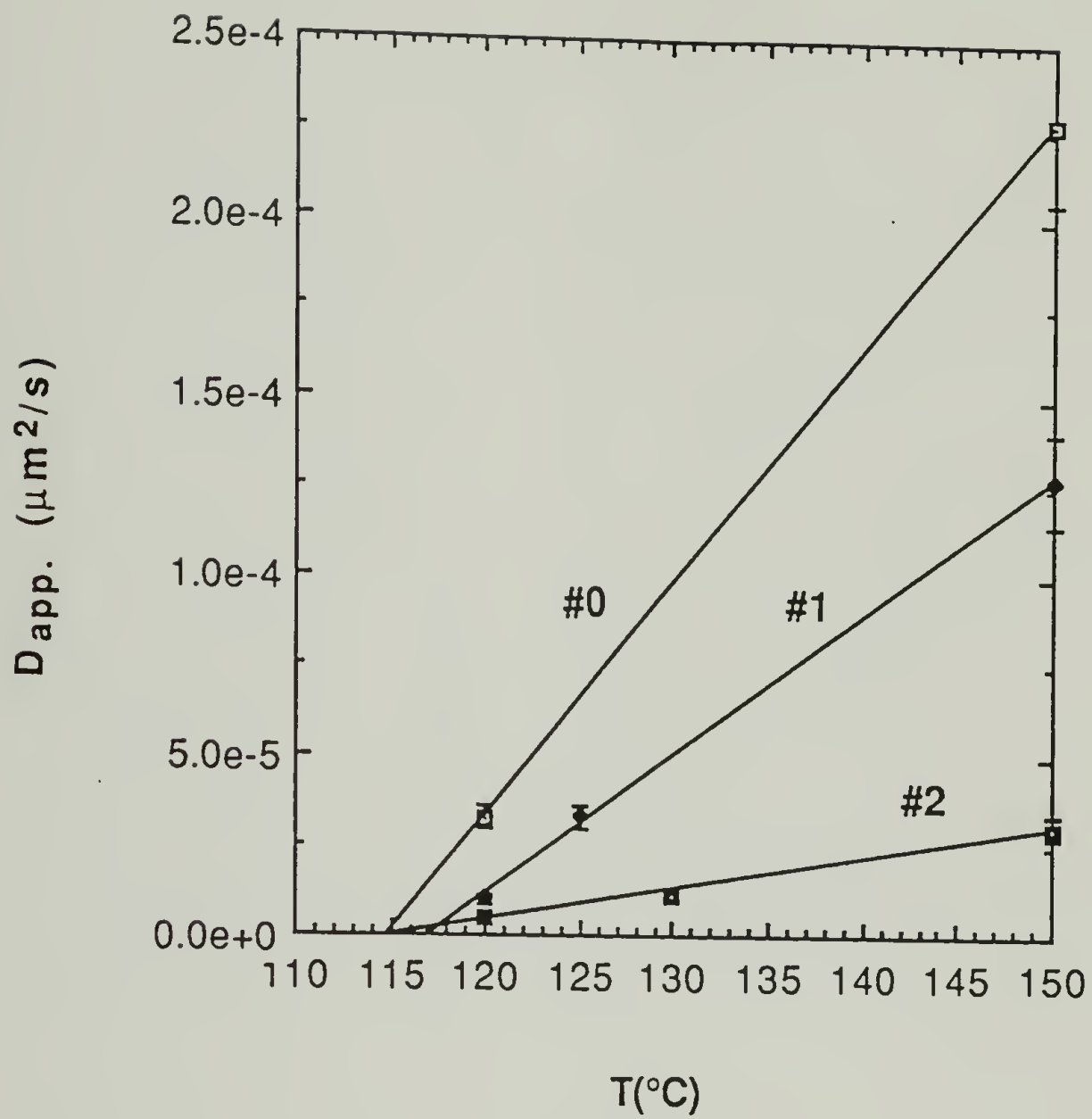
Figure 6.19 The apparent diffusion constant in the phase separating system for the samples #0, #1, and #2 at different temperatures. The spinodal point is extrapolated to be 116°±2°C.
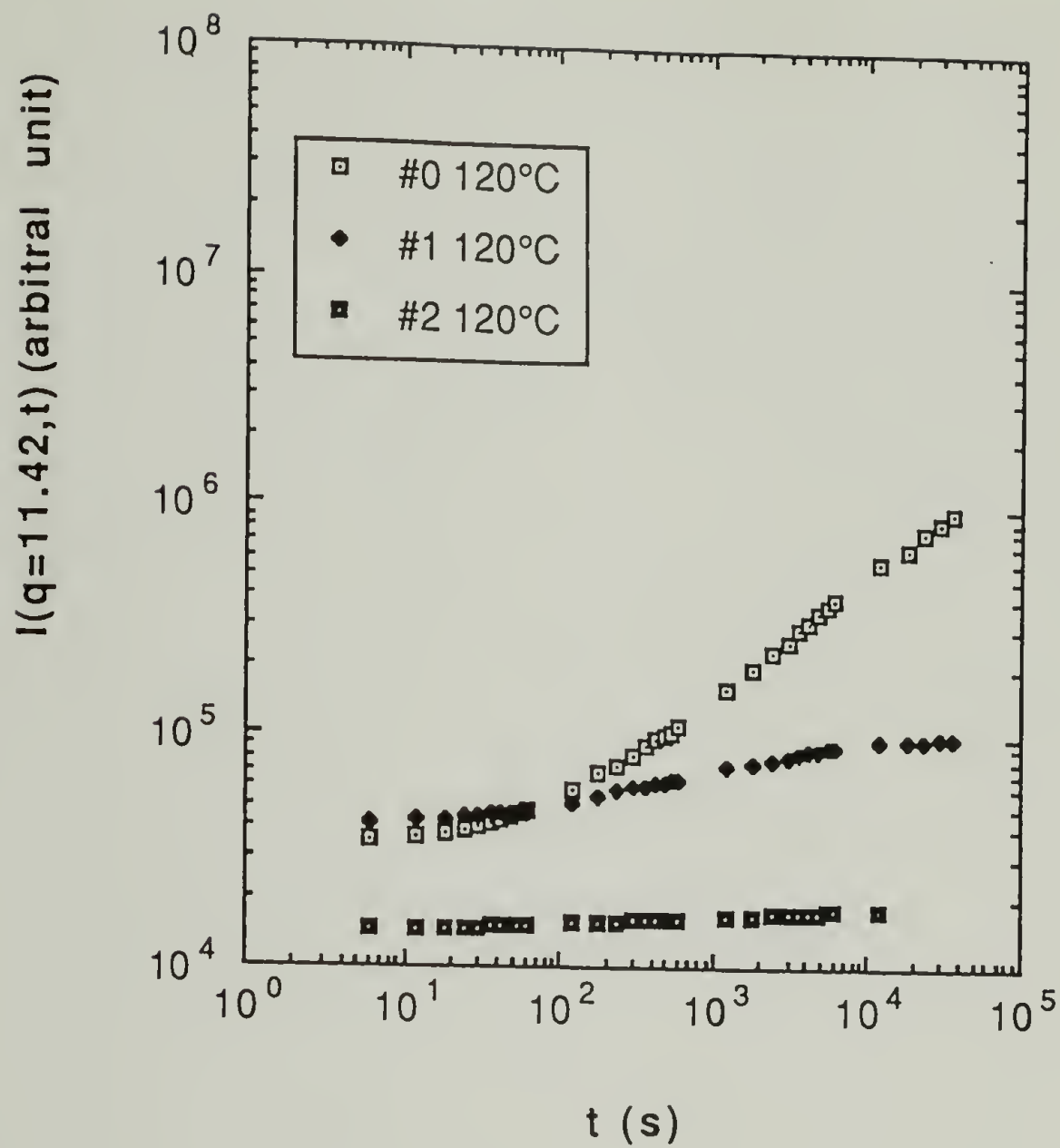
Figure 6.20 The long term time dependence of wide angle light scattering at a scattering vector, $q=11.42(\mu m^{-1})$, for the samples #0, #1, and #2 at 120°C.
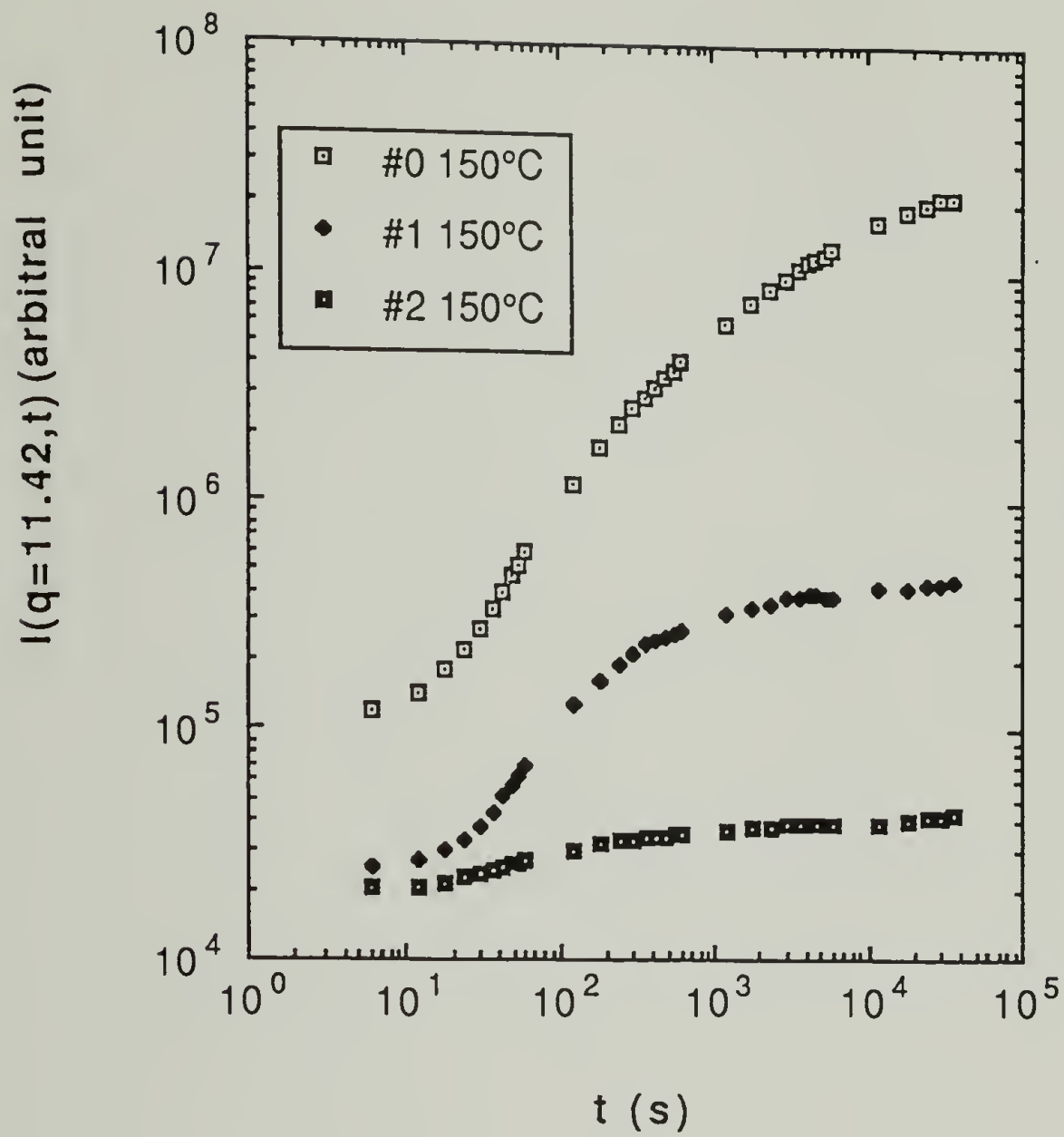
Figure 6.21 The long term time dependence of wide angle light
scattering at a scattering vector, $q=11.42(\mu m^{-1})$, for the
samples #0, #1, and #2 at 150°C.

APPENDIX C

PROGRAMS

MAIN PROGRAM: OMA_III.PAS

```pascal
{$I+,R+,N-}
program OMA_III_array_conversion_with_reduction_of_data ;
uses oma_lib;
type
  oma_data_type_ptr_array
                   = array[1..oma_max_memories] of oma_data_type_ptr ;
  oma_data_type_ptr_array_ptr
                   = ^oma_data_type_ptr_array ;

function arcsin (x : real) : real ;      {arcsine}
begin
  arcsin := arctan(x/sqrt(1.0-sqr(x))) ;
end;


function log_10 (x : real) : real ;      {log_10(x)}
begin
  if x > 0.0 then log_10 := ln(x)/ln(10)
  else begin
         writeln('Illegal function call to log_10(x) was made with x =
',x);
         halt(1);
       end;
end;


procedure convert_OMA ( main_file,
                        output_file,
                        background_file,
                        dye_file,
                        water_file    : string);
const
  c5       = 7.1707128047e-12 ;     {a[6]}  {use p_fit.pas to calculate}
  c4       = -9.3612057740e-9 ;
  c3       = 4.6820027158e-6 ;
  c2       = -1.1188217240e-3 ;
  c1       = 2.5442759011e-1 ;
  c0       = -3.8107920644e1 ;        {a[1]}
  th_laser = 34 ;
  th_det   = 16 ;
  lamda    = 0.6328 ;{um}
  n_sample = 1.45 ;
  s        = ','   ; {separation character for SC4 .csv file}
  max_volt = 10000.0 ; { maximum input to A/D conv. of OMA III in mV}
  sector   = 16     ; {must be power of 2, including 2^0=1}
{sector 16-> 25.4mm/512*16=0.8mm and 32-1 data points}
  t_unit   = 6      ; { i = 400 each 6 sec is unit time }
```

```pascal
var
  input,back,dye,water
                          : oma_dataset_type_ptr;
  p                       : oma_data_type_ptr;
  data                    : oma_data_type_ptr_array_ptr ;
  i,j,mem,k               : integer;
  sector2                 : integer ;
  q                       : array[1..oma_data_size] of real;
  c                       : real ; {channel}
  th,th4                  : real ; {angle deg}
  t1,t2,t3,t4             : real ; {angle rad}
  factor                  : real ; {average intensity at around 256 ch for dye}
  av,av0                  : real ; {average over sector}
  t,ab,alpha              : real ; {time, optical thickness}
  outfile                 : text ;

begin
  new(input);                     {input main data to a heap pointed by
'input'}
  input^.filename := main_file;
  read_oma(input) ;
  mem := input^.memories ;
  p := input^.data_head ;
  new(data) ;
  for i := 1 to mem do
    begin
      data^[i] := p ;
      p := p^.next ;
    end ;
  new(back);                      {input back ground data to heap 'back'}
  back^.filename := background_file;
  read_oma(back);
  if(back^.memories<>1) then
    begin
      writeln('inproper data for back ground');
    end;
  new(dye);                       {input dye data to heap 'dye'}
  dye^.filename := dye_file;
  read_oma(dye);
  if(dye^.memories<>1) then
    begin
      writeln('inproper data for dye');
    end;
  new(water);                     {input water data to heap 'water'}
  water^.filename := water_file;
  read_oma(water);
  if(water^.memories<>1) then
    begin
      writeln('inproper data for water');
    end;
{get absorption coef. alpha p28 for dye sample}
  alpha := ln((water^.data_head^.data[oma_data_size]
              -back^.data_head^.data[oma_data_size])
            /(dye^.data_head^.data[oma_data_size]
              -back^.data_head^.data[oma_data_size]));
{ Obtain intensity calibration factor }
{ by the fluorescence intensity of dye. }
{Use nile blue water solution. Its absorption must be less than 10 %}
```

```
  for j := 1 to oma_data_size -1 do
    begin
      dye^.data_head^.data[j] := dye^.data_head^.data[j]
                               - water^.data_head^.data[j] ;
    end;
  factor := 0.0 ;
  for j := ((oma_data_size-1) div 2)-sector+1 to ((oma_data_size-1) div
2)+sector do
    begin
      factor := factor + dye^.data_head^.data[j] ;
    end ;
{intensity calib. factor array}
  factor := factor /(2*sector) ;{normalize with center 2 sector}
  for j := 1 to oma_data_size -1 do
    begin
      if(abs(factor)<1.0) then
        begin
          dye^.data_head^.data[j] := 1.0 ;
        end
      else if (dye^.data_head^.data[j]>0.0) then
        begin
          dye^.data_head^.data[j] :=factor /dye^.data_head^.data[j] ;
        end
      else
        begin
          dye^.data_head^.data[j] := 0.0 ; { invalid data }
        end
    end;
{s.comp conversion to input milivolt assuming i=400}
  q[oma_data_size]:=0.0;
  for i := 1 to mem do
    begin
      data^[i]^.data[oma_data_size] :=
              (data^[i]^.data[oma_data_size]
            - back^.data_head^.data[oma_data_size])*max_volt/6553600.0;
    end ;
{back ground substraction and intensity calibration }
{ using dye/water data}
  for j:=1 to oma_data_size-1 do
    begin
      c:=j;
      t1   := th_laser/180*pi ;
      t2   := arcsin(sin(t1)/n_sample) ;
      th   := (((((c5*c+c4)*c+c3)*c+c2)*c+c1)*c+c0 ;
              {channel to angle conv.}
      th4 := th + th_det ;
      t4   := th4/180*pi ;
      t3   := arcsin(sin(t4)/n_sample) ;
      t    := alpha*(1-cos(t2)/cos(t3));
      ab   := exp(alpha);
      if (abs(t)>0.0001) then {six digit cf. p 27-28}
        begin
          ab   := ab *t/(exp(t)-1.0);
        end;
      q[j]:= 4*pi*n_sample * sin((t2+t3)/2.0) / lamda ;
            {scattering vector}
      for i := 1 to mem do
        begin
```

```pascal
            data^[i]^.data[j] := (data^[i]^.data[j]-
back^.data_head^.data[j])
                                * dye^.data_head^.data[j]
                                * ab ;
                                { ab : absorption crrection}
        end;
    end;
{output routine}
  writeln(' ===== output =====');
  assign(outfile,output_file);
  rewrite(outfile);
{ ===== heading ===== }
  writeln(outfile,'"OMA_III:',main_file,'"');
  writeln(outfile,s,'"=== converted by OMA_III.PAS(Ver. 3.0 /
programmer: Osamu Aoki(U. of Mass.) ==="');
  writeln(outfile,s,'"This data format(*.csv) is compatible with Lotus
1-2-3, SC4 and other programs."');
  writeln(outfile,s,'"Sector by"',s,sector:3);

writeln(outfile,s,'"Contents"',s,'"filename"',s,s,'"memories"',s,'"file_
label"');
  writeln(outfile,s,'"Main"',s,'"',main_file
,'"',s,s,input^.memories,s,input^.file_label);
  writeln(outfile,s,'"Back"',s,'"',background_file ,'"',s,s,
back^.memories,s,back^.file_label );
  writeln(outfile,s,'"Dye"',s,'"',dye_file
,'"',s,s,dye^.memories,s,dye^.file_label);
  writeln(outfile,s,'"Water"',s,'"',water_file ,'"',s,s,
water^.memories,s,water^.file_label );
  writeln(outfile);
{ ===== row data ==== }
  writeln(outfile,s,'"I(q,t) row data"') ;
  write(outfile,s,'"memories"',s,'"--->"',s,'"--->"',s);
  for i := 1 to input^.memories do
    begin
      write(outfile,i,s);
    end;
  writeln(outfile);
  write(outfile,s,'"channel"',s,'"q"',s,'"q^2\time"',s);
  for i := 1 to input^.memories do   {time for p3.ksp:i=400:time unit=6
sec}
    begin
    if       i<11 then write(outfile,t_unit*(i-1),s)
    else if i<20 then write(outfile,t_unit*(i-10)*10.0,s)
    else if i<29 then write(outfile,t_unit*(i-19)*100.0,s)
    else              write(outfile,t_unit*(i-28)*1000.0,s)  ;
    end;
  writeln(outfile);
  write(outfile,s,s,s,'"log(time)"',s) ;
  for i := 1 to input^.memories do      {log(time) for p3.ksp:i=400:time
unit=6 sec}
    begin
    if       i=1  then write(outfile,'-1',s)
    else if i<11 then write(outfile,log_10(t_unit*(i-1)),s)
    else if i<20 then write(outfile,log_10((i-10)*10.0*t_unit),s)
    else if i<29 then write(outfile,log_10((i-19)*100.0*t_unit),s)
    else              write(outfile,log_10((i-28)*1000.0*t_unit),s) ;
    end;
```

102

```
    writeln(outfile);
    sector2 := sector div 2 ;
{output average value over each sector}
    for j := 1 to ((oma_data_size-1) div sector)-1 do
        begin
{average channel position over q}
        av := 0.0 ;
        for k := (j-1)*sector+1+sector2 to j*sector+sector2 do
            begin
            av:= av+k;
            end ;
        av := av /sector ;
        write(outfile,s,av,s);
{average q over sector}
        av := 0.0 ;
        for k := (j-1)*sector+1+sector2 to j*sector+sector2 do
            begin
            av:= av+q[k];
            end ;
        av := av /sector ;
        write(outfile,av,s,sqr(av),s);
{average data over sector}
        for i := 1 to mem do
            begin
            av := 0.0 ;
            for k := (j-1)*sector+1+sector2 to j*sector+sector2 do
                begin
                av:= av+data^[i]^.data[k];
                end ;
            av := av /sector ;
            write(outfile,av,s);
            end;
        writeln(outfile);
    end;
{out put s.comp. value as mV}
    write(outfile,s,'"SC(t)"',s,'"--->"',s,'"--->"',s);
    for i := 1 to mem do
        begin
        av:=data^[i]^.data[oma_data_size];
        write(outfile,av,s);
        end;
    writeln(outfile);
{out put s.comp. value as NORMALIZED}
    write(outfile,s,'"SC(t)/SC(0)"',s,'"--->"',s,'"--->"',s);
    for i := 1 to mem do
        begin
        av:=data^[i]^.data[oma_data_size]/data^[1]^.data[oma_data_size];
        write(outfile,av,s);
        end;
    writeln(outfile);
    writeln(outfile);   {vacant line}
{parameters}          { do not output }
{
    writeln(outfile,s,'"parameters"',s,'"main"',s,'"back"');
    for i := 1 to oma_parameter_size do
        begin
```

103

```pascal
    writeln(outfile,s,'"para',i:3,'"',s,input^.parameters[i],s,back^.paramet
ers[i]);
      end;
  }
    close(outfile);
end;

{main}
var
   filename : array[1..5] of string;
   i        : integer ;

begin {main}
   writeln;
   writeln('++++++++++ conversion program for OMA-III data
++++++++++++++');
   writeln('                        programmed by Osamu Aoki');
   if (paramcount <> 5) then
     begin
       writeln('Enter command as "C:\>oma_III main output back dye
water"');
       writeln('Comment: All files may be specified as
d:\dir\filename.ext.');
       writeln('              Both main_file and background_file are generated
by OMA-III''s');
       writeln('              "OMA-III -> MS-DOS" command in Disk-screen.');
       writeln('              The back, dye and water have only one memory and
shares the same');
       writeln('              exposute time and number of scans/memory with
the main.');
       halt(1);
     end ;
   writeln('---------- using files  ----------');
   for i := 1 to 5 do
     begin
       filename[i] := paramstr(i);
       writeln('filename[',i:1,']=',filename[i]);
     end;

convert_oma(filename[1],filename[2],filename[3],filename[4],filename[5])
;
end.
```

104

```pascal
{$I+,R+,N-}
unit oma_lib;
interface
const
  oma_data_size        = 513 ;
  oma_parameter_size   = 88 ;
  oma_max_memories     = 200 ;
type
  oma_data_type_ptr    = ^oma_data_type;
  oma_data_type        = record
                           next : oma_data_type_ptr;
                           data : array[1..oma_data_size] of real;
                         end;
  oma_dataset_type     = record
                           filename   : string;
                           memories   : integer;
                           data_head  : oma_data_type_ptr;
                           file_label : string;
                           parameters : array[1..oma_parameter_size] of
real;
                         end;
  oma_dataset_type_ptr = ^oma_dataset_type;

procedure read_OMA( input : oma_dataset_type_ptr);
function uppercase(x :string) : string ;

implementation
function uppercase(x :string) : string ;
var
 i : integer ;
 c : char     ;
 y : string   ;
begin
  y:='';
  for i := 1 to length(x) do
    begin
      c := upcase(x[i]);
      y := concat(y,c);
    end;
  uppercase := y ;
end ;

procedure read_OMA( input : oma_dataset_type_ptr);

var
  p,q                              : oma_data_type_ptr;
  i,j                              : integer;
  section,buf                      : string;
  line,IOerror                     : integer;
  end_of_file                      : boolean;
  infile                           : text;
  read_flag                        : boolean;

  function read_buf                : string;
```

```pascal
    begin;
       line := line + 1;
       {$I-}
       readln(infile,buf);
       {$I+}
       IOerror:=IOresult;
       if(IOerror<>0)then
         begin
           writeln('I/O error at ',section,' line:',line:5);
           writeln('MS-DOS error code:',IOerror:5);
           halt(1);
         end;
       read_buf := buf;
    end;

    procedure error_message;
    begin;
       writeln
         ('Non-OMA file having incompatible data at ',section,'
line:',line:5);
       writeln(buf);
       halt(1);
    end;

    function convert_int( buf : string) : integer ;
    var
       code,intbuf       : integer ;
    begin;
       {$R-}
       val(buf,intbuf,code);
       {$R+}
       if(code<>0)then error_message;
       convert_int := intbuf ;
    end;


    function convert_real( buf : string) : real ;
    var
       code              : integer;
       realbuf           : real ;
    begin;
       {$R-}
       val(buf,realbuf,code);
       {$R+}
       if(code<>0)then error_message;
       convert_real := realbuf ;
    end;

begin;                                                    {read_OMA}
   if uppercase(input^.filename)<>'NUL' then   { real file name ?}
     begin
       read_flag := true ;
     end
   else
     begin
       read_flag := false ;
     end ;
   assign(infile,input^.filename);
```

```pascal
reset(infile);
line:=0;
section:='Header';
if read_flag then
  begin
    if(length(read_buf)<>0)then error_message;
    input^.memories := convert_int(read_buf);
    if((input^.memories<1) or (input^.memories>oma_max_memories))
        then error_message;
    if(convert_int(read_buf)<>1) then error_message;
    if(convert_int(read_buf)<>oma_data_size) then error_message;
  end
else
  begin
    input^.memories := 1 ;
  end ;
{read data to heap area with record type data_type}
for j:=1 to input^.memories do
  begin;
    str(j:5,buf);
    section:='data of memory '+buf;
    line:=0;
    if j=1 then
      begin
        new(p);
        input^.data_head := p;
        p^.next := nil ;
      end
    else
      begin
        q := p ;
        new(p);
        q^.next := p ;
        p^.next := nil ;
      end;
    for i:=1 to oma_data_size do
      begin;
        if read_flag then
          begin
            p^.data[i]:=convert_real(read_buf);
          end
        else
          begin
            p^.data[i]:= 0 ;
          end;
      end;
    if( read_flag and (length(read_buf)>0))then error_message;
  end;
section:='file label';
line:=0;
if read_flag then
  begin
    input^.file_label:=read_buf ;
    section:='parameters';
    line:=0;
    for i:=1 to oma_parameter_size do
      begin;
        input^.parameters[i]:=convert_real(read_buf);
```

107

```pascal
            end;
        if(length(read_buf)>0)then error_message;
        {$I-}
        end_of_file:=eof(infile);
        {$I+}
        IOerror:=IOresult;
        if ((IOerror<>0) or (not end_of_file))then
          begin
            writeln('Non-OMA file: end_of_file=',end_of_file,'
IOerror=',IOerror);
          end;
      end
    else
      begin
        input^.file_label :='"All data = 0.0 , 1 memory and undefined
parameters"';
        for i := 1 to oma_parameter_size do input^.parameters[i] := 0.0 ;
        input^.parameters[2]  := 512 ;
        input^.parameters[4]  := 0.0 ;
        input^.parameters[8]  := 2 ;
        input^.parameters[10] := 0 ; {i}
        input^.parameters[11] := 1 ; {j}
        input^.parameters[12] := 0 ; {k}
      end;
    close(infile);
  end;
  end.                                                    {read_OMA}
```

REFERENCES

1. Bruins, P. F., *Polyblends and Composites*, (Wiley-Interscience, New York 1981).

2. Klempner, D., and K. C. Frisch. *Polymer Alloys - Blends, Blocks, Grafts and Interpenetrating Networks, Polymer Science and Technology, vol. 10*, (Plenum, New York 1979).

3, Olabisi, O., L. M. Robeson, and M. T. Shaw. *Polymer-Polymer Miscibility*, (Academic Press, New York 1979).

4, Paul, D. R., and S. Newman. *Polymer Blends*, (Academic Press, New York 1978).

5, Sperling, L. H., *Interpenetrating Polymer Networks and Related Materials* (Plenum Press, New York 1981).

6, Walsh, D. J., J. S. Higgins, and A. Moconnachie. *Polymer Blend and Mixtures, NATO ASI Series E: Applied Sciences-No.89* (Martinus Nijhoff Publisers, Boston 1985).

7, Frisch, H. L., *British Polym. J.*, **17**, 149 (1985).

8, Nishi, T., T. T. Wang, and T. K. Kwei. *Macromolecules*, **8**, 227 (1975).

9. Hashimoto, T., J. Kumaki, and H. Kawai. *Macromolecules*, **16**, 641 (1983).

10. Snyder, H. L., P. Meakin, and S. Reich. *Macromolecules*, **16**, 757 (1983).

11, Halary, J. L., J. M. Ubrich, J. M. Nunzi, L. Monnerie, and R. S. Stein. *Polymer*, **25**, 957 (1984).

12, Shibayama, M., H. Yang, R. S. Stein, and C. C. Han. *Macromolecules*, **18**, 2179 (1985).

13, Yang, H., M. Shibayama, R. S. Stein, N. Shimizu, and T. Hashimoto. *Macuromolecules*, **19**, 1667 (1986).

14, Han, C. C., M. Okada, Y. Muroga, F. L. McCrackin, B. J. Bauer, and Q. Tran-Cong. *Polym. Eng. Sci.*, **26**, 3 (1986).

15,   Han, C. C., M. Okada, Y. Muroga, B. J. Bauer, and Q. Tran-Cong. *Polym. Eng. Sci.*, **26**, 1208 (1986).

16,   Hashimoto, T., J. Kumaki, and H. Kawai. *Macromolecules*, **16**, 641 (1983).

17,   Hashimoto, T., K. Sasaki, and H. Kawai. *Macromolecules*, **17**, 2812 (1984).

18,   Sasaki, K., and T. Hashimoto. *Macromolecules*, **17**, 2818 (1984).

19,   Inoue, T., T. Ougizawa, O. Yasuda, and K. Miyasaka. *Macromolecules*, **18**, 57 (1985).

20,   Russell, T. P., G. Hadziioannou, and W. K. Warburton. *Macromolecules*, **18**, 78 (1985).

21,   Strobl, G. R., *Macromolecules*, **18**, 558 (1985).

22,   Okada, M., and C. C. Han. *J. Chem. Phys.*, **85**, 5317 (1986).

23,   Kumaki, J., and T. Hashimoto. *Macromolecules*, **19**, 763 (1986).

24,   Hashimoto, T., M. Itakura, and H. Hasegawa. *J. Chem. Phys.*, **85**, 6118 (1986).

25,   Hashimoto, T., M. Itakura, and N. Shimidzu. *J. Chem. Phys.*, **85**, 6773 (1986).

26,   Yang, H., M. Shibayama, R. S. Stein, N. Shimizu, and T. Hashimoto. *Macromolecules*, **19**, 1667 (1986).

27,   Sato, T., and C. C. Han. *J. Chem. Phys.*, **88**, 2057 (1988).

28,   Han, C. C., B. Bauer, J. C. Clark, Y. Muroga, Y. Matsushita, M. Okada, Q. Tran-Cong, T. Chang, and I. C. Sanchez. *Polymer*, **29**, 2003 (1988).

29,   Bauer, B. J., R. M. Briber, and C. C. Han. *Polym. Prepr. (Am. Chem. Soc., Div. Polym. Chem.)* **28**(2), 169 (1987).

30,   Briber, R. M., and B. J. Bauer. *Macromolcules*, **21**, 3296 (1988).

31,   Bauer, B. J., R. M. Briber, and C. C. Han. *Macromolcules*, **22**, 940 (1989).

32,   Dary, L. E., U. S. Patent 2,439,202; April 6 (1948); assigned to United States Rubber Company.

33, Backnall, C. B., *Toughened Plastics* (Applied Science Publishers LTD, London 1977)

34, Binder, K., and H. L. Frisch. *J. Chem. Phys.*, **81**, 2126 (1984).

35, Onuki, A., *Proceedings for the meeting Dynamics of Ordering Processes in Condensed Matter*, held in Kyoto, Japan, August (1987).

36 Onuki, A., *J. Phys. Soc. Jpn. Lett.*, **57**, 699 (1988).

37. Flory, P. J., *J. Chem. Phys.*, **9**, 660(1941).

38, Flory, P. J., *J. Chem. Phys.*, **10**, 51 (1942).

39, Huggins, M. L., *J. Chem. Phys.*, **9**, 440 (1941).

40, Flory, P. J., *Principles of polymer Chemistry* (Cornell University, Ithaca 1953).

41, Flory, P. J., and J. Rehner. Jr., *J. Chem. Phys.*, **11**, 521 (1943).

42, Flory, P. J., *J. Chem. Phys.*, **18**, 108, (1950).

43, Neuburger, N. A., and B. E. Eichnger. *Macromolecules*, **21**, 3060 (1988).

44, Dusek, K., *J. Polym. Sci.*, **B3**, 209 (1965).

45, Dusek, K., *J. Polym. Sci.*, **C16**, 1289 (1967).

46, Dusek, K., and W. Prins. *Adv. Polym. Sci.*, **6**, 1 (1969).

47, Dusek, K., *Polymer Networks. Structure and Mechanical Properties*, A. J. Chompff, S. Newman, Eds., (Plenum Press, New York 1971).

48, Flory, P. J., *J. Chem. Phys.*, **66**, 5720 (1977).

49, Flory, P. J., and B. Erman. *Macromolecules*, **15**, 800 (1982).

50, Erman, B., and P. J. Flory. *Macromolecules*, **15**, 806 (1982).

51, Mark, J. E., and B. Erman. *Rubberlike Elasticity* (Wiley-Interscience, New York 1988).

52, J. W. Cahn and J. E. Hilliard, *J. Chem. Phys.*, **28**, 258 (1958).

53,   Cahn, J. W., *J. Chem. Phys.*, **30**, 1121 (1959).

54,   Cahn, J. W., and J. E. Hilliard. *J. Chem. Phys.*, **31**, 688 (1959).

55,   Cahn, J. W., *J. Chem. Phys.*, **42**, 93 (1965).

56,   Binder, K., *J. Chem. Phys.*, **79**, 6387 (1983).

57,   Binder, K., *Phys. Rev.*, **A29**, 341 (1984).

58,   Binder, K., *Colloid. Polym. Sci.*, **265**, 237 (1987).

59,   de Gennes, P. G., *Scaling Concept in Polymer Physics*, (Cornell University, Ithaca 1979).

60,   de Gennes, P. G., *J. Chem. Phys.*, **72**, 4756 (1980).

61,   Pincus, P., *J. Chem. Phys.*, **75**, 1996 (1981).

62,   Brandrup, J., *Polymer Handbook*, (Wiley-Interscience, NewYork 1975).

63,   R. S. Stein and J. J. Keane, *J. Polym., Sci.*, **17**, 21 (1955).

64,   Stein, R. S., R. E. Prud'homme, L. Bourland, and R. T. Natarajan. *J. Polym., Sci., Polym. Physics Ed.*, **12**, 1955 (1974).

65,   Stein, R. S., R. T. Natarajan, R. E. Prud'homme, and L. Bourland. *J. Polym., Sci., Polym. Physics Ed.*, **14**, 1541 (1976).

66,   Roland, C. M., and G. G. A. Böhm. *J. Polym. Sci., Polym. Phys. Ed.*, **22**, 79 (1984).

67,   Vrahopoulou-Gilbert, E., and A. J. McHugh. *Macromolecules*, **17**, 2657 (1984).

68,   Fredrickson, G. H., *J. Chem. Phys.*, **85**, 5306 (1986).

69,   Rangel-Nafaile, C., A. B. Metzner, and K. F. Wissbrun. *Macromolecules*, **17**, 1187 (1984).

70,   Candau, S., J. Bastide, and M. Delsanti. *Adv. Polym. Sci.*, **44**, 27 (1982).

71.   Boue, F., B. Farnoux, J. Bastide, A. Lapp, J. Herz, and C. Picot. *Europhys. Lett.*, **1**, 637 (1986).

72, Bastide, J., M. Buzier, and F. Boue. *Polymer Motion in Dense Systems: Springer Proceedings in Physics 29* (Springer-Verlag, Berlin, 1987).

73, Tsay, H. M., and R. Ulman. *Macromolecules,* **21**, 2963 (1988).

74, Tran-Cong, Q., T. Nagaki, O. Yano, and T. Soen. *Macromolecules,* **22**, 2720 (1989).